AD NUMBER

AD478724

LIMITATION CHANGES

TO:

Approved for public release; distribution is unlimited.

FROM:

Distribution authorized to U.S. Gov't. agencies and their contractors; Administrative/Operational Use; NOV 1965. Other requests shall be referred to Defense Advanced Research Projects Agency, ASBD-TIO, Attn: Nuclear Test Detection Office, 675 North Randolph Street, Arlington, VA 22203-2114.

AUTHORITY

onr ltr, 28 jul 1977

MISSING PAGE
NUMBERS ARE BLANK
AND WERE NOT
FILMED

SU-SEL-65-097

Acoustic-Gravity Waves in the Atmosphere

by

T. A. Potemra

November 1965

Technical Report No. 110

Prepared under
Office of Naval Research Contract
Nonr-225(64), NR 088 019, and
Advanced Research Projects Agency ARPA Order 196-65

RADIOSCIENCE LABORATORY

STANFORD ELECTRONICS LABORATORIES

STANFORD UNIVERSITY · STANFORD, CALIFORNIA

SEL-65-097

ACOUSTIC-GRAVITY WAVES IN THE ATMOSPHERE

by

T. A. Potemra†

November 1965

Technical Report No. 110

Prepared under
Office of Naval Research Contract
Nonr-225(64), NR 088 019, and
Advanced Research Projects Agency ARPA Order 196-65

†Now at Applied Physics Laboratory, The Johns Hopkins University

Radioscience Laboratory
Stanford Electronics Laboratories
Stanford University Stanford, California

ABSTRACT

The purpose of this research was to obtain a panoramic view of acoustic-gravity-wave motions throughout the atmosphere. A one-dimensional array of particles and springs, conceived by Newton to study sound waves in the atmosphere, was extended to two dimensions. Variations of density and pressure with altitude are represented by variations in mass and spring constants.

The validity of this extension of Newton's model in faithfully imitating motions in the atmosphere is limited by the ability of the particle-and-spring array to support shear waves, whereas the atmosphere cannot. By careful restriction of energy sources, this model proved feasible for simulating on a computer a portion of the atmosphere measuring 300 km high by 500 km wide. A motion picture--automatically plotted by the computer, a frame at a time--provides greater detail and perspective of mechanical wave motions in the atmosphere than has ever been obtainable before. Ground-level and 100-km-high explosions were investigated with this computer model, and the resulting transient motions of the atmosphere were displayed by means of a motion picture produced by digital techniques. Computed ground-level barograms resulting from a ground-level explosion compare well with experimental barograms recorded during ground-level nuclear explosions.

CONTENTS

ILLUSTRATIONS

NOTATION

c	velocity of sound
d_o	equilibrium spacing between particles
e	voltage
f	force
g	gravitational constant
i	current
k	spring modulus
m	particle mass
n_x, n_y	refractive indexes in x and y directions
p	pressure
p_o	ambient-pressure
r	radial distance from source
s	speed; propagation of a mechanical wave
t	time
$\bar{u}_x, \bar{u}_y$	direction vectors
v_p	phase velocity
$\vec{v}$	perturbational velocity
v_x, v_y	perturbational velocities in the x and y directions
x	horizontal coordinate
y	altitude coordinate
z	horizontal coordinate
C	electrical capacitance
D/Dt	Eulerian derivative
E_d	energy density

H	scale height of atmosphere
H_o, J_o	Bessel functions
L	electrical inductance
Y	admittance
Z	impedance
β	propagation constant
γ	ratio of specific heats
δp	perturbational pressure
$\delta \rho$	perturbational density
$\vec{\kappa}$	wave-number vector
κ_x, κ_y	wave numbers in x and y directions
ρ	density
ρ_o	ambient density
χ	velocity gradient
ω	frequency
ω_c	atmospheric frequency cutoff
Δp	overpressure
$\Delta \rho$	overdensity

ACKNOWLEDGMENT

I wish to express my appreciation to Professor O. G. Villard, Jr., and Dr. G. H. Barry for their guidance and inspiration during the course of this work. I am also grateful to Professor O. Buneman, who provided invaluable assistance in the final development of this problem, and for the comments of members of the RAND Corporation, especially Dr. W. Meecham during a presentation arranged by Dr. P. Tamarkin.

The patient and efficient computer programming by D. E. Westover was of great help and is deeply appreciated.

I. INTRODUCTION

Pressure disturbances in the atmosphere are caused by a variety of natural and man-made sources. Atmospheric tides result from the revolution of the earth on its axis and have periods of about one day, or about 1,000 min. Airplanes, volcanoes, explosions, and auroral activity cause higher-frequency pressure disturbances, audible to the human ear, known as acoustic waves. Acoustic waves extend over a very wide frequency range and have periods as long as a few minutes. Acoustic-gravity waves fill the gap in the frequency spectrum between atmospheric tides and acoustic waves, having periods ranging from 10 to 1,000 min and wavelengths from 100 to 10,000 km.

A. ACOUSTIC-GRAVITY WAVES

The equilibrium surface of a liquid in a uniform gravitational field is a plane. When this surface is moved from its equilibrium position, motion will occur in the liquid which will propagate as waves throughout the fluid. These mechanical waves are due to the force of the gravitational field as well as to pressure and inertial forces.

The atmosphere is highly compressible and has no definite surface boundary as does an ordinary fluid, but equilibrium conditions in the atmosphere are also defined by the earth's gravitational field. Gravity compresses the air in the surrounding atmosphere to such a degree that air density and pressure decrease exponentially with altitude. For wave motion with wavelengths short in comparison to this scale, only pressure and inertial forces may be considered--defining these disturbances as acoustic waves. Low-frequency disturbances with wavelengths much greater than the vertical scale of the atmosphere are affected by the gravitational field and are called "acoustic-gravity waves."

Impedance in acoustic systems is proportional to air density. The exponential variation of air density with altitude in the atmosphere represents a tapered acoustical transmission line. For sufficiently low frequencie and long wavelengths, wave propagation ceases along the tapered transmission line so that a low-frequency cutoff exists for

vertically traveling pressure waves in the atmosphere. This low-frequency cutoff in the atmosphere is dependent on the vertical variation of mass density determined by the earth's gravitational field and by the vertical temperature variations within the atmosphere. At sea level this atmospheric cutoff corresponds to wave periods of 5 to 10 min, depending on the precise structure of the atmosphere. Disturbances with frequencies above this cutoff are termed acoustic waves and disturbances with lower frequencies are called acoustic-gravity waves. Since the atmosphere is essentially uniform in any horizontal direction parallel to the surface of the earth, a horizontal cutoff frequency is not apparent. Waves propagating at angles between the vertical and horizontal would experience different cutoff frequencies, depending on these propagation angles.

The atmosphere also has the characteristic of an electrical transformer. Consider a pressure disturbance propagating vertically in the atmosphere. If we ignore three-dimensional spreading losses for the moment and assume the speed of sound to vary slowly with altitude, the much less dense air at high altitudes must oscillate more violently than an equal volume of air at ground level with the same kinetic energy. A small pressure disturbance on the ground will produce a large pressure disturbance by the time it propagates to high altitudes. Pressure is analogous to voltage in an electrical system; thus the atmosphere is analogous to an electrical transformer with a turns ratio proportional to the vertical distance between "input" and "output" altitudes in the atmosphere.

In summary, the two types of mechanical wave propagation in the atmosphere (acoustic and acoustic-gravity) are differentiated by the extent to which gravity influences the wave motion. A cutoff frequency related to the gravitational field and vertical temperature profile in the atmosphere separates the mechanical disturbances in the frequency domain.

B. IMPORTANCE TO IONOSPHERIC PHYSICS

Radio experimenters have been detecting large-scale traveling irregularities in the E and F regions of the ionosphere for many years [Refs. 1, 2]. In the E region, only one particle in 10^8 is an electron

and, in the F region, one particle in 10^3 is an electron. Mechanical disturbances in the ambient neutral atmosphere will carry along the few electrons just as sparsely spaced beads in a vibrating gelatin. Density variations in the neutral fluid in the E region are directly reproduced in the charged fluid of electrons. At higher altitudes in the F region, however, electrons would be constrained to move along magnetic field lines like beads on an abacus. An understanding of ionospheric radio propagation is incomplete without considering the enclosing neutral atmosphere. Therefore an analysis of mechanical waves such as acoustic or acoustic-gravity waves in the atmosphere is of great importance to the radio physicist.

Conversely, ionospheric radio propagation has provided an effective tool for studying the atmosphere at ionosphere heights. Aeronomists (atmospheric physicists) are no longer restricted to making ground-level measurements or limited range measurements with balloons or rockets. Radio probes provide these researchers with "high altitude barometers."

C. AIR-CELL COMPUTER MODEL OF THE ATMOSPHERE

This research has been concerned with a digital-computer model of the atmosphere that provides solutions for energy distributions, overpressures, density perturbations, and particle velocities resulting from various acoustic-gravity sources.

An analogy between a fluid and a mechanical lattice, first used by Newton in the 18th Century [Ref. 3], is the basis for the computer modeling. The fluid equations describing the earth's atmosphere are re-written into a form describing discrete "cells of air" rather than a fluid continuum, so that the atmosphere is divided into a number of cells, as shown in Fig. 1. The number of air molecules contained within each cell, and therefore the total mass of each cell, are fixed, while changes in dimensions of the cell represent density and pressure perturbations. The resulting finite-difference equations describing wave propagation in the atmosphere are nearly equivalent to the equations describing mechanical wave propagation in the two-dimensional lattice of particles

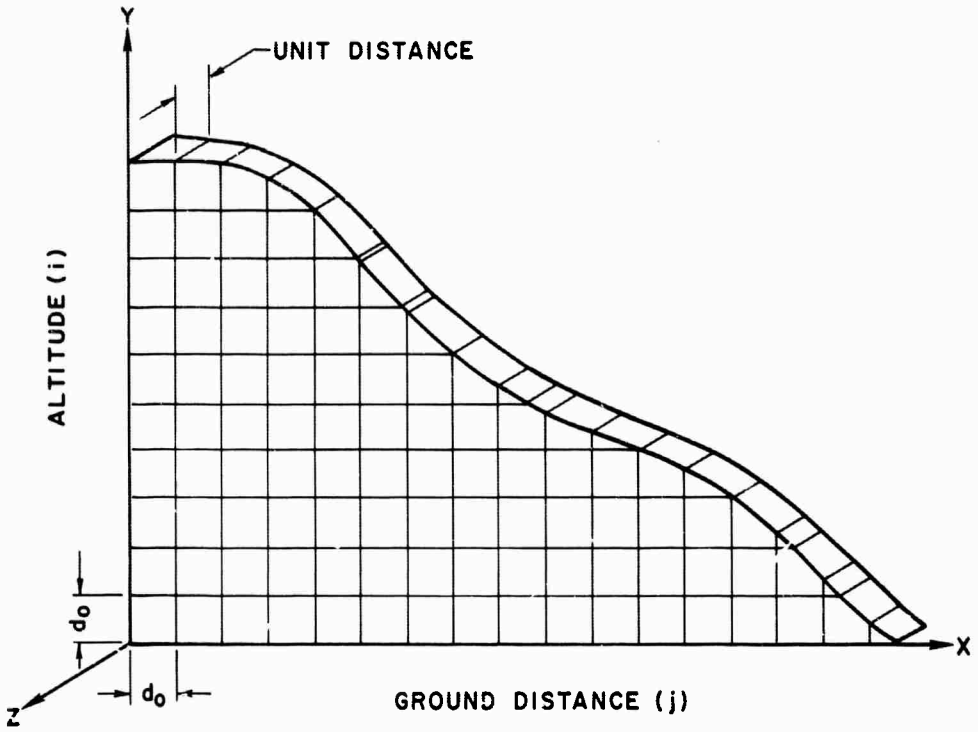

34353

FIG. 1. TWO-DIMENSIONAL ARRAY OF AIR CELLS REPRESENTING THE ATMOSPHERE.

and springs shown in Fig. 2, but differ in the following way. In general, any fluid (including the atmosphere) is unable to endure or support a shear stress--a shear stress is a force tangent to a surface per unit area of that surface. The particle-and-spring array can sustain a certain amount of shear stress; however, this property limits the usefulness of the particle-and-spring model to imitate atmospheric oscillations and raises the question as to why the mechanical analogy was invoked at all.

A rigorous finite-difference solution to the hydrodynamic equations of the atmosphere was programmed, but instabilities resulted in the computer solution. These instabilities were immediately eliminated by programming the equations of motion for the mechanical lattice in Fig. 2. The mechanical-lattice approach represents an extension of Newton's one-dimensional analog to two dimensions and has a heuristic value in explaining phenomena in the real atmosphere, such as frequency cutoffs and energy-trapping effects.

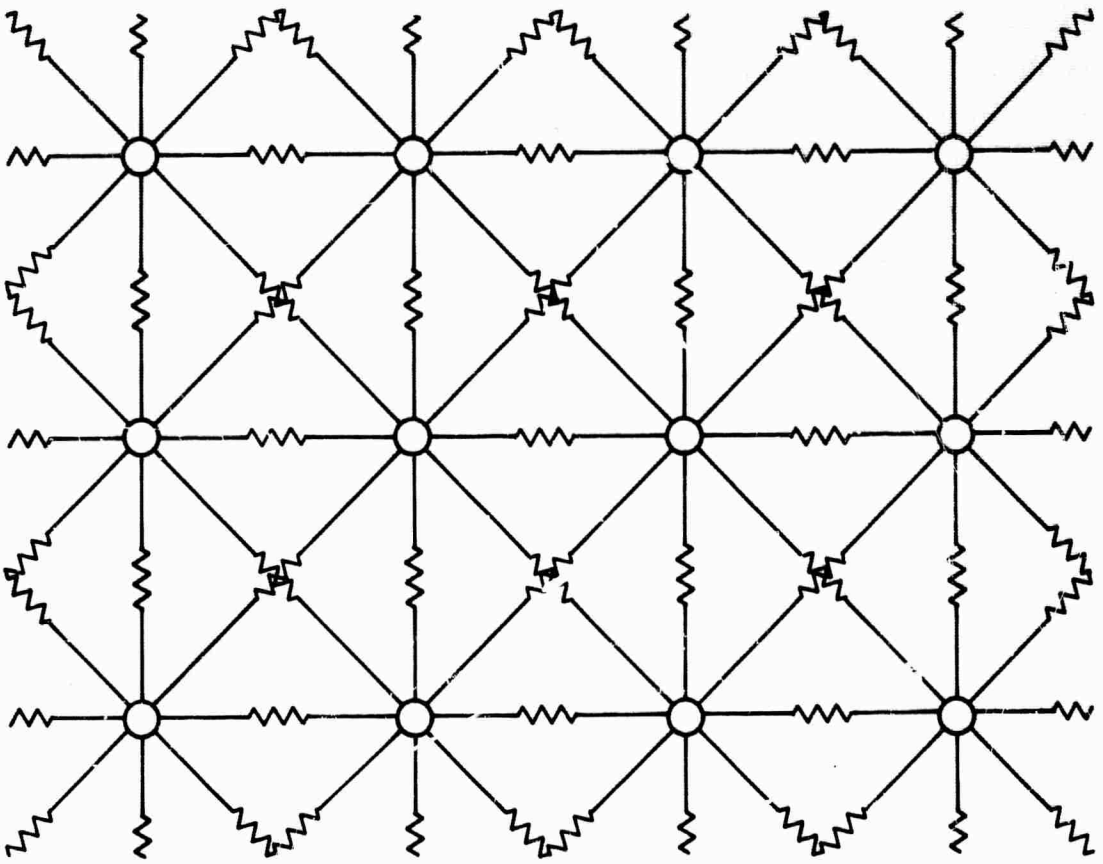

34354

FIG. 2. TWO-DIMENSIONAL LATTICE OF MASSES AND SPRINGS REPRESENTING THE ATMOSPHERE.

The discrepancy between the mechanical model and the atmosphere may be eliminated by requiring the energy source to be "shear-stress free." Isotropic point sources (or, in the two-dimensional case, isotropic line sources) satisfy this requirement and were the only type of source considered in this analysis. A detailed mathematical development supporting the validity of the mechanical model is contained in Chapter III.

A portion of the atmosphere was modeled in which densities and pressures vary through 11 orders of magnitude. If masses comparable to ping-pong balls were used to construct the top row of particles in an actual mechanical model, a single particle in the bottom row would weigh 10-million tons--equal to the total annual steel production for America.

Long-wavelength disturbances propagate with no difficulty through a linear array of masses and springs. But, as the wavelength is decreased

to such a value that a half wavelength is comparable to the intermass spacing, a resonance condition is realized and propagation ceases. At this frequency the velocity of propagation throughout the mechanical lattice is reduced to zero and the lattice is no longer a valid model of the atmospheric fluid. The air-cell computer model was found to be valid for frequencies as high as 5 mc (millicycles per second) (0.005 cps).

Sinusoidal point sources were considered first to check the computer-model results with existing geometrical acoustic-wave theory in the higher acoustic-frequency range. The source frequency was then decreased to study the steady-state distribution of energy throughout the atmosphere. A high-altitude sinusoidal source was also studied. Finally, a pulse input was applied to the model to simulate an explosion to observe the transient behavior of the atmosphere. Transient phenomena and large-scale motions resulting from these explosions are visualized with the motion-picture output of the computer model. This movie provides greater detail and insight into mechanical wave motions in the atmosphere than has ever been obtainable before.

D. SCOPE

The early theoretical work in atmospheric studies by Newton and Laplace, and experimental work beginning with the Krakatoa eruption in 1883 are reviewed.

The present state of understanding of acoustic-gravity-wave propagation is reviewed with a description of the two most prominent analyses: homogeneous wave-guide theory by which normal modes are calculated, and ray theory in which refractive-index concepts are used. Ray theory is extended to provide a cursory analysis of atmospheric oscillations and energy distributions throughout the atmosphere resulting from acoustic-gravity-wave sources.

The air-cell computer model of the atmosphere is described in detail and the results of the model are presented.

II. BACKGROUND FOR ACOUSTIC-GRAVITY-WAVE ANALYSIS

A. HISTORY OF EXPERIMENTAL INTEREST

First published reports of pressure waves traveling through the atmosphere relate to the Krakatoa volcanic eruption in 1883 [Refs. 4-6]. Long-period pressure disturbances were observed to circulate two or three times around the earth. Audible sounds were heard over distances of thousands of miles. It has been estimated by modern researchers [Ref. 7] that the Krakatoa eruption was equivalent to a modern nuclear explosion with the yield on the order of 50 MT of TNT. The Great Siberian Meteor of 1908 [Ref. 8] provided another dramatic source of long-period atmospheric oscillations recorded on barographs. Experimental observations of acoustic-gravity wave propagation in the atmosphere were infrequent until the age of high-yield nuclear explosions. In the last few decades a world-wide network of barographic and seismic stations [Refs. 7, 9] have been established recording atmospheric waves from both the American and Russian nuclear tests.

B. HISTORY OF THEORETICAL DEVELOPMENT

Theoretical analyses of atmospheric motions date back to Laplace with the publication of Traite de Mechanique Celeste [Ref. 10] at the end of the 18th Century. Laplace considered the problem of tidal motions in an ocean of shallow depth covering a rotating earth and extended his work to oscillations in an atmosphere of uniform temperature. Lamb [Ref. 11], in his first edition of Hydrodynamics, published in 1879, provided the basic equation for analyzing long waves (acoustic-gravity waves) in the atmosphere. And, beginning with the equations of motion, continuity, and state, he derived a set of equations used as a starting point by a majority of researchers on the subject today. The equations of motion, continuity, and adiabatic state are:

$$\rho_o \frac{\partial \vec{v}}{\partial t} + \nabla p + \rho_o \vec{g} = 0 \qquad (2.1)$$

$$\frac{D\rho}{Dt} + \rho_o \chi = 0 \qquad (2.2a)$$

$$\chi \equiv \nabla \cdot \vec{v} \qquad (2.2b)$$

$$\frac{Dp}{Dt} = c^2 \frac{D\rho}{Dt} \, . \qquad (2.3)$$

The Eulerian derivative is denoted by

$$\frac{D}{Dt} \equiv \frac{\partial}{\partial t} + \vec{v} \cdot \nabla \, . \qquad (2.4)$$

Pressure, density and velocity perturbations are indicated by p, ρ, and v, with "o"-subscript quantities denoting ambient values. The velocity of sound c is determined from $c^2 = \gamma p_o / \rho_o$, where γ is the ratio of specific heats. Lamb noted that ambient values of pressure and density varied greatly with altitude in the atmosphere, but the same quantities were well behaved in any horizontal direction, parallel to the earth's surface. Therefore solutions could be expanded in a conventional set of cylindrical harmonics in any horizontal plane as

$$\exp\,[i\omega t]\, J_o(\kappa r) \qquad \text{or} \qquad \exp\,[i\omega t]\, H_o^{(2)}(\kappa r) \qquad (2.5)$$

where r is the horizontal distance from the source. Other investigators [Ref. 1] have expanded solutions in rectangular harmonics where quantities vary as $\exp\,[j(\omega t \pm \vec{\kappa} \cdot \vec{x})]$. A rectangular coordinate system was used for the air-cell computer model with uniformity assumed in one horizontal direction, reducing the problem to two dimensions.

Inserting the cylindrical variations, Eq. (2.5), into Eqs. (2.1), (2.2), and (2.3) provides the following popular form:

$$c^2 \frac{d^2\chi}{dy^2} + \left(\frac{d}{dy} c^2 + \gamma g\right) \frac{d\chi}{dy}$$

$$+ \left\{\omega^2 - \kappa^2 c^2 - \frac{g^2\kappa^2}{\omega^2}\left[\frac{d}{dy} c^2 - (\gamma - 1)g\right]\right\}\chi = 0 \qquad (2.6)$$

$$(\omega^4 - g^2\kappa^2)v_y = -\omega^2 c^2 \frac{d\chi}{dy} - g(\gamma\omega^2 - \kappa^2 c^2)\chi = 0 \ , \qquad (2.7)$$

where y is the altitude coordinate and v_y is the velocity in this direction.

The difficulty now resides in solving these equations for quantities varying with altitude. Solutions to Lamb's equations above are provided by Pekeris [Refs. 12, 13], Press and Harkrider [Refs. 14, 15] and Pfeffer and Zarichny [Refs. 16-18] for different atmospheric models. The simplest models were considered by Pekeris in 1947, who assumed the atmosphere to have a constant temperature gradient up to a certain altitude, where in one case the atmosphere was terminated and in another a constant temperature was assumed for higher altitudes. Pekeris solved for phase and group velocities vs wave period in an effort to explain dispersive effects (group velocity decreasing with decreasing wave period) observed in barograms recorded in England during disturbances caused by the Great Siberian Meteor in 1908.

1. Mode Theory

With the advent of high-speed digital computers, more complicated, multilayered atmospheric models were considered by Pfeffer, and by Press and Harkrider. The techniques used by these or later investigators may be termed a "Mode Analysis," in contrast to a "Ray Theory" as defined by Tolstoy [Ref. 19]. The mode technique requires the atmosphere to be divided into a number of isothermal layers approximating the actual temperature profile. The equations of motion are solved in each layer subject to boundary conditions requiring continuity at each layer interface. The number of discrete isothermal layers used to simulate the atmosphere is

limited by computational parameters, but usually 20 to 40 layers were used up to a certain altitude, where various terminations were made.

Horizontal phase and group velocities corresponding to horizontal wave numbers and periods were calculated. Multivalued solutions of velocities for a given wave period lead to the definition of "modes." A source is imbedded in a particular layer in which boundary and initial conditions are matched. Synthetic barograms resulting from explosions have been computed with a great deal of success in this manner [Ref. 15]. Accuracy is limited only by the number of modes for which one is willing to spend computer time.

Solutions for atmospheric oscillations at any given point in the atmosphere are available by means of this analysis. A panoramic view of oscillations throughout the atmosphere is also obtainable, at least in principle, from mode theory, but would require an enormous amount of computer time.

2. Ray Analysis

Hines [Ref. 1] has used ray theory to study acoustic-gravity waves in the atmosphere. A two-dimensional rectangular coordinate system was used with y denoting altitude in the atmosphere and x denoting horizontal distance.

Assuming that pressure, density, and velocity vary as

$$\exp\left[i(\omega t - \kappa_x x - \kappa_y y)\right], \tag{2.8}$$

Hines derived dispersion relationships from which refractive-index surfaces could be calculated. Inserting the assumed Fourier variation, expression (2.8), into the equations of motion, continuity, and adiabatic state leads to the following equations for overpressure Δp, overdensity $\Delta\rho$, and perturbation velocities v_x and v_y.

$$\frac{\Delta p}{p_o R} = \frac{\Delta\rho}{\rho_o R} = \frac{v_x}{X} = \frac{v_y}{Y} = A \exp\left(\frac{\gamma g}{2c^2} y\right) \exp\left[i(\omega t - \kappa_x x - \kappa_y y)\right], \tag{2.9}$$

where:

$$P = \gamma\omega^2\left[\kappa_y - i\left(1 - \frac{\gamma}{2}\right)\frac{g}{c^2}\right] \tag{2.10}$$

$$R = \omega^2\kappa_y + i(\gamma - 1)g\kappa_x^2 - i\gamma g\frac{\omega^2}{2c^2} \tag{2.11}$$

$$X = \omega\kappa_y c^2\left[\kappa_y - i\left(1 - \frac{\gamma}{2}\right)\frac{g}{c^2}\right] \tag{2.12}$$

$$Y = \omega\kappa_x^2 c^2 \ . \tag{2.13}$$

The dispersion relationship is

$$\kappa_x^2\left[(\gamma - 1)g^2 - \omega^2c^2\right] - \kappa_y^2\omega^2c^2 + \left(\omega^4 - \gamma^2g^2\frac{\omega^2}{4c^2}\right) = 0 \tag{2.14}$$

$$n_x^2\left[\frac{g^2}{c^2}(\gamma - 1) - \omega^2\right] - n_y^2\omega^2 + \left(\omega^2 - \frac{\gamma^2g^2}{4c^2}\right) = 0 \ . \tag{2.15}$$

The refractive index n is defined by $\vec{n} = c\vec{\kappa}/\omega$, and the gravitational constant g and ratio of specific heats γ are very nearly constant and equal to: $g = 9.8$ m/sec^2, $\gamma = 1.5$. It should be emphasized that these waves have real propagation constants in both the horizontal and vertical directions, thus calling for Hines' definition of internal gravity waves, since they propagate within the entire fluid.

The dispersion equation above, defining refractive-index surfaces, can be examined for some interesting features. For frequencies such that $\omega^2 > \gamma^2g^2/4c^2$, the refractive-index surfaces are elliptical; for higher frequencies the surfaces degenerate into circles, indicating little or no spatial dispersion. The waves corresponding to these frequencies are

acoustic waves and may be analyzed approximately by ignoring the effects of gravity. The frequency for which $\omega^2 = \gamma^2 g^2/4c^2$ represents a cutoff for the acoustic mode, and at ground level corresponds to a period of about 5 min (300 sec). For frequencies such that $\omega^2 < (g^2/c^2)(\gamma - 1)$, the refractive-index surfaces are hyperbolic opening on the horizontal axis. The waves corresponding to these frequencies are termed acoustic-gravity waves and the frequency $\omega^2 = (g^2/c^2)(\gamma - 1)$ is a resonance of the atmosphere called the Väisälä frequency [Ref. 1]. Waves of this type have also been termed thermobaric waves, since the wave motion involves thermodynamic and gravitational quantities [Ref. 20].

A difficulty may be seen in the fact that the sound velocity c is a rapidly varying function of altitude causing these refractive-index surfaces also to vary rapidly with altitude. It should be recalled that a vector drawn from the origin to this surface has the same direction as the phase velocity of the wave, and a vector drawn normal to the surface at this point has the sense of energy or group velocity. The progress of these vectors defines phase-front and energy raypaths throughout the atmosphere. Since the refractive-index surfaces for acoustic-gravity waves are hyperbolic, it is not possible to draw a normal to this surface that is also pointing vertically, verifying the idea that, below the "atmospheric cutoff," waves may not propagate vertically. Further, a maximum-energy takeoff angle at a specific wave period is defined by the normal to the corresponding hyperbola asymptote. For increasing wave periods this angle decreases to zero, indicating that very low-frequency disturbances will be confined to the horizontal direction

Consider the refractive-index surface for a constant wave period at different altitudes in the atmosphere. Since the sound velocity generally decreases with increasing altitude (at least above a certain altitude), a particular wave period will correspond to a family of hyperbolic refractive surfaces closing on the horizontal axis with increasing altitude. The altitude at which the vertical wave number vanishes defines the reflection height. A plot of the maximum-energy takeoff angle and reflection height plotted vs wave period calculated from the arguments above is presented in Fig. 3.

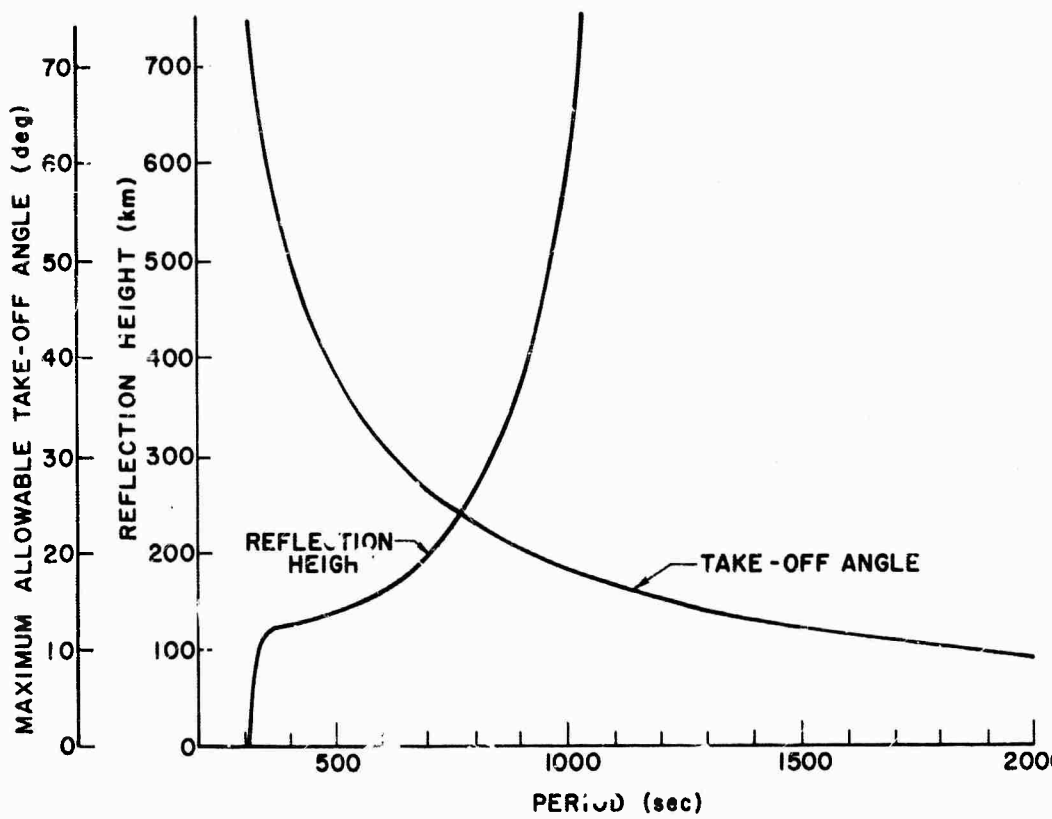

34355

FIG. 3. MAXIMUM TAKEOFF ANGLE AND REFLECTION HEIGHT VS ACOUSTIC-GRAVITY-WAVE PERIOD.

Below a certain cutoff frequency, wave propagation in the atmosphere appears to cease in the vertical direction and to be confined more and more to the horizontal direction. This analysis is pursued in greater detail by Hines, who calculated the spectrum of wave periods expected at various ionospheric heights limited by viscosity and reflections.

The necessary criteria and limitations for the application of ray theory have been defined by Tolstoy [Ref. 19]. The concepts involved in ray theory are valid only when the propagation medium is "slowly varying" within the space of one wavelength. This criterion is violated for the study of acoustic-gravity waves because atmospheric parameters change several orders of magnitude within a single wavelength. Conclusions obtained from ray theory concerning the propagation of acoustic-gravity waves in the atmosphere are therefore questionable.

C. HISTORY OF WAVE ANALYSIS WITH MECHANICAL LATTICES

Newton observed that the sound heard at a distance from a cannon lagged the visible flash by a few fractions of a second. To analyze the propagation of the sound pulse through the atmosphere, he conceived of a mechanical analogy consisting of particles and springs. The mass of the individual particles was to represent air density and the springs provided a linear representation of the pressure forces. Newton calculated the velocity of propagation along this array to be $d(k/m)^{1/2}$. Newton's formula for the speed of sound c was therefore proportional to $(p/\rho)^{1/2}$, where p and ρ are atmospheric pressure and density. This analogy was nearly correct, except that, as pointed out by Laplace in 1822, Newton's calculations of the spring constants were in error, since they implied an isothermal expansion of air while in reality, for sound propagation, adiabatic expansions must be considered. The corrected expression for the sound velocity included the ratio of specific heats γ. Therefore sound speed equals $(\gamma p/\rho)^{1/2}$. The concept of the mechanical analogy for analyzing wave propagation in a fluid emerged as the major contribution to knowledge. Descriptions of a continuous fluid represented an insurmountable problem at that time and the concept of partial differential equations had not yet been introduced.

Wave propagation in a mechanical system was considered in the 18th Century by Taylor in his famous analysis and, in the 19th Century, Cauchy used Newton's model to study dispersion of optical waves. In analyzing Newton's model of masses and springs, Lord Kelvin discovered the concept of "cutoff frequency" where disturbances with sufficiently low frequencies refused to propagate. His work was extended to consider ideas about frequency "stop" and "pass" bands, thereby developing mechanical filters. In 1898 Vincent actually constructed a model consisting of pendulums and springs that became the first practical mechanical filter. The first electrical filter was constructed in 1906. In this century Born extended Kelvin's analysis to study wave propagation in crystal lattices, but the later work of Brillouin [Ref. 21] represents the most complete treatise on wave propagation throughout multidimensional lattices.

Chapter III describes how the earth's atmosphere was modeled with a two-dimensional mechanical lattice. The actual construction of such an array with balls and springs, such as was done by Vincent, appeared to be impractical because of the tremendous range of values of masses and spring constants required. Construction of a two-dimensional physical model introduces further problems. Waves propagate in a rectangular array of balls and springs only parallel to the two axes. If diagonal-coupling springs are added as shown in Fig. 2, the model more properly represents an elastic solid since a shear elasticity has been introduced. While a more complex mechanical model (involving pulleys or linkages) might be devised to approximate a fluid more accurately, digital computer simulation of the simpler mechanical model appeared most practical.

D. COMPUTER MODELS OF FLUIDS

Since the computer sciences are comparatively new, specialized uses such as solving fluid-dynamical problems by a digital computer are in the infant stages of development. Recent computer experiments describing incompressible-fluid flow have been reported by Harlow and Fromm [Ref. 22]. The computer techniques were developed by Kolsky [Ref. 23] and Evans and Harlow [Ref. 24] who divided a two-dimensional field into a network of fixed cells through which the fluid (represented by fixed-mass particles) flowed. The coordinates of these particles are calculated as a function of time providing a Lagrangian coordinate system superimposed upon an Eulerian one. Results of this model compared quite well with values obtained from actual fluid-flow experiments.

III. AIR-CELL COMPUTER MODEL OF THE ATMOSPHERE

A. INTRODUCTION

The purpose of this chapter is to describe a two-dimensional mechanical lattice that models the atmospheric fluid and to find a solution to the hydrodynamic equations describing the atmosphere to provide a panoramic view of oscillations resulting from various input conditions.

The fluid equations are rewritten into a form describing discrete "cells of air," rather than a fluid continuum. The resulting "air-cell" equations are equivalent (for irrotational sources of energy) to equations describing a mechanical system consisting of particles and springs. The mechanical lattice is attractive because boundary and initial conditions are greatly simplified and because of the heuristic value of describing wave propagation in a fluid with a system of particles and springs. The limitations and advantages of the air-cell model are discussed in detail in the following sections.

Finite-difference equations describing wave propagation in the air-cell model are solved by a digital computer that produces values for overpressures, density fluctuations, and air-particle orbits throughout the atmosphere resulting from a variety of input conditions. Sinusoidal-filament sources are considered first to calculate the steady-state distribution of energy throughout the atmosphere. Ground-level and 100-km-high sources were programmed into the computer model. Ground-level and 100-km-high pulse-input-simulating explosions were programmed to study the transient behavior of the atmosphere. Transient motions resulting from these explosive sources were studied by means of a digitally produced motion picture.

1. Plan of Solution

Assuming small perturbational values of pressures, densities, and particle velocities, I have used a linear analysis to solve the hydrodynamic equations for the atmosphere so that second- and higher-order effects are ignored. A rectangular coordinate system is used on a flat earth where altitude in the atmosphere is designated by y and horizontal distances parallel to the surface of the earth are denoted by x

and z. The problem is reduced to two dimensions by requiring all variables to be independent of the z coordinate. Energy inputs are thereby restricted to be line, rather than point sources, resulting in cylindrical wavefronts extending infinitely in the z direction, as shown in Fig. 4. The two-dimensional atmosphere (i.e., the x-y plane) is divided into cells with equal height and width and unit depth as shown in Fig. 5a. The location of the center of each cell is specified by the time varying coordinates $\bar{x}(i,j,t)$ and $\bar{y}(i,j,t)$, where i and j specify the row and column. The position and velocity of all air molecules contained within a cell (per unit depth) are approximately given by $\bar{x}(i,j,t)$, $\bar{y}(i,j,t)$ and $(d/dt)\bar{x}(i,j,t)$, $(d/dt)\bar{y}(i,j,t)$. The number of molecules within each cell, and therefore the total mass of each cell, are fixed, while changes in dimensions of the cell represent density and pressure perturbations. The walls of any cell may move in both horizontal and

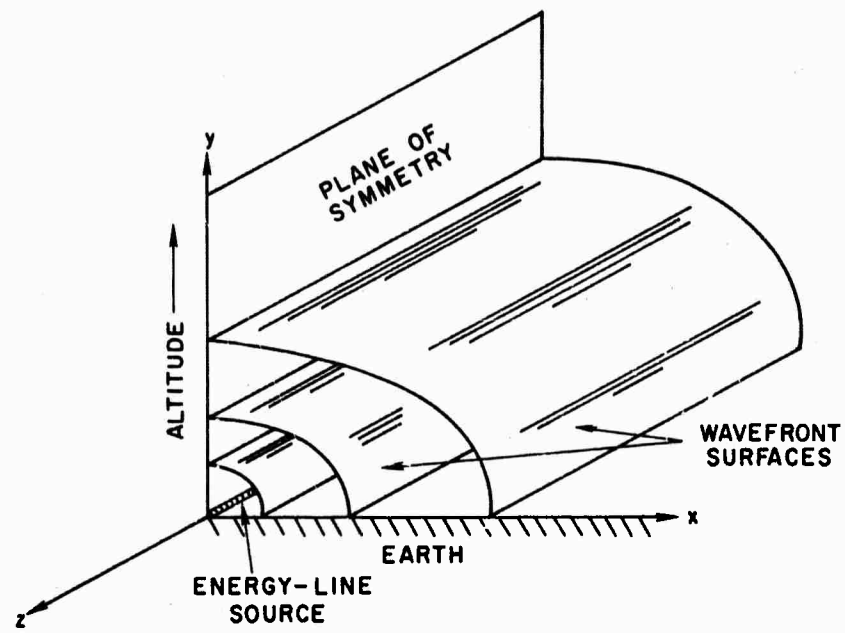

35388

FIG. 4. COORDINATE SYSTEM OF THE AIR-CELL MODEL.

vertical directions and are located approximately halfway between cell midpoints. Cell overlap, as shown in Fig. 5b, is a second-order effect and is ignored, preserving continuity. The magnitude and direction of gravity are taken to be constant.

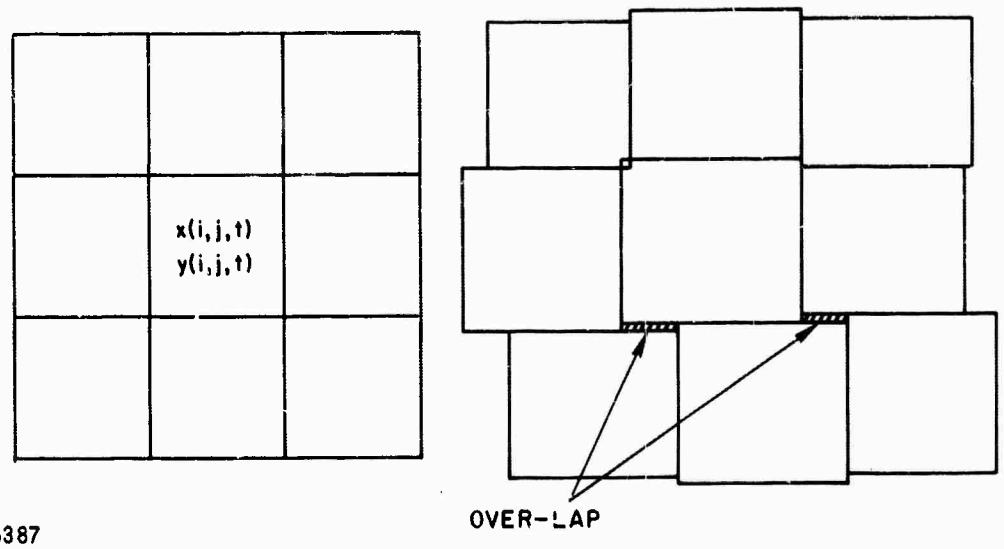

a. Stationary positions of cells

b. Perturbed positions of cells

FIG. 5. CELL-OVERLAP EFFECT.

2. Hydrodynamic Equations

The hydrodynamic equations describing oscillations in the atmosphere are:

$$(\rho_o + \delta\rho)\frac{\partial \vec{v}}{\partial t} + \nabla(p_o + \delta p) - (\rho_o + \delta\rho)\vec{g} = 0 \qquad (3.1)$$

$$\frac{d(p_o + \delta p)}{d(\rho_o + \delta\rho)} = c^2 \qquad (3.2)$$

$$\frac{\partial}{\partial t}(\rho_o + \delta\rho) + \nabla \cdot (\rho_o + \delta\rho)\vec{v} = 0 \ . \qquad (3.3)$$

These are equations of motion, adiabatic state, and continuity for the atmospheric fluid where ρ_o and p_o are the ambient density and pressure, $\delta\rho$, δp, and $\vec{v}$ are the perturbational density, pressure, and velocity, and c is the velocity of sound. As stated previously, a small-signal analysis will be used, so that it is assumed that $\rho_o \gg \delta\rho$ and $p_o \gg \delta p$.

The stationary condition of the atmosphere is obtained, from Eq. (3.1), by

$$\nabla p_o - \rho_o \vec{g} = 0 \ . \tag{3.4}$$

For an adiabatic process $p = \rho^{\gamma}$, and the speed of sound c is given, by Eq. (3.3), as

$$c^2 = \gamma \frac{p_o}{\rho_o} \ , \tag{3.5}$$

where γ is the ratio of specific heats. Under the conditions that the speed of sound c is a slowly varying function of altitude, Eqs. (3.4) and (3.5) are combined and integrated, giving

$$p_o \propto \rho_o \propto \exp\,[-y/H] \tag{3.6}$$

where $H \equiv c^2/\gamma g$. The quantity H is defined as the scale height of the atmosphere.

The continuity Eq. (3.3) is satisfied by the definition of the cell structure ignoring cell overlap, as previously mentioned.

The equations of motion (3.1) and adiabatic state (3.2) are rewritten, removing stationary terms, as

$$\rho_o \frac{\partial \vec{v}}{\partial t} + \nabla(\delta p) - \delta\rho\vec{g} = 0 \tag{3.7}$$

and

$$\nabla(\delta p) = c^2 \nabla(\delta\rho) \tag{3.8}$$

and combined to give

$$\frac{\partial \vec{v}}{\partial t} + \frac{c^2}{\rho_o} \nabla(\delta\rho) - \frac{\delta\rho}{\rho_o} \vec{g} = 0 \ . \tag{3.9}$$

3. Density Gradient

Equation (3.9) is solved by a finite-difference technique whereby the density gradient is approximated in the following manner. The horizontal density gradient evaluated at the center of the $(i,j)^{th}$ cell is approximated by

$$\frac{d}{dx}(\delta\rho) \approx \frac{\delta\rho(i,j+1,t) - \delta\rho(i,j-1,t)}{d_o} \tag{3.10}$$

(refer to Fig. 5a).

The vertical density gradient, evaluated at the same point, is

$$\frac{d}{dy}(\delta\rho) \approx \frac{\delta\rho(i+1,j,t) - \delta\rho(i-1,j,t)}{d_o} \ . \tag{3.11}$$

Since the density and pressure within any given air cell are determined by the width and height of that air cell, the density gradients above depend on the time-varying positions of the four sides of each of the four neighboring cells: the $(i+1,j)$, $(i-1,j)$, $(i,j+1)$, and the $(i,j-1)$ air cells (Fig. 6).

The physical significance of the preceding evaluation of the density (or pressure) gradient may be exemplified by imagining an array of "elastic bags" filled with air, as shown in Fig. 7a. A horizontal force will be exerted on the middle bag by the neighboring two bags if

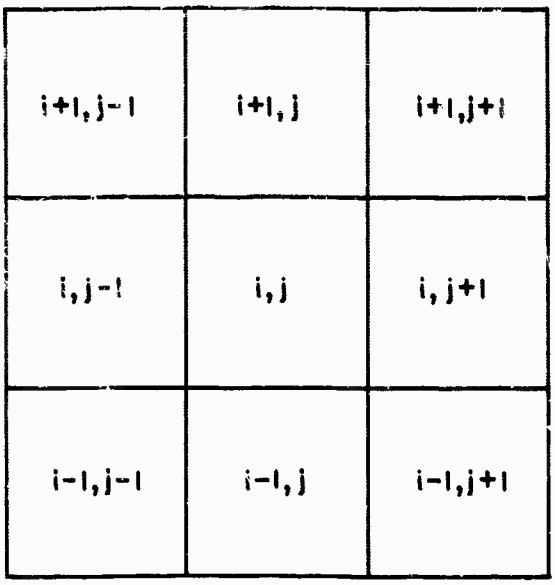

FIG. 6. INDEXING OF AIR CELLS.

the center of either of these two bags is moved in a horizontal direction and the walls between the bags are moved, as shown in Fig. 7b.

It is also possible to exert a force on the center bag by pushing on the top or bottom of either of the neighboring two bags, even with the centers of these bags remaining fixed, as in Fig. 7c.

In summary, a horizontal force is exerted on the middle bag by either a horizontal displacement of the center of a neighboring bag or a change in the position of the top or bottom boundary of a neighboring bag.

4. Mechanical-Lattice Analogy

The purpose of this section is to describe briefly a two-dimensional lattice consisting of particles and springs that may be used to model the atmosphere. The mass contained within a given air cell is represented by a single particle located at the center of that cell; pressure forces are represented by springs connected between particles.

A first guess at a two-dimensional lattice to represent a fluid is shown in Fig. 8, in which the boundaries of the air cells are represented by the dotted lines. A horizontal displacement of the $(i,j-1)^{th}$

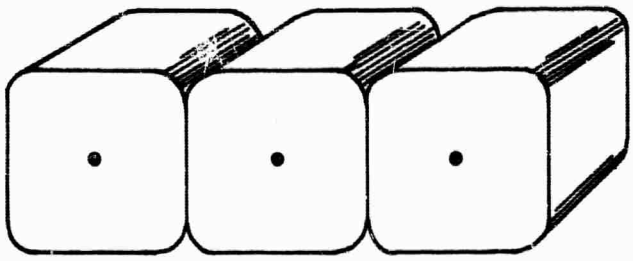

a. Initial array

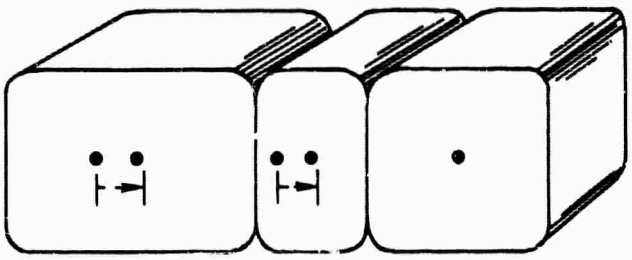

b. Horizontal displacement of a neighboring bag

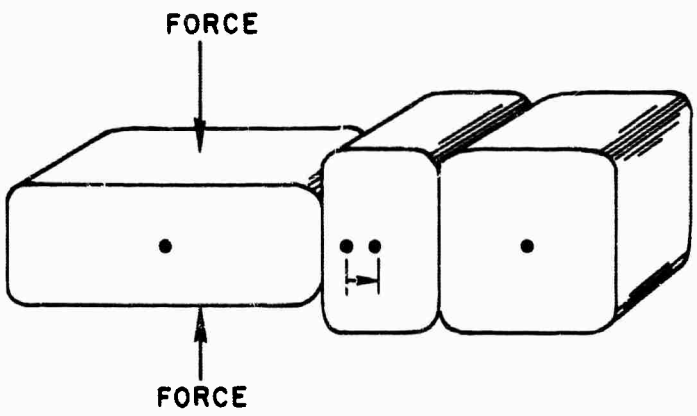

35385

c. Depression of a neighboring bag

FIG. 7. ELASTIC-BAG ANALOGY.

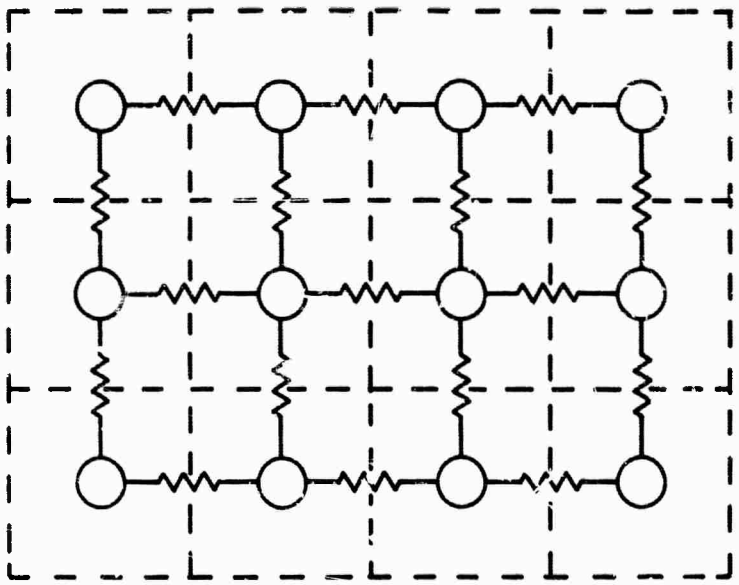

35389

FIG. 8. FIRST APPROXIMATION TO A TWO-DIMENSIONAL LATTICE.

particle (as in Fig. 6) will exert a horizontal force on the neighboring $(i,j)^{th}$ particle. This is analogous to a horizontal displacement of the wall between the $(i,j-1)^{th}$ and $(i,j)^{th}$ air cells, causing a pressure force that tends to displace the $(i,j)^{th}$ cell. The mechanical-lattice analogy, however, fails to represent a horizontal force on the $(i,j)^{th}$ cell when the top or bottom of the $(i,j-1)^{th}$ cell is moved.

This problem may be better visualized by picturing the mechanical equivalent of a single air cell as in Fig. 9. The two "boxes" are equivalent since vertical or horizontal forces on the top, bottom, or sides of each box will be balanced by the same restoring forces (Figs. 9a and 9b). The inertia of the mechanical air cell is provided by the mass in the center of the box. A diagonal force on the mechanical cell, however, as in Fig. 9c, will nearly collapse the box, assuming the springs to have only a compressional modulus.

As a second estimate to include this force, a set of diagonal springs might be included, as was shown in Fig. 2. Now a vertical displacement of the $(i+1,j-1)^{th}$ particle, representing a push on the top of the $(i,j-1)^{th}$ air cell, will cause a horizontal force on the $(i,j)^{th}$ particle as wanted. But a horizontal displacement of the $(i+1,j-1)^{th}$

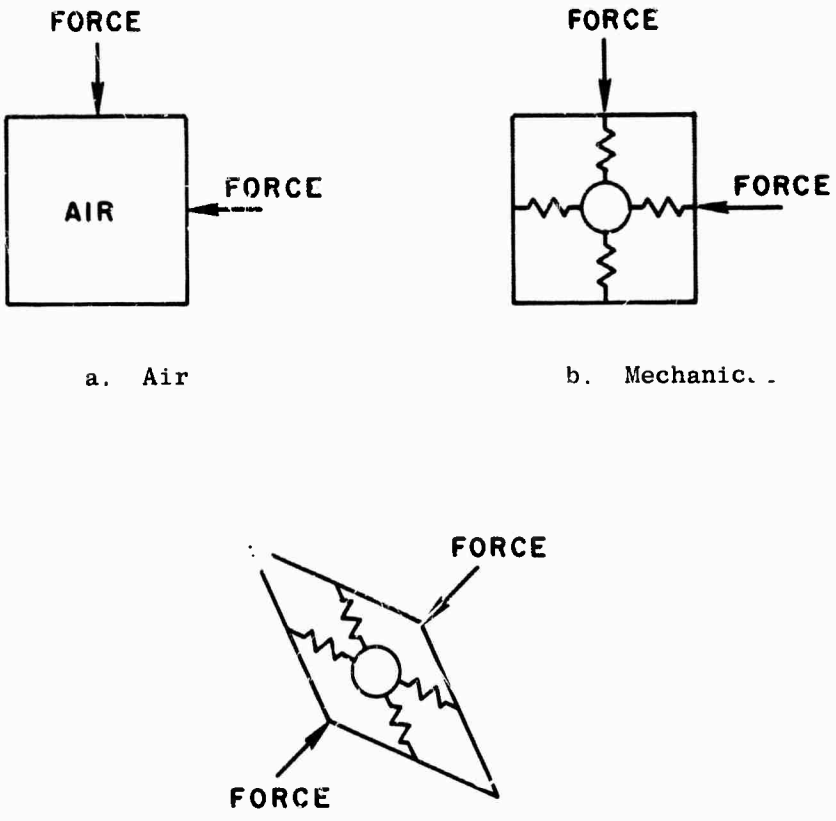

a. Air

b. Mechanical

c. Diagonal instability of mechanical air cell

FIG. 9. REPRESENTATION OF MECHANICAL AIR CELL.

particle will also exert a horizontal force on the $(i,j)^{th}$ particle, representing a shear force that does not exist in an inviscid fluid. This represents a limitation of the air-cell model unless energy sources are imitated in the mechanical lattice in such a way as to prevent excitation of shear modes. Isotropic-filament sources, which cannot excite shear waves (at least in a uniform fluid), were the only type of source configuration considered in this analysis of a nonuniform fluid. Results of the air-cell model were checked with geometric acoustic-ray theory [Ref. 25]. The lattice of particles and springs pictured in Fig. 2 was found to imitate realistically the behavior of the atmosphere.

A rigorous derivation of the density gradients and a solution to Eq. (3.9) by finite-difference techniques are contained in the following sections. These finite-difference equations strengthen the analogy with the mechanical lattice of particles and springs. The preceding discussion was intended to provide physical insight into the processes involved in wave propagation in a fluid by examining various analogies and to describe the air-cell computer model used to solve the hydrodynamic equations governing atmospheric motions.

B. SOLUTION OF THE HYDRODYNAMIC EQUATIONS

The purpose of this section is to derive rigorously the finite-difference equations that were solved by a digital computer to provide solutions to the hydrodynamic equations describing the atmosphere. Equation (3.9) is solved by this technique, providing solutions in terms of the coordinates of particles representing the center of each air cell. Newton's one-dimensional mechanical analog is reviewed, first to illustrate the finite-difference technique that is used and also to establish mathematically the analogy between a fluid and a mechanical lattice. This one-dimensional solution is extended to represent a vertical column of air in the atmosphere by taking into account the ambient vertical variation of pressure and density with altitude. Finally, the finite-difference equations for a two-dimensional atmosphere are derived and an analogy to a two-dimensional mechanical array of particles and springs is established.

1. Uniform One-Dimensional Lattice

Newton used a mechanical lattice consisting of equal masses spaced equally along the direction of propagation to derive an equation for the speed of sound in the atmosphere (Fig. 10a). The equilibrium spacing between particles is d_o, the mass of each particle is m, and the spring modulus is k for each spring. To calculate the speed of propagation s of a mechanical wave along this lattice, consider the first particle to be slowly displaced to the right with a velocity v. After

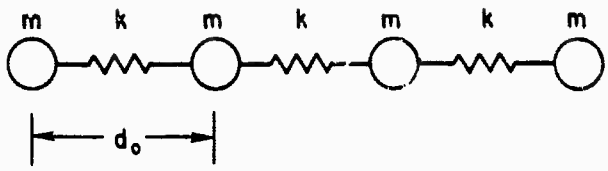

a. Initial array

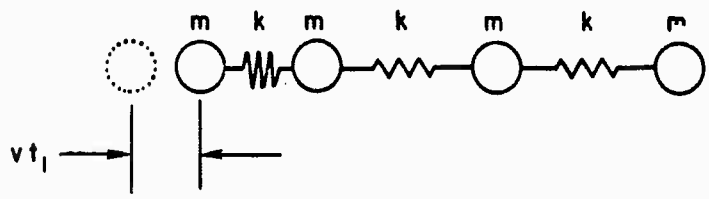

35375

b. Displacement of first particle

FIG. 10. NEWTON'S ONE-DIMENSIONAL LATTICE.

a time t_1 has elapsed, the neighboring particle will have the same motion as the first particle, where t_1 is given by

$$t_1 = d_o/s \ . \tag{3.12}$$

At time t_1 the first ball has moved a distance equal to vt_1, as shown in Fig. 10b. The tension in the spring connecting the first and second particles is: Tension = kvt_1. The momentum of the first ball is: Momentum = mv. And the inertial force of the first ball at time t_1 is approximately

$$f = \frac{d}{dt} \text{ (momentum)} = \frac{mv}{t_1} \ . \tag{3.13}$$

The inertial force must balance the restoring force;

$$\frac{mv}{t_1} = kvt_1 \ . \tag{3.14}$$

The velocity of propagation s is found by substituting Eq. (3.12) into Eq. (3.14), yielding

$$s = d_o(k/m)^{1/2} \quad . \tag{3.15}$$

The equations of motion describing mechanical wave propagation along this lattice are derived by equating the restoring forces acting on each particle to the inertial force of that particle. The time-varying coordinate of the j^{th} particle is specified by $\bar{x}(j,t)$, as shown in Fig. 11a, where

$$\bar{x}(j,t) = x_o(j) + x(j,t) \quad . \tag{3.16}$$

The stationary position of the j^{th} particle is $x_o(j)$, and $x(j,t)$ is the time-varying displacement from this equilibrium position. Then

$$x_o(j+1) - x_o(j) = x_o(j) - x_o(j-1) = d_o \quad . \tag{3.17}$$

The force tending to move the j^{th} particle from its equilibrium position as a result of a displacement of the neighboring $(j-1)^{th}$ particle is

$$f(j-1) = k[x(j-1,t) - x(j,t)] \quad . \tag{3.18}$$

The force tending to move the j^{th} particle as a result of a displacement of the neighboring $(j+1)^{th}$ particle is

$$f(j+1) = k[x(j+1,t) - x(j,t)] \quad . \tag{3.19}$$

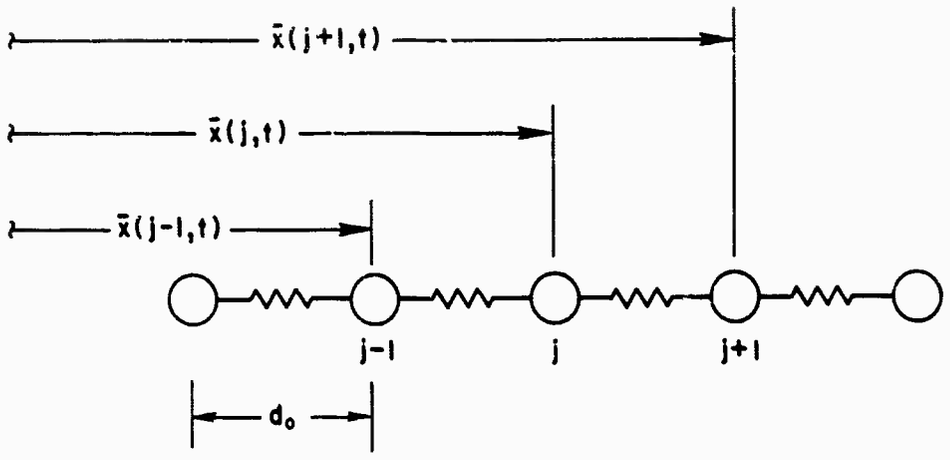

a. Mechanical lattice

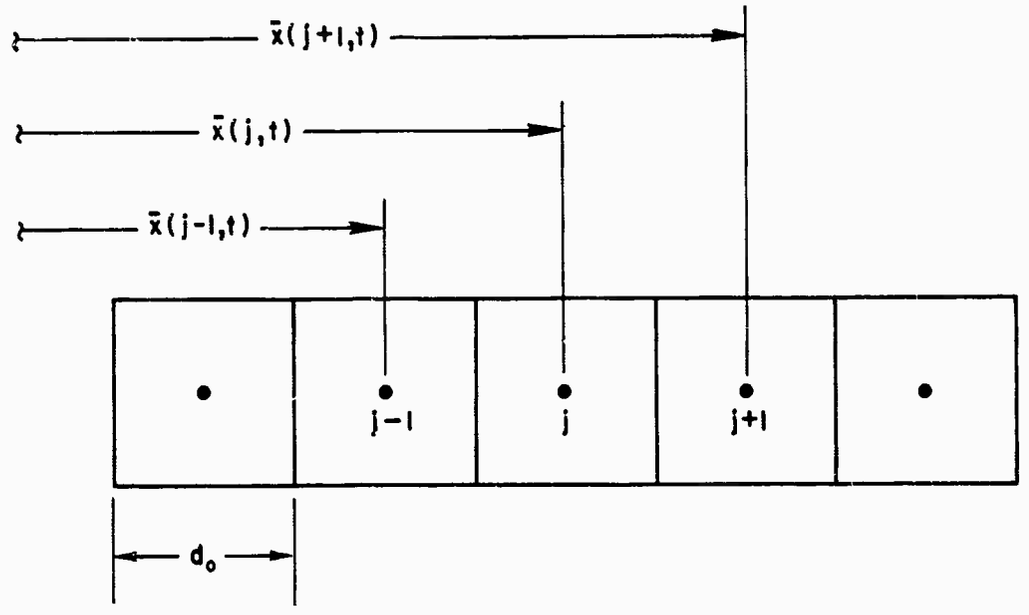

35392 b. Air-cell array

FIG. 11. COORDINATES FOR ONE-DIMENSIONAL ARRAY.

The sum of these two forces must be balanced by the inertia of the j^{th} particle,

$$m \frac{d^2}{dt^2} x(j,t) = k[x(j+1,t) + x(j-1,t) - 2x(j,t)] . \qquad (3.20)$$

If $(d^2/dt^2)x(j,t)$ is written as $(d/dt)v_x(j,t)$, Eq. (3.20) becomes

$$\frac{d}{dt} v_x(j,t) = \frac{k}{m} [x(j+1,t) + x(j-1,t) - 2x(j,t)] . \qquad (3.21)$$

Equation (3.21) is the equation of motion for mechanical wave motion in a uniform one-dimensional lattice and also describes wave propagation in a fluid, as shown below.

Fluid equation (3.9) will be solved in one dimension for a uniform atmosphere,

$$\frac{d}{dt} v_x + \frac{c^2}{\rho_o} \frac{d}{dx} (\delta\rho) = 0 .$$

Consider a linear array of air cells instead of particles, where now the coordinate $\bar{x}(j,t)$ locates the center of the j^{th} air cell as shown in Fig. 11b. The dimensions of the j^{th} air cell are:

$$\text{width} = d_o + \delta x(j,t)$$

$$\text{height} = d_o$$

$$\text{depth} = d_o ,$$

where $\delta x(j,t)$ is the time-varying horizontal stretch of the j^{th} cell.

The density of air in the j^{th} air cell is given by

$$\rho_o + \delta\rho(j,t) = \frac{m_o}{(d_o + \delta x) d_o^2} . \qquad (3.22)$$

A normalized density perturbation is derived from Eq. (3.22); assuming $\delta x \ll d_o$, as

$$\frac{\delta\rho(j,t)}{\rho_o} = - \frac{\delta x(j,t)}{d_o} \quad . \tag{3.23}$$

The density gradient is evaluated at the j^{th} cell by

$$\frac{d}{dx} (\delta\rho)\Big|_j \approx \frac{\delta\rho(j+1,t) - \delta\rho(j-1,t)}{d_o} \tag{3.24}$$

Substituting Eq. (3.23) into (3.24) gives

$$\frac{d}{dx} \frac{\delta\rho}{\rho_o}\Big|_j \approx - \frac{\delta x(j+1,t) - \delta x(j-1,t)}{d_o^2} \quad . \tag{3.25}$$

Substituting Eq. (3.25) into fluid equation (3.9) gives;

$$\frac{d}{dt} v_x(j,t) = \frac{c^2}{d_o^2} [\delta x(j+1,t) - \delta x(j-1,t)] \quad . \tag{3.26}$$

The stretch of each cell δx must be related to the air-cell coordinate $\bar{x}$ in order to solve Eq. (3.26). It will be assumed that the walls of each cell are located approximately halfway between cell midpoints. However, as seen from Fig. 12, this assumption leads to an inconsistency because the "air-cell center" is no longer at the center of the air cell! For the small signal analysis assumed, however, this discrepancy between the actual cell center and the defined center will be small and should not affect the ultimate solution of the hydrodynamic equations as long as the finite difference equations are consistent. This assumption is at least reasonable for the neighboring $(j+1)^{th}$ and $(j-1)^{th}$ cells when evaluating the force exerted on the j^{th} cell. The stretches of these neighboring cells, as defined in Fig. 13, are:

$$\delta x(j-1,t) + d_o = 2\left[\frac{\bar{x}(j,t) - \bar{x}(j-1,t)}{2}\right] = x(j,t) - x(j-1,t) + d_o$$

$$\delta x(j+1,t) + d_o = 2\left[\frac{\bar{x}(j+1,t) - \bar{x}(j,t)}{2}\right] = x(j+1,t) - x(j,t) + d_o$$

$$\delta x(j-1,t) = x(j,t) - x(j-1,t) \qquad (3.27)$$

$$\delta x(j+1,t) = x(j+1,t) - x(j,t) \; . \qquad (3.28)$$

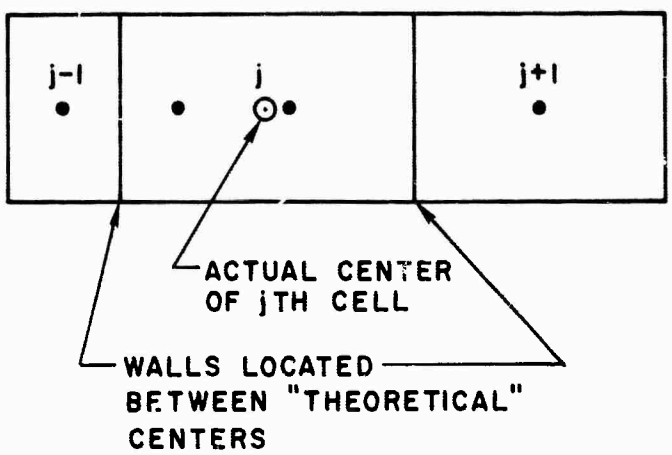

FIG. 12. PARADOX OF AIR-CELL CENTER.

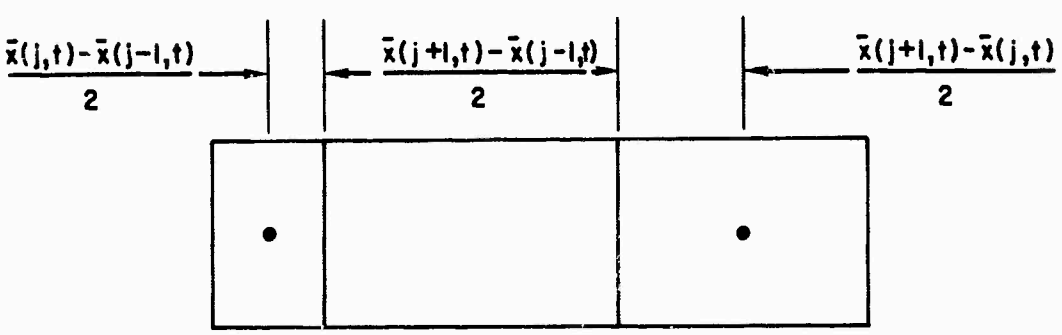

35390

FIG. 13. DIMENSIONS OF AN AIR CELL.

Inserting Eqs. (3.27) and (3.28) into (3.26) gives

$$\frac{d}{dt} v_x(j,t) = \frac{c^2}{d_o^2} [x(j+1,t) + x(j-1,t) - 2x(j,t)] , \qquad (3.29)$$

where $(d/dt)x(j,t) = v_x(j,t)$.

The finite-difference equation, (3.29), is solvable for the motion of the center of the j^{th} air cell with the time derivative $(d/dt)v_x$ approximated by $(\Delta/\Delta t)v_x$.

A comparison of Eq. (3.29) with (3.21) verifies the analogy between the fluid approximated by discrete air cells and the mechanical lattice, provided that

$$\frac{c^2}{d_o^2} = \frac{k}{m} ,$$

which agrees with Newton's formula, Eq. (3.15). The one-dimensional air-cell model of a fluid represents a finite-difference approximation to the hydrodynamic equations and is equivalent to a one-dimensional mechanical lattice consisting of particles connected by springs.

2. Tapered One-Dimensional Lattice

The one-dimensional mechanical lattice may be used to represent a vertical column of air in the atmosphere by varying masses and springs with distance along the lattice to imitate the real variation of density and pressure with altitude. The starting point is again Eq. (3.9);

$$\frac{d}{dt} v_y + \frac{c^2}{\rho_o} \frac{d}{dy} (\delta\rho) + \frac{\delta\rho}{\rho_o} = 0 . \qquad (3.30)$$

The coordinate y and the index i denote altitude. Density ρ_o and sound velocity c are functions of y or i. The model now consists of a vertical column of air cells with the center of the i^{th}

cell denoted by the coordinate $\bar{y}(i,t)$ as shown in Fig. 14. As before, $\bar{y}(i,t) = y_o(i) + \delta y(i,t)$ and $y_o(i+1) - y_o(i) = d_o$, where $y_o(i)$ is the stationary location of the i^{th} cell and $y(i,t)$ is the time-varying perturbation from this value.

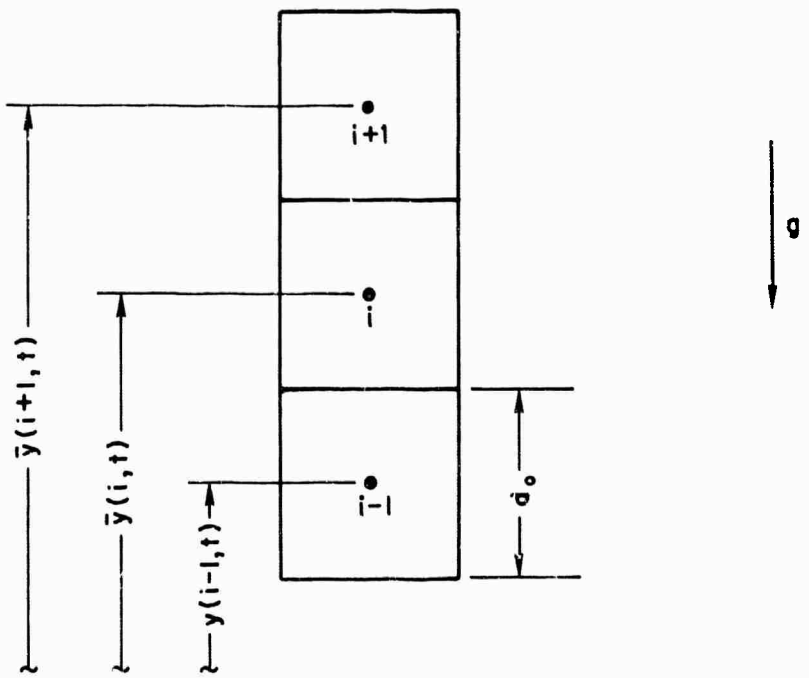

35376

FIG. 14. COORDINATES FOR ONE-DIMENSIONAL VERTICAL AIR-CELL ARRAY.

The dimensions of the i^{th} cell are:

$$\text{height} = d_o + \delta y(i,t)$$

$$\text{width} = d_o$$

$$\text{depth} = d_o \ ,$$

where $\delta y(i,t)$ is the time-varying vertical stretch of the i^{th} cell.

The normalized density perturbation is

$$\frac{\delta\rho(i,t)}{\rho_o(i)} = - \frac{\delta y(i,t)}{d_o} \ . \qquad (3.31)$$

The density gradient at the i^{th} cell is approximated by

$$\frac{d}{dy}(\delta\rho)\Big|_i = \frac{\delta\rho(i+1,t) - \delta\rho(i-1,t)}{d_o} . \qquad (3.32)$$

Substituting Eq. (3.31) into (3.32) gives:

$$\frac{d}{dy}(\delta\rho) = -\frac{1}{d_o^2}\left[\rho_o(i+1)\,\delta y(i+1,t) - \rho_o(i-1)\,\delta y(i-1,t)\right] . \qquad (3.33)$$

The stretches of the $(i+1)^{th}$ and $(i-1)^{th}$ cells are approximated by expressions similar to the uniform case:

$$\delta y(i+1,t) \approx y(i+1,t) - y(i,t) \qquad (3.34)$$

$$\delta y(i-1,t) \approx y(i,t) - y(i-1,t) . \qquad (3.35)$$

The stretch of the i^{th} cell is given by

$$\delta y(i,t) \approx y(i,t) - y(i-1,t) \approx y(i+1,t) - y(i,t) \approx \frac{y(i+1,t) - y(i-1,t)}{2} . \qquad (3.36)$$

Inserting Eqs. (3.34) and (3.35) into Eq. (3.33) and combining with Eq. (3.36) to solve Eq. (3.30) gives

$$\frac{d}{dt}v_y(i,t) - \frac{c^2(i)}{d_o^2}\left\{\left[\frac{\rho_o(i+1)}{\rho_o(i)} + \frac{d_o g}{2c^2(i)}\right] y(i+1,t) + \left[\frac{\rho_o(i-1)}{\rho_o(i)} - \frac{d_o g}{2c^2(i)}\right] y(i-1,t) - \frac{\rho_o(i+1) + \rho_o(i-1)}{\rho_o(i)}\, y(i,t)\right\} = 0 . \qquad (3.37)$$

Equation (3.37) is the finite-difference approximation to the hydrodynamic equation, (3.30), describing motion in a vertical column of

air in the atmosphere. It will be shown in the following that Eq. (3.37) also describes wave motion in a mechanical lattice of nonuniform particles and springs.

Consider the lattice of nonuniform particles and springs pictured in Fig. 15. If, as done for the uniform lattice in the previous section, the restoring forces acting on the i^{th} particle are equated to the inertial force of that particle, the following equation of motion is derived:

$$\frac{d}{dt} v_y(i,t) = \frac{k'(i)}{m(i)} y(i+1,t) + \frac{k''(i)}{m(i)} y(i-1,t) - \frac{k'(i) + k''(i)}{m(i)} y(i,t)$$

$$= 0 \ . \qquad (3.38)$$

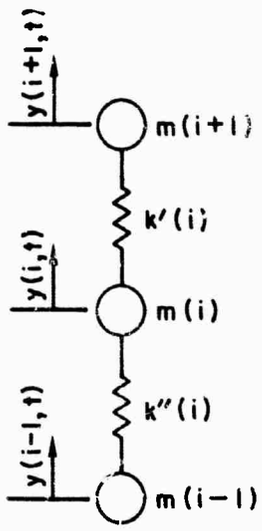

FIG. 15. ONE-DIMENSIONAL VERTICAL ARRAY.

The hydrodynamic equation, (3.37), and mechanical-lattice equation, (3.38), are equal if the spring constants are defined as follows:

$$\frac{k'(i)}{m(i)} = \frac{c^2(i)}{d_o^2}\left[\frac{\rho_o(i+1)}{\rho_o(i)} + \frac{d_o g}{2c^2(i)}\right] = \frac{c^2(i)}{d_o^2}\left[\frac{\rho_o(i+1)}{\rho_o(i)} + \frac{d_o}{2H\gamma}\right] \qquad (3.39)$$

$$\frac{k''(i)}{m(i)} = \frac{c^2(i)}{d_o^2}\left[\frac{\rho_o(i-1)}{\rho_o(i)} - \frac{d_o g}{\gamma c^2(i)}\right] = \frac{c^2(i)}{d_o^2}\left[\frac{\rho_o(i-1)}{\rho_o(i)} - \frac{d_o}{2H\gamma}\right] \qquad (3.40)$$

and it is noted that

$$\frac{k'(i) + k''(i)}{m(i)} = \frac{c^2(i)}{d_o^2}\left[\frac{\rho_o(i+1) + \rho_o(i-1)}{\rho_o(i)}\right] \approx 2\,\frac{c^2(i)}{d_o^2} \; . \qquad (3.41)$$

Therefore a vertical one-dimensional segment of air in the atmosphere is equivalent to a one-dimensional lattice of particles and springs with masses and spring modulii adjusted to simulate the variation of mass density and air pressure with altitude in the real atmosphere.

The spring constants defined by Eqs. (3.39) and (3.40) may be reduced further. From (3.6) the following is true for an atmosphere with a constant sound velocity:

$$\frac{\rho_o(i+1)}{\rho_o(i)} = \frac{\exp -[(y + d_o)/H]}{\exp [-y/H]} = \exp\left(-\frac{d_o}{H}\right) \approx 1 - \frac{d_o}{H} \; , \qquad (3.42)$$

and

$$\frac{\rho_o(i-1)}{\rho_o(i)} \approx 1 + \frac{d_o}{H} \; . \qquad (3.43)$$

Substituting Eqs. (3.42) and (3.43) into Eqs. (3.38) and (3.39) gives

$$\frac{k'(i)}{m(i)} = \frac{c^2(i)}{d_o^2}\left[1 - \frac{d_o}{H}\left(1 - \frac{1}{2\gamma}\right)\right] \qquad (3.44)$$

$$\frac{k''(i)}{m(i)} = \frac{c^2(i)}{d_o^2}\left[1 - \frac{d_o}{H}\left(1 - \frac{1}{2\gamma}\right)\right]. \qquad (3.45)$$

The ratio of specific heats γ is approximately equal to 1.5 in the atmosphere. For d_o less than the scale height H, a uniform fluid is approximated by the air-cell model and the springs above and below each particle in the mechanical analog are nearly equal.

To complete the rigorous development of the mechanical analog, the following inconsistency must be resolved. The spring connecting the i^{th} particle and the $(i+1)^{th}$ particle is the same spring, but in the air-cell model it has two definitions. In one case this spring above the i^{th} particle is defined as

$$k'(i) = m(i) \frac{c^2(i)}{d_o^2} . \qquad (3.46a)$$

This same spring is also defined below the $(i+1)^{th}$ particle, as

$$k''(i) = m(i+1) \frac{c^2(i+1)}{d_o^2} . \qquad (3.46b)$$

Since these springs are in general not equal, a single spring with the average modulus of the two theoretical springs was used;

$$k(i \text{ to } i+1) = \frac{k'(i) + k''(i+1)}{2} . \qquad (3.47)$$

A vertical, one-dimensional segment of air in the atmosphere is approximated by a one-dimensional lattice of particles and springs with masses and spring constants analogous to the variable mass density and air pressure in the real atmosphere.

3. Two-Dimensional Lattice

A two-dimensional array of air cells is now considered as pictured in Fig. 4. As defined before, the horizontal coordinate of each cell is given by $\bar{x}(i,j,t)$ and the vertical coordinate by $\bar{y}(i,j,t)$. The starting point is Eq. (3.9) again;

$$\frac{d}{dt} v_x + \frac{c^2}{\rho_o} \frac{d}{dx} (\delta\rho) = 0 \qquad (3.48)$$

and

$$\frac{d}{dt} v_y + \frac{c^2}{\rho_o} \frac{d}{dy} (\delta\rho) + \frac{\delta\rho}{\rho_o} g = 0 \ . \qquad (3.49)$$

The dimensions of the $(i,j)^{th}$ cell are:

width = $d_o + \delta x(i,j,t)$

height = $d_o + \delta y(i,j,t)$

depth = d_o.

The horizontal and vertical stretch (δx and δy) of each cell are defined in terms of the cell coordinates $\bar{x}$ and $\bar{y}$ as done previously for the one-dimensional models.

The mass density associated with each air cell is

$$\rho_o(i,j) + \delta\rho(i,j,t) = \frac{m(i,j)}{(d_o + \delta x)(d_o + \delta y)d_o} \ . \qquad (3.50)$$

From Eq. (3.50) a normalized density perturbation is derived, assuming that δx and $\delta y \ll d_o$, as

$$\frac{\delta\rho(i,j,t)}{\rho_o(i,j)} = - \frac{1}{d_o} [\delta x(i,j,t) + \delta y(i,j,t)] \ . \qquad (3.51)$$

The horizontal and vertical density gradients of Eqs. (3.48) and (3.49) are evaluated as

$$\frac{d}{dx} (\delta\rho)\Big|_{i,j} = \frac{\delta\rho(i,j+1,t) - \delta\rho(i,j-1,t)}{d_o} \qquad (3.52)$$

and

$$\frac{d}{dy}(\delta\rho)\Big|_{i,j} = \frac{\delta\rho(i+1,j,t) - \delta\rho(i-1,j,t)}{d_o} . \qquad (3.53)$$

Substituting Eq. (3.51) into Eqs. (3.52) and (3.53) gives:

$$\frac{d}{dx}(\delta\rho)\Big|_{i,j} = -\frac{\rho_o(i)}{d_o^2}[\delta x(i,j+1,t) + \delta y(i,j+1,t) - \delta x(i,j-1,t) - \delta y(i,j-1,t)] \qquad (3.54)$$

and

$$\frac{d}{dy}(\delta\rho)\Big|_{i,j} = -\frac{\rho_o(i+1)}{d_o^2}[\delta x(i+1,j,t) + \delta y(i+1,j,t)] + \frac{\rho_o(i-1)}{d_o^2}[\delta x(i-1,j,t) + \delta y(i-1,j,t)] . \qquad (3.55)$$

Equations (3.54) and (3.55) are substituted into Eqs. (3.48) and (3.49) and the stretch of each cell (δx and δy) is evaluated in terms of the coordinates of each cell (x and y) measured from the stationary positions, as done previously for the one-dimensional lattices.

$$\frac{d}{dt}v_x(i,j,t) = \frac{c^2(i)}{d_o^2}[x(i,j+1,t) + x(i,j-1,t) - 2x(i,j,t)] + \frac{c^2(i)}{2d_o^2}[y(i+1,j+1,t) - y(i-1,j+1,t) - y(i+1,j-1,t) + y(i-1,j-1,t)] \qquad (3.56)$$

$$\frac{d}{dt} v_y(i,j,t) = \frac{c^2(i)}{d_o^2}\left[\frac{\rho_o(i+1)}{\rho_o(i)} + \frac{gd_o}{2c^2}\right] y(i+1,j,t)$$

$$+ \frac{c^2(i)}{d_o^2}\left[\frac{\rho_o(i-1)}{\rho_o(i)} - \frac{gd_o}{2c^2}\right] y(i-1,j,t)$$

$$- \frac{c^2(i)}{d_o^2}\,\frac{\rho_o(i+1) + \rho_o(i-1)}{\rho_o(i)}\, y(i,j,t)$$

$$+ \frac{c^2(i)}{2d_o^2}\,\frac{\rho_o(i+1)}{\rho_o(i)}\,[x(i+1,j+1,t) - x(i+1,j-1,t)]$$

$$- \frac{c^2(i)}{2d_o^2}\,\frac{\rho_o(i-1)}{\rho_o(i)}\,[x(i-1,j+1,t) - x(i-1,j-1,t)]$$

$$+ \frac{g}{2d_o}\,[x(i,j+1,t) - x(i,j-1,t)] \,. \qquad (3.57)$$

Equations (3.56) and (3.57) are the finite-difference approximations to the hydrodynamic equations, (3.48) and (3.49), describing motions in a two-dimensional atmosphere. Under certain conditions Eqs. (3.56) and (3.57) also describe wave motions in a two-dimensional lattice of particles and springs pictured in Fig. 2.

The equations of motion for the two-dimensional mechanical lattice are derived by equating the total restoring force acting on a single particle to the inertial force of that particle. A detailed picture of the two-dimensional lattice is shown in Fig. 16. In this figure, the diagonal springs are shown half as stiff as the vertical and horizontal springs because the former springs are stretched over a distance $\sqrt{2}$ further than the latter springs and, from Eq. (3.15),

$$k_{diag} = \frac{m\,c^2}{(\sqrt{2}\,d_o)^2} = \frac{k}{2} \quad . \tag{3.58}$$

Since the horizontal and vertical forces acting on the $(i,j)^{th}$ particle have been derived in previous sections, it is necessary only to calculate the effect of the diagonal springs.

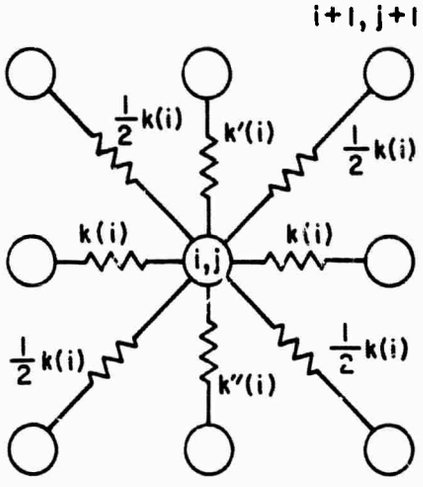

53777

FIG. 16. TWO-DIMENSIONAL LATTICE.

The horizontal or vertical component of the force acting on the $(i,j)^{th}$ particle as a result of stretching a diagonal spring is

$$F(i,j) = \frac{1}{\sqrt{2}}\, k_{diag}\, \Delta s \quad , \tag{3.59}$$

where k_{diag} is the diagonal spring constant derived in Eq. (3.58) and Δs is the stretch of the diagonal spring given by

$$\Delta s = \Big\{[x(i+1,j+1,t) - x(i,j,t) + d_o]^2 + [y(i+1,j+1,t) - y(i,j,t) + d_o]^2\Big\}^{1/2} - \sqrt{2}\, d_o \quad . \tag{3.60}$$

For small displacements,

$$\Delta s \cong \frac{1}{\sqrt{2}} \left[x(i+1,j+1,t) + y(i+1,j+1,t) - x(i,j,t) - y(i,j,t)\right], \quad (3.61)$$

and the total horizontal or vertical component of the force acting on the $(i,j)^{th}$ particle is

$$\text{Force}\,(i,j) = \frac{k}{4} \left[x(i+1,j+1,t) + y(i+1,j+1,t) - x(i,j,t) - y(i,j,t)\right] . \quad (3.62)$$

Adding the forces that are due to the remaining springs and setting these equal to the inertial force of the $(i,j)^{th}$ particle results in

$$\begin{aligned} m(i) \frac{d}{dt} v_x(i,j,t) = {} & k(i) \left[x(i,j+1,t) + x(i,j-1,t) - 2x(i,j,t)\right] \\ & + \frac{k(i)}{4} \left[y(i+1,j+1,t) - y(i-1,j+1,t)\right. \\ & \qquad \left. - y(i+1,j-1,t) + y(i-1,j-1,t)\right] \\ & + \frac{k(i)}{4} \left[x(i+1,j+1,t) + x(i-1,j+1,t)\right. \\ & \qquad \left. + x(i+1,j-1,t) + x(i-1,j-1,t)\right] \end{aligned} \quad (3.63)$$

$$\begin{aligned} m(i) \frac{d}{dt} v_y(i,j,t) = {} & k'(i)\, y(i+1,j,t) + k''(i)\, y(i-1,j,t) \\ & - \left[k'(i) + k''(i)\right] y(i,j,t) \\ & + \frac{k(i)}{4} \left[x(i+1,j+1,t) - x(i+1,j-1,t)\right. \\ & \qquad \left. + y(i+1,j+1,t) + y(i+1,j-1,t)\right] \end{aligned}$$

$$+ \frac{k(i)}{4} [x(i-1,j+1,t) - x(i-1,j-1,t)$$

$$- y(i-1,j+1,t) - y(i-1,j-1,t)]. \quad (3.64)$$

An equivalency between the mechanical equations, (3.63) and (3.64), and the hydrodynamic equations, (3.56) and (3.57), may be shown by arbitrarily defining the following "diagonal springs" from Eqs. (3.39) and (3.40).

$$\frac{k'_d(i)}{m(i)} = \frac{c^2(i)}{d_o^2} \frac{\rho_o(i+1)}{\rho_o(i)} \approx \frac{c^2(i)}{d_o^2} \qquad \text{(for small } d_o\text{)} \qquad (3.65)$$

$$\frac{k''_d(i)}{m(i)} = \frac{c^2(i)}{d_o^2} \frac{\rho_o(i-1)}{\rho_o(i)} \approx \frac{c^2(i)}{d_o^2} \qquad \text{(for small } d_o\text{)}. \qquad (3.66)$$

Assuming that the stationary height and width d_o is less than the scale height H, so that the last term of Eq. (3.57) may be ignored, Eqs. (3.56) and (3.57) are rewritten as

$$m(i) \frac{d}{dt} v_x(i,j,t) = k(i) [x(i,j+1,t) + x(i,j-1,t) - 2x(i,j,t)]$$

$$+ \frac{k(i)}{2} [y(i+1,j+1,t) - y(i-1,j+1,t)$$

$$- y(i+1,j-1,t) + y(i-1,j-1,t)] \qquad (3.67)$$

$$m(i)\frac{d}{dt}v_y(i,j,t) = k'(i)\,y(i+1,j,t) + k''(i)\,y(i-1,j,t)$$

$$- [k'(i) + k''(i)]\,y(i,j,t)$$

$$+ \frac{k(i)}{2}\,[x(i+1,j+1,t) - x(i+1,j-1,t)]$$

$$+ \frac{k(i)}{2}\,[x(i-1,j+1,t) - x(i-1,j-1,t)] \quad . \qquad (3.68)$$

Equations (3.67) and (3.68) are still the hydrodynamic equations of the atmosphere, but with the constants in Eqs. (3.65) and (3.66) inserted. It will be shown below that the hydrodynamic equations of motion are curl-free. Because of this fact it will be further shown that the hydrodynamic equations, (3.67) and (3.68), are equivalent to the mechanical lattice equations if only curl-free motions are considered--i.e., energy sources are restricted to isotropic filaments.

To prove that the hydrodynamic equations are curl-free, consider the displacement vector $\vec{r}$ defined as

$$\vec{r} = x(i,j,t)\bar{u}_x + y(i,j,t)\bar{u}_y \quad ,$$

where $\bar{u}_x$ and $\bar{u}_y$ are direction vectors in the x and y directions.

The displacement vector $\vec{r}$ may be expressed as the gradient of a scalar from Eq. (3.9), as

$$\frac{\partial^2\vec{r}}{\partial t^2} = \frac{\partial\vec{v}}{\partial t} = -\frac{c^2}{\rho_o}\nabla(\delta\rho) + \frac{\delta\rho}{\rho_o}\vec{g} \qquad (3.69)$$

and

$$\frac{\partial^2\vec{r}}{\partial t^2} = -c^2\nabla\left(\frac{\delta\rho}{\rho_o}\right) + (\gamma + 1)\vec{g}\,\frac{\delta\rho}{\rho_o} \quad . \qquad (3.70)$$

For the values of sound velocity c, ratio of specific heats γ, and gravitational constant g specified earlier and for wave motions such that the second term on the right side of Eq. (3.70) is small compared to the first term, a double integration reduces this equation to

$$\vec{r} = -c^2 \nabla \left(\iint \frac{\delta \rho}{\rho_o} \, dt^2 \right) . \tag{3.71}$$

And, finally,

$$\nabla \times \vec{r} = 0 . \tag{3.72}$$

Therefore the hydrodynamic equations described by Eqs. (3.67) and (3.68) are curl-free. Equation (3.72) may then be rewritten as

$$\frac{\partial}{\partial y} x(i,j,t) = \frac{\partial}{\partial x} y(i,j,t) . \tag{3.73}$$

With the restriction that only curl-free motion be considered, Eq. (3.73) is evaluated by the finite-difference technique described in the previous sections, and the hydrodynamic equations, (3.67) and (3.68), are equivalent to the mechanical-lattice Eqs. (3.63) and (3.64). In other words, to minimize the possibility of exciting shear waves in the mechanical lattice, energy sources must be restricted to isotropic filaments.

This latter restriction limits the usefulness of the mechanical lattice to imitate atmospheric oscillations and raises the question as to why the mechanical analogy was invoked at all. The mechanical-lattice approach was an extension of Newton's one-dimensional analogy to two dimensions. This array of particles and springs is very useful for demonstrating various phenomena in the real atmosphere, such as frequency cutoffs and energy-trapping effects. The hydrodynamic equations, (3.56) and (3.57), were programmed but instabilities resulted in the computer solution. These instabilities were immediately eliminated by programming the mechanical lattice represented by Eqs. (3.63) and (3.64). This latter solution does not represent the only cure for the instability, since an

exhaustive study was not carried out to eliminate the difficulties resulting from a direct programming of Eqs. (3.56) and (3.57). A suggestion for future work is to discover and eliminate the source of the computer instability resulting from programming the hydrodynamic equations.

C. ENERGY SOURCES

Since the atmosphere is modeled by a mechanical lattice consisting of particles and springs, energy sources are imitated by forcing a group of particles to oscillate. The simulation of point sources is greatly simplified by the fact that the particles may be moved independently. A cylindrical wavefront of energy resulting from a point source located at the $(i,j)^{th}$ particle is simulated by forcing the eight surrounding particles to move as shown in Fig. 17a. The total energy of this wavefront is calculated by summing the kinetic energy $(1/2)mv^2$ of each of the eight particles. Energy distributions throughout the atmospheric model are conveniently found by calculating the fraction of total source energy in each particle over a given contour, as will be shown in the next chapter. A quadrant of the cylindrical wavefront pictured in Fig. 17a was actually programmed into the air-cell model, as shown in Fig. 17b.

D. BOUNDARY CONDITIONS

Four boundary conditions must be specified for the mechanical lattice on the top, bottom, right, and left sides of the two-dimensional array of particles and springs. Since the problem is reduced to a purely mechanical one, the boundary conditions are greatly simplified.

Only line sources of energy will be considered, parallel to the bottom boundary (representing the ground plane) and lying in the symmetry plane (Fig. 18). The top and right boundaries represent "perfect terminations," so that waves impinging on these boundaries will not be reflected back toward the source.

1. The Ground Plane

The particles on the ground plane are allowed to move only in the horizontal direction, and the motion of particles above this plane is imaged in the ground plane as shown in Fig. 19. To calculate the horizontal displacement of a particle on the ground, represented by $x(0,j,t)$,

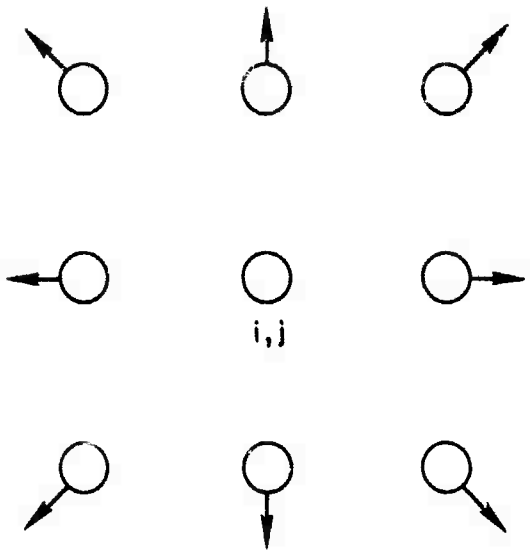

a. At the $(i,j)^{th}$ particle

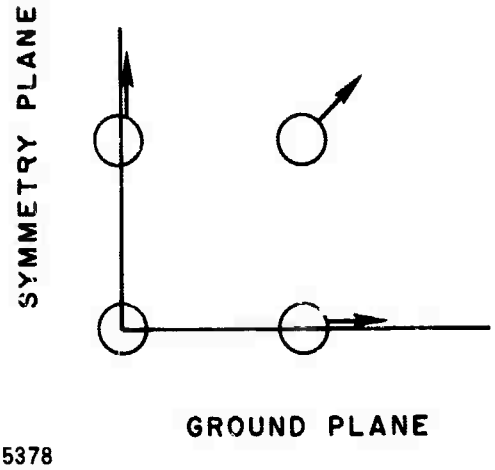

b. At grourd level

FIG. 17. COMPUTER SIMULATION OF FILAMENT SOURCES.

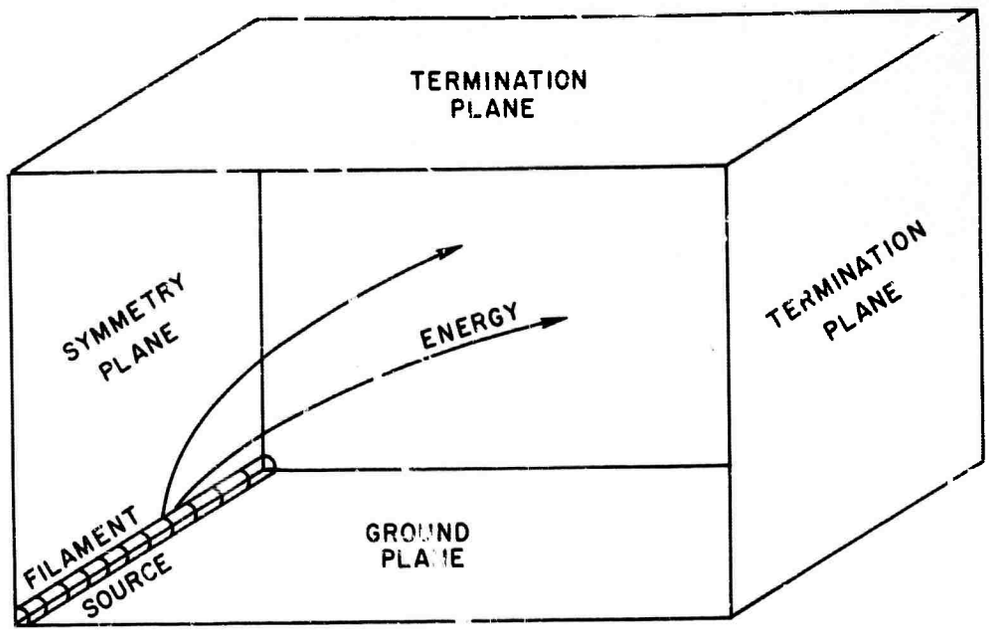

FIG. 18. BOUNDARY CONDITIONS.

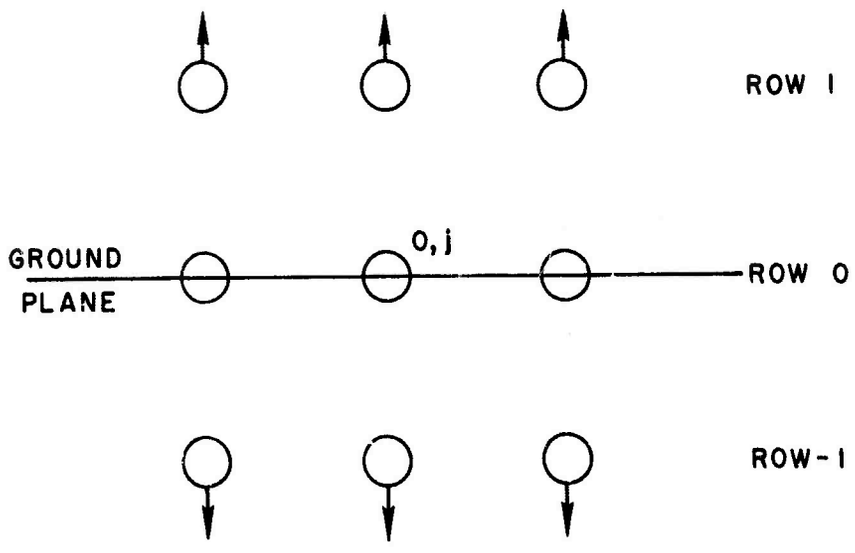

35382

FIG. 19. GROUND-PLANE IMAGING.

the displacements of the eight neighboring particles are needed--particles $(0,j-1)$, $(1,j-1)$, $(1,j)$, $(1,j+1)$, $(0,j+1)$, $(-1,j+1)$, $(-1,j)$, and $(-1,j-1)$. The last three particles lie below the ground plane and are images of the particles above the ground plane, so that

$$x(-1,j+1,t) = x(1,j+1,t) \qquad y(-1,j+1,t) = -y(1,j+1,t)$$

$$x(-1,j,t) = x(1,j,t) \qquad \text{and} \qquad y(-1,j,t) = -y(1,j,t)$$

$$x(-1,j-1,t) = x(-1,j-1,t) \qquad y(-1,j-1,t) = -y(1,j-1,t) \ .$$

2. The Symmetry Plane

The particles in the symmetry plane are allowed to move only vertically and the motion of particles will be symmetric with respect to this plane, as shown in Fig. 20. In calculating the vertical displacement of the $(i,0)^{th}$ particles, the displacements of the eight surrounding particles will be related by

$$y(i+1,-1,t) = y(i+1,1,t) \qquad x(i+1,-1,t) = -x(i+1,1,t)$$

$$y(i,-1,t) = y(i,1,t) \qquad \text{and} \qquad x(i,-1,t) = -x(i,1,t)$$

$$y(i-1,-1,t) = y(i-1,1,t) \qquad x(i-1,-1,t) = -x(i-1,-1,t) \ .$$

3. The Right Termination Plane

The termination of a one-dimensional mechanical lattice is derived from Eq. (3.21). Let the j^{th} particle represent the last particle in the array, as shown in Fig. 21. In order to calculate the displacement of the j^{th} particle, the displacement of the $(j+1)^{th}$ particle must be known. It is assumed that

$$x(j+1,t) = x\left(j,t - \frac{d_o}{c}\right) , \tag{3.74}$$

where c is the velocity of sound propagation. The displacement of the j^{th} particle may be calculated from

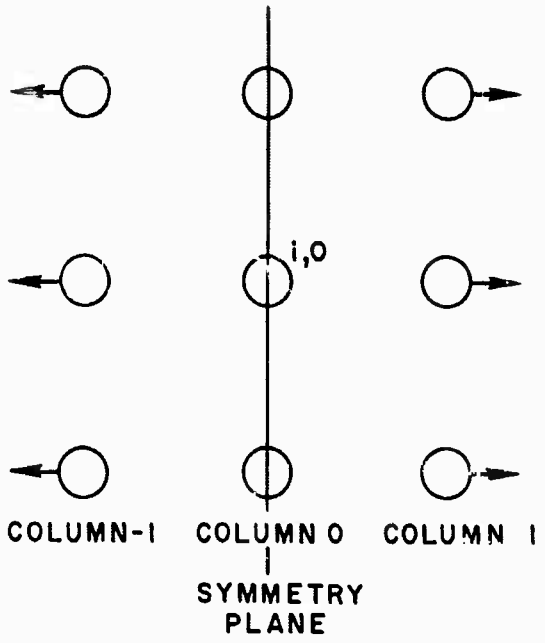

35382

FIG. 20. SYMMETRY-PLANE IMAGING.

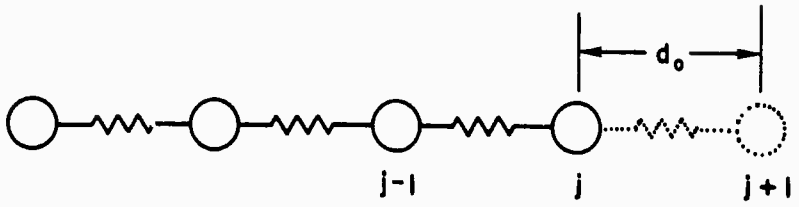

35381

FIG. 21. TERMINATION OF ONE-DIMENSIONAL ARRAY.

$$\frac{d}{dt} v_x(j,t) = \frac{k}{m}\left[x\left(j,t-\frac{d_o}{c}\right) + x(j-1,t) - 2x(j,t)\right] . \qquad (3.75)$$

To extend this termination condition to the two-dimensional lattice, it will be assumed that waves arriving at the right boundary are very nearly plane waves traveling normal to the boundary (Fig. 22). Particles on this boundary will move only in the horizontal direction; all vertical displacements are zero. Equation (3.74) may be applied to the last column $(j = j_L)$ of particles:

$$x(i,j_{L+1},t) = x\left(i,j_L,t-\frac{d_o}{c}\right) \qquad (3.76)$$

where c is the velocity of sound at the altitude corresponding to the i^{th} particle.

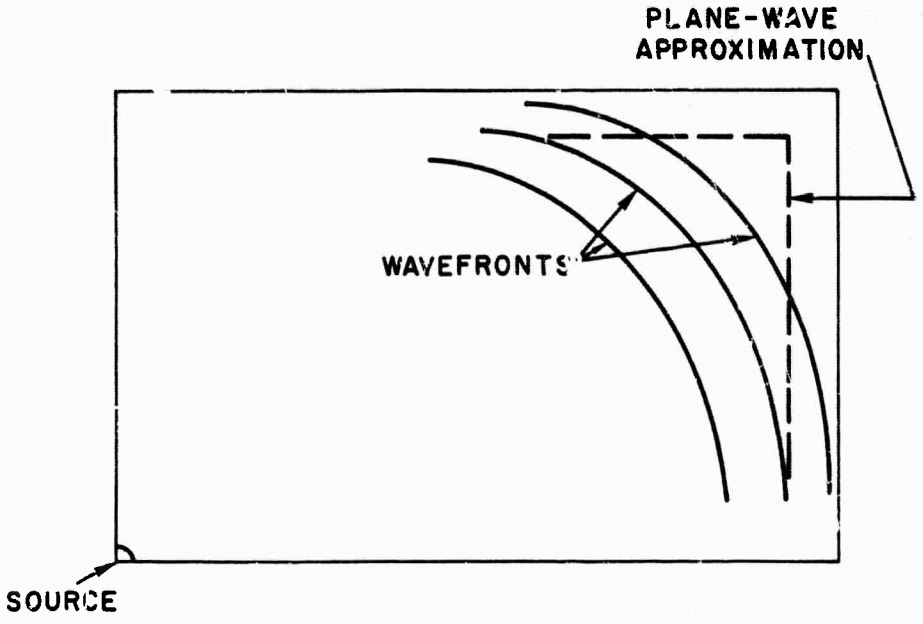

35381

FIG. 22. PLANE-WAVE APPROXIMATION.

4. The Top Termination

As for the right side, it has been assumed that waves arriving at the top boundary will be nearly plane waves and the horizontal displacements of particles on this boundary are set equal to zero. This situation is shown in Fig. 22. The vertical termination is expressed similar to Eq. (3.76) for the top row $(i = i_T)$ of particles;

$$y(i_{T+1},j,t) = y\left(i_T,j,t-\frac{d_o}{c}\right) . \qquad (3.77)$$

E. FREQUENCY LIMITATIONS

As is the case for any system described by a second-order differential equation, the mechanical lattice of particles and springs possesses natural or resonant frequencies, which depend on the velocity of propagation throughout the array and the spacing between particles. The mechanical lattice represents a valid model of the atmosphere for frequencies above these resonances; therefore sources supplying energy to the lattice must be limited. Pulse inputs simulating explosions in the atmosphere must be "filtered" to remove higher-frequency harmonics that could excite resonances in the mechanical array. Because of the variations of masses and springs, the natural modes of the air-cell model are quite awkward to calculate but were conveniently found by computer experiments. For an interparticle spacing d_o equal to 10 km and a velocity of propagation equal to the speed of sound in the atmosphere, the highest useful frequency of the air-cell model was determined to be 10 mc (corresponding to a wave period of 100 sec--shorter than the vertical cutoff of the atmosphere of 300 sec).

F. CORRECTIONS TO THREE-DIMENSIONAL GEOMETRY

As pictured in Fig. 1, the air-cell model of the atmosphere restricts energy sources to be infinite filaments rather than point sources, resulting in cylindrical wavefronts. It is desirable to correct the values of energy densities determined from the cylindrical geometry to a three-dimensional geometry, with an axis of symmetry replacing the plane of symmetry, and point sources replacing the filament sources, producing spherical wavefronts instead. In a uniform fluid this correction is made by dividing energy-density values by the distance between the source and the field point (i.e., cylindrical spreading implies a $1/r$ variation while spherical-spreading variation is $1/r^2$). This correction is also a good approximation at large distances (compared to a wavelength) from the source in a nonuniform fluid.

At distances very close to a filament source in the nonuniform air-cell representation of the atmosphere, the medium is very nearly uniform, so that the energy source may be physically represented by a cylindrical

wavefront symmetrical about the filament source. This symmetrical wavefront is simulated in the mechanical array by forcing the proper particles to oscillate as discussed in Section III.C.

In summary, it is assumed that, at very close distances (on the order of a cell dimension d_o) to a filament source, waves begin to propagate as if in a uniform fluid, forming symmetrical cylindrical wavefronts, but at greater distances are deformed because of nonuniformity of the medium. A point source in the spherical geometry is corrected to a filament source in cylindrical geometry by the $1/r$ factor. The same $1/r$ factor is used to correct energy densities calculated at great distances from the source from the cylindrical system back to the spherical system. It should be appreciated that solutions determined in the cylindrical and spherical coordinate systems are related by much more complicated expressions than a simple $1/r$ factor, and must be described by more subtle mathematical and physical concepts than can be expressed in this analysis. It might be suggested that the two-dimensional lattice of particles (or more accurately, rods extending infinitely in the z direction) and springs be replaced by rings concentric to the symmetry line and springs to obtain a three-dimensional model. However, the purpose of this analysis was to develop, as conveniently and economically as possible, a computer model to provide qualitative insight to the large-scale effect of acoustic-gravity waves in the atmosphere, since accurate answers at only particular points in the atmosphere are already available from a more elegant mathematical treatment involving normal mode expansions [Refs. 14-18].

In an attempt to provide a very rough check of barograms (calculated from the computer model) with experimental data, the approximate conversion factor of $1/r$ was applied as described.

G. SUMMARY

This chapter has described a two-dimensional lattice of particles interconnected by springs that models the behavior of a two-dimensional

fluid. The array of particles and springs is very useful for demonstrating various phenomena in the real atmosphere, such as frequency cutoffs and energy trapping, and facilitates computer calculations that provide convenient panoramic displays of oscillations in the atmosphere.

A limitation of the particle-and-spring model would be the introduction of shear forces. These forces are insignificant for the case of linear acoustic-gravity waves in the real atmosphere. In order to avoid the possibility of exciting shear waves, energy sources were restricted to isotropic filaments. The validity of the computer model in the light of this limitation was checked with geometrical acoustic ray theory [Ref. 25]. The model was found to imitate well the behavior of the atmosphere, as will be described in the following chapter.

The mechanical lattice is limited at high frequencies by the natural modes of the particles and springs. However, as the purpose of this analysis was to examine very low-frequency wave propagation in the atmosphere (below 0.001 cps), energy sources were filtered to eliminate harmonics that might excite any resonant modes.

The limitations of the air-cell computer model are justified by the convenient and simplified computer calculations that can be made to provide dramatic, qualitative displays of atmospheric oscillations. A treatment involving normal mode expansion of solutions [Refs. 14-18] can provide highly accurate answers at particular points in the atmosphere. The accuracy of this latter analysis, however, is limited by the number of modes for which one is willing to spend computer time.

The qualitative displays provided by the air-cell computer model provide insight into the large-scale perturbations of the atmosphere and ionosphere caused by acoustic-gravity waves.

IV. COMPUTER-MODEL RESULTS

A. INTRODUCTION

A segment of atmosphere measuring 300 km in height by 500 km in width was modeled with 1500 air cells in a lattice measuring 30 by 50 cells. Pressure, density, and specific-heat ratios were taken from the "U.S. Standard Atmosphere, 1962" [Ref. 26]. Displacements and velocities were evaluated at 10-sec increments of time. Values for horizontal and vertical displacements and velocities of every air cell at each increment of time were solved for, resulting from various energy sources in the atmosphere, by an IBM 7090 digital computer and recorded on magnetic tape. These magnetic tapes were then processed to provide air-cell orbits, synthetic barograms, and even motion pictures. These motion pictures were plotted frame by frame on a Stromberg-Carlson 4020 High-Speed Microfilm Recorder. The atmosphere is represented by a lattice of gyrating "dots" on a motion picture screen. Only "steady-state" or "equilibrium" motions can be presented in this paper, but the motion picture of transient motions in the atmosphere may be obtained from the author. Ground-level, sinusoidal point sources were considered first to gain an appreciation of energy dispersion throughout the atmosphere for different source frequencies. A relatively high acoustic frequency was considered first to compare with results already available from geometric acoustic theory. Successively lower frequencies were considered to bridge the transition from the acoustic range to the acoustic-gravity range. A high-altitude, sinusoidal point source was programmed into the computer model revealing a mixture of acoustic- and acoustic-gravity-wave propagation.

The transient behavior of the atmosphere was studied by programming an impulse (properly filtered to eliminate the high frequencies above the useful limit of the computer model) simulating an explosion both at ground level and at a high altitude. Barograms computed from the ground-level explosion are compared with available experimental barograms recorded during nuclear tests. High-altitude barograms are also presented.

B. GROUND-LEVEL, SINUSOIDAL POINT SOURCES

Figure 23a is a computer plot, produced after transients have died down in the computer, displaying the equilibrium air-cell orbits

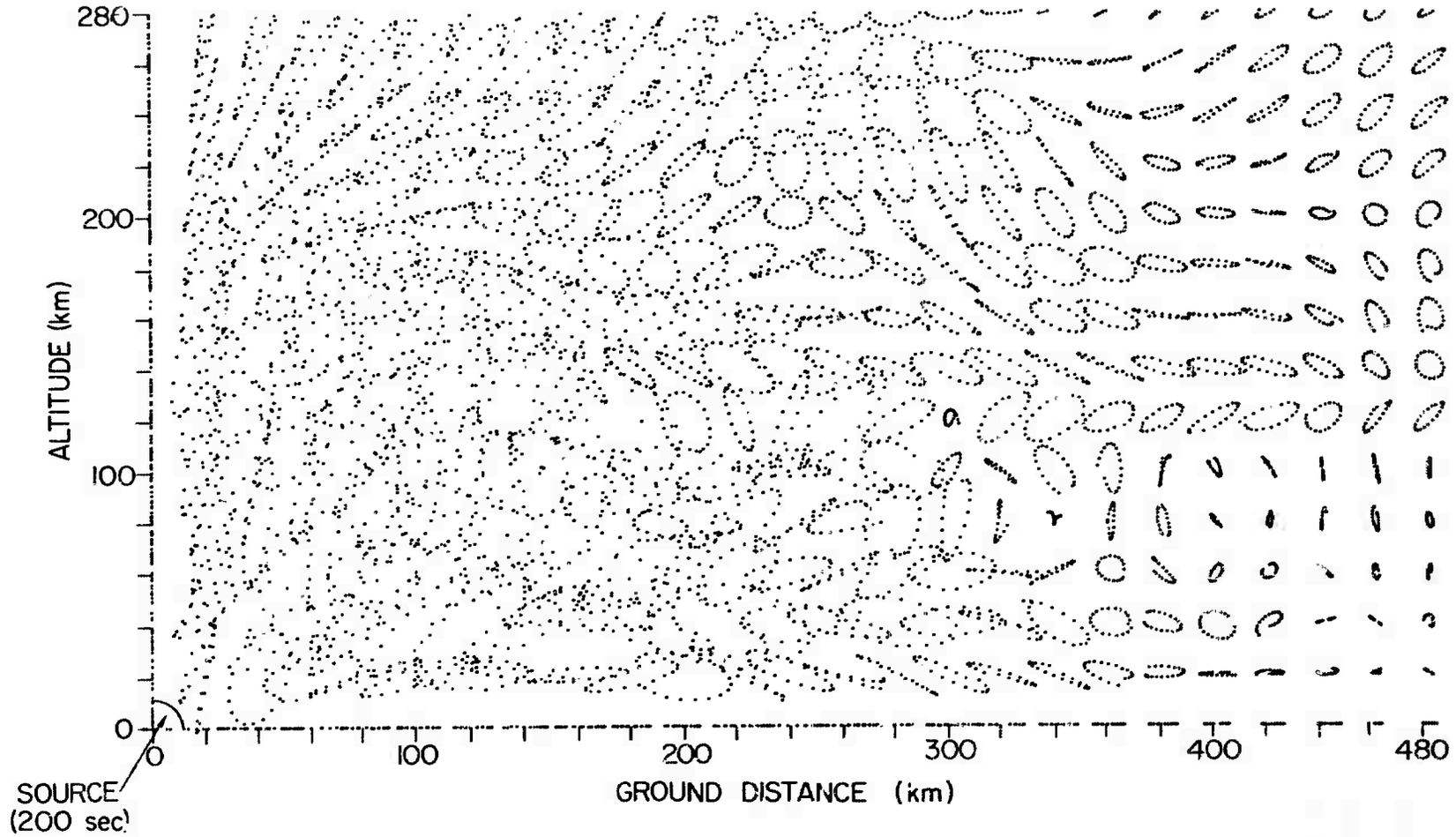

a. Computer output

FIG. 23. EQUILIBRIUM AIR-CELL ORBITS RESULTING FROM A 200-SEC, SINUSOIDAL POINT SOURCE.

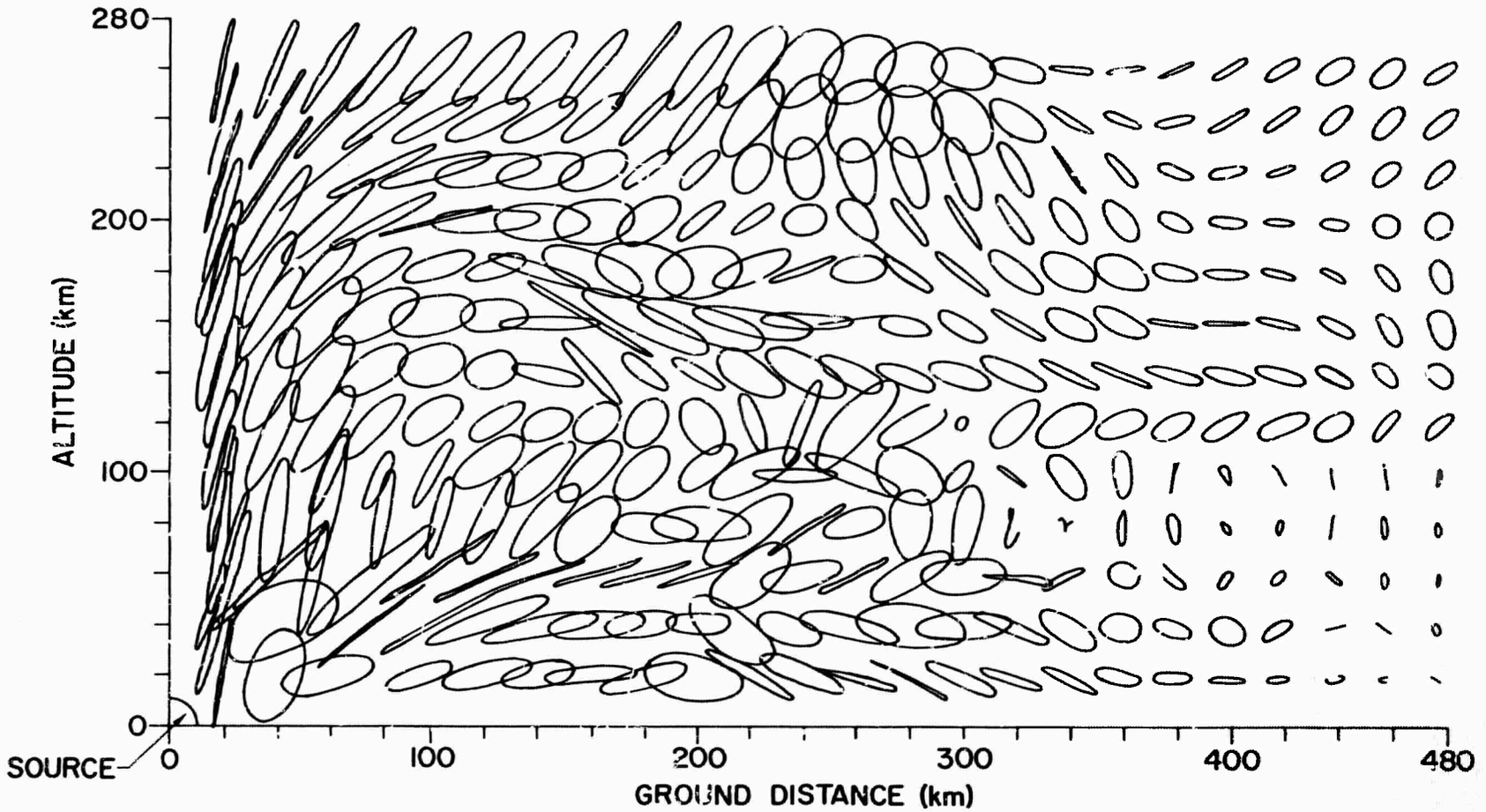

b. Retrace (for clarity)

FIG. 23 (CONTINUED)

resulting from a ground-level, sinusoidal point source with a 200-sec period.

Because of the transformer characteristic of the atmosphere described in Chapter I, and the great difference in mass between the top and bottom particles in the lattice, the particles at the top of the mechanical lattice must vibrate more violently than the particles on the bottom. The top particles weigh 10^{-11} of the bottom particles, and therefore will be displaced $10^{11/2}$ further in order to satisfy conservation-of-energy requirements. Therefore, particle displacements have been normalized in Fig. 23 by arbitrary numbers varying with altitude in the lattice to fit the data on a single plot.

In Fig. 23b, the air-cell orbits have been retraced for clarity. The direction of energy flow is revealed by the orientation of the major axis of each ellipse.

Figure 24 displays acoustic raypaths computed by a method in which the atmosphere is horizontally stratified into a number of isothermal slabs and Snell's law is satisfied at each boundary. The direction of acoustic-energy flow throughout the atmosphere shown by the air-cell computer

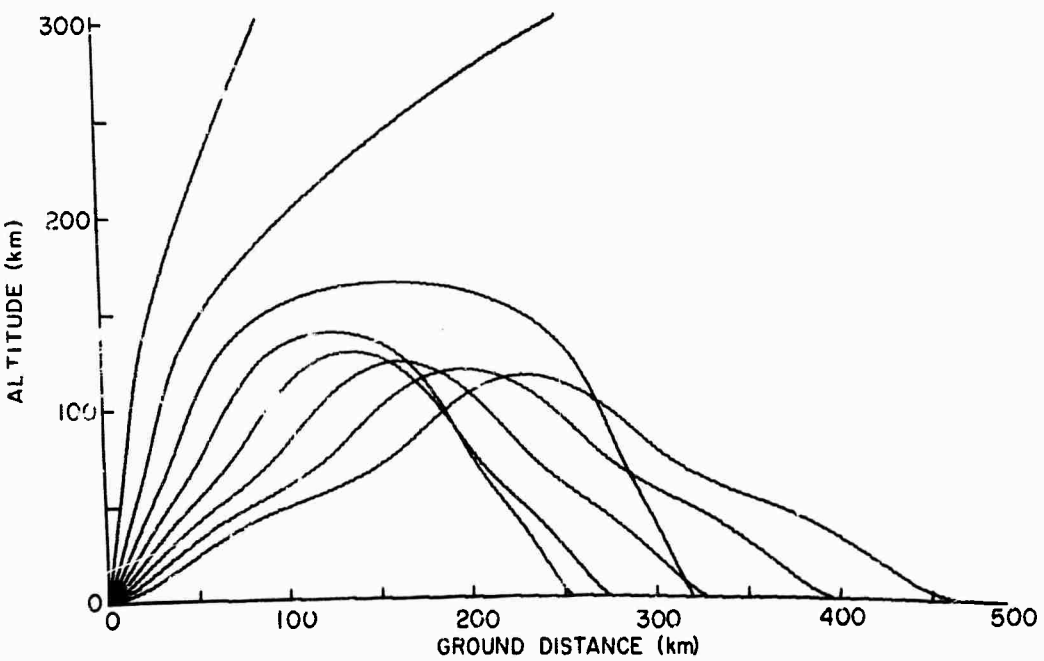

FIG. 24. ACOUSTIC RAYPATHS FOR A GROUND-LEVEL SOURCE

model in Fig. 23b compares well with the geometric raytracings in Fig. 24, supporting the validity of the computer model.

As the source frequency is decreased (period and wavelength lengthened) a geometrical raytracing technique is no longer valid because wavelengths are now much greater than the vertical scale of the atmosphere. The steady-state distribution of energy throughout the atmosphere at longer source periods is shown in the sequence of Figs. 25 through 28. The same numbers as used in Fig. 23b have been used to normalize the particle orbits in the series of plots in these figures. These figures dramatically display the frequency-dependent, spatial dispersion of acoustic-gravity waves. As the source frequency is decreased, the released energy becomes more confined to low altitudes in the atmosphere. Sources with periods longer than 600 sec are observed to distribute nearly all of their energy on the ground.

1. Energy Distributions

Energy distributions are conveniently found from the air-cell model by calculating the kinetic energy $(1/2)mv^2$ of each air cell around any given contour. Figure 29 is a plot of the fraction of source energy contained in an air cell along a vertical path located 100 km away (ground distance) from the source. A greater fraction of energy is trapped in the two sound ducts (regions of temperature and sound-velocity minima) located at altitudes of approximately 20 and 90 km. The fraction of total energy in each air cell decreases with altitude because of the bending of raypaths (as can be seen from the raypath plots in Fig. 24) and because of the spreading due to the increase in total distance from the source. Figure 30 shows the vertical distribution of energy 100 km away from a 300-sec, ground-level point source. This 300-sec period corresponds to the vertical cutoff frequency of the atmosphere at ground level. The distribution of energy is similar to the 200-sec case with energy trapped in the two sound ducts but, in addition, a greater amount of energy is seen to reside immediately on the ground. A much greater amount of energy is seen to remain at low altitudes for the 400-sec source in Fig. 31. However, at a greater ground distance from the source the vertical energy distribution looks more like that for the higher-frequency acoustic case.

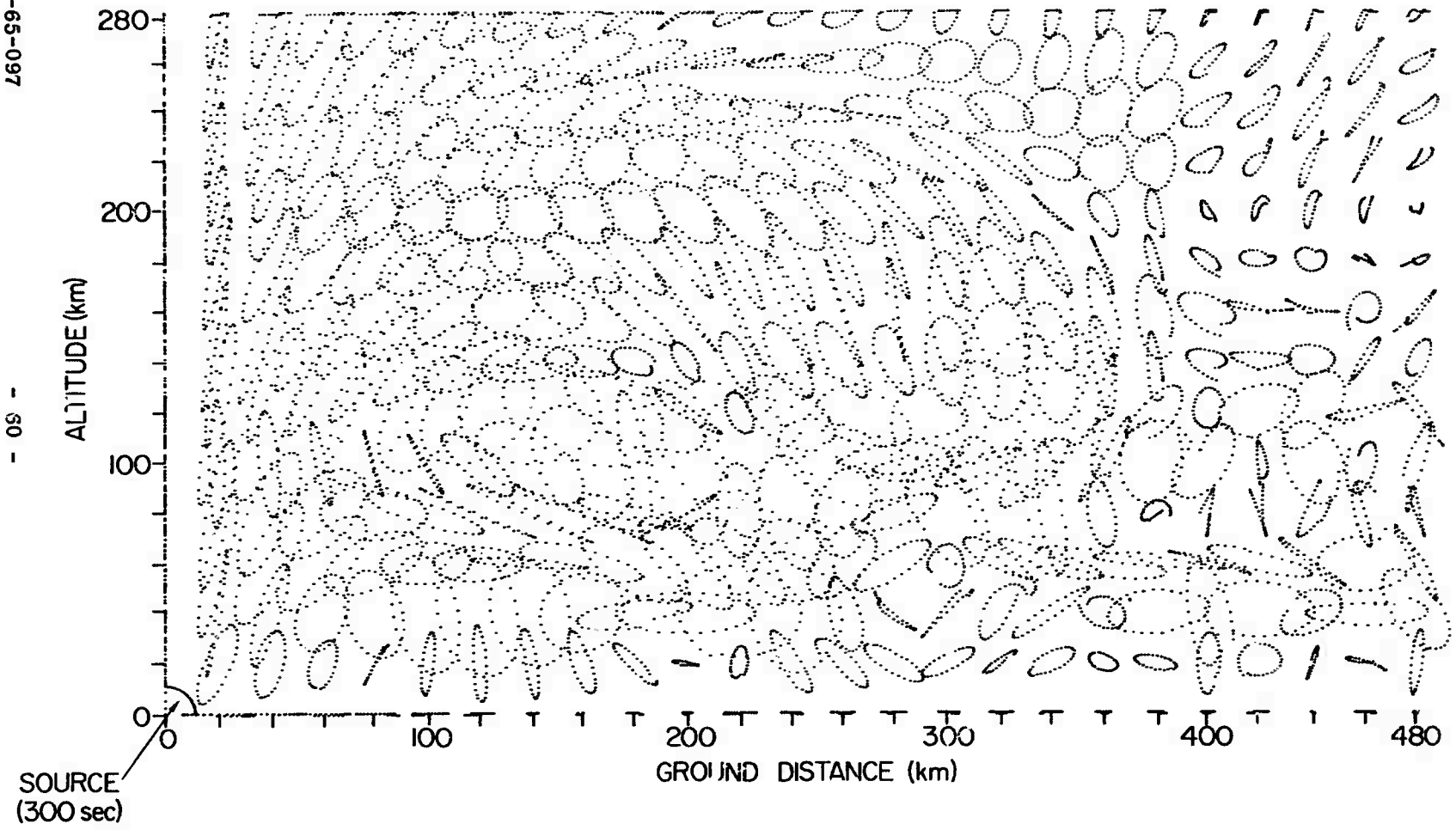

FIG. 25. EQUILIBRIUM AIR-CELL ORBITS RESULTING FROM A 300-SEC, SINUSOIDAL POINT SOURCE.

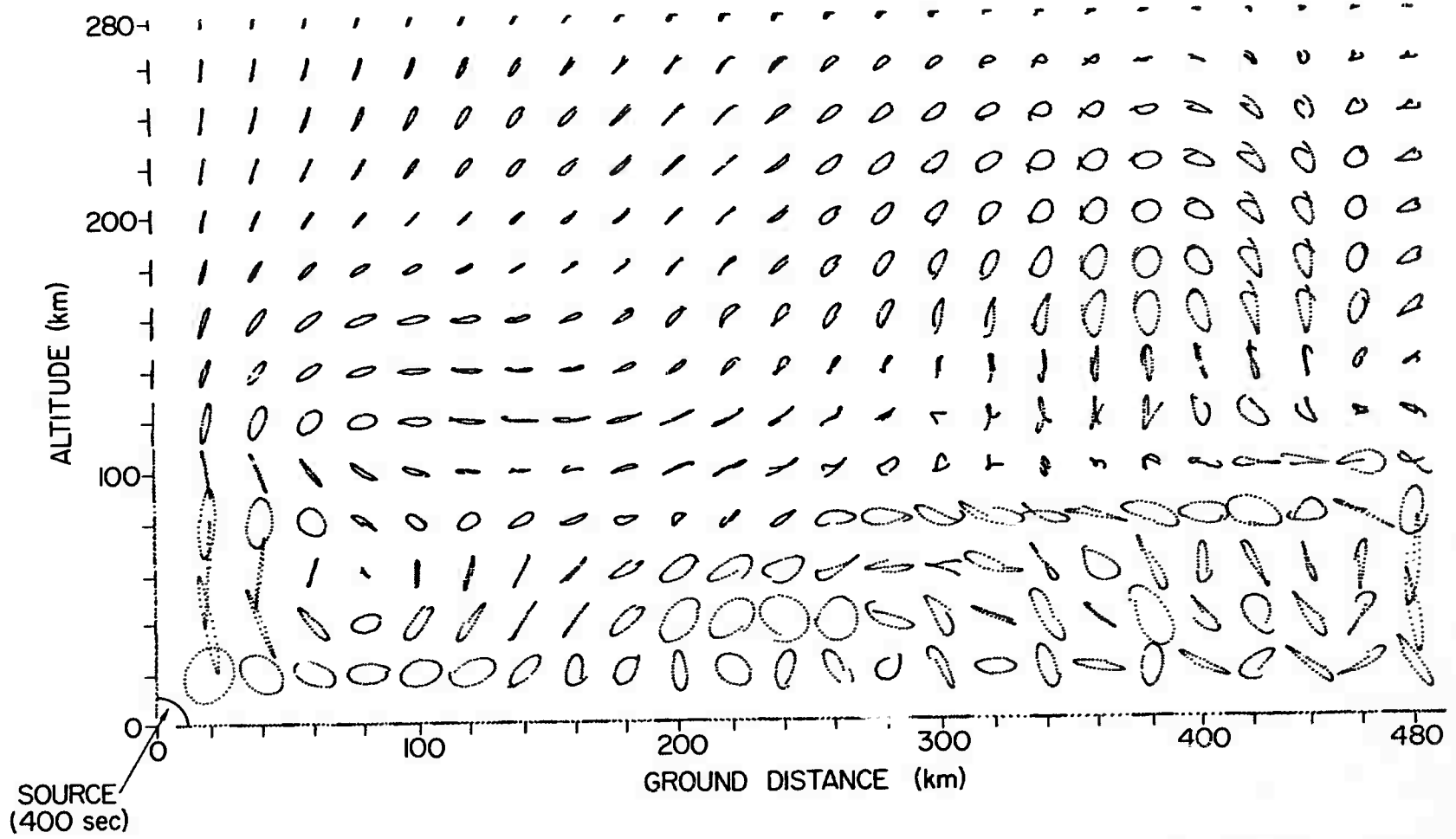

FIG. 26. EQUILIBRIUM AIR-CELL ORBITS RESULTING FROM A 400-SEC, SINUSOIDAL POINT SOURCE.

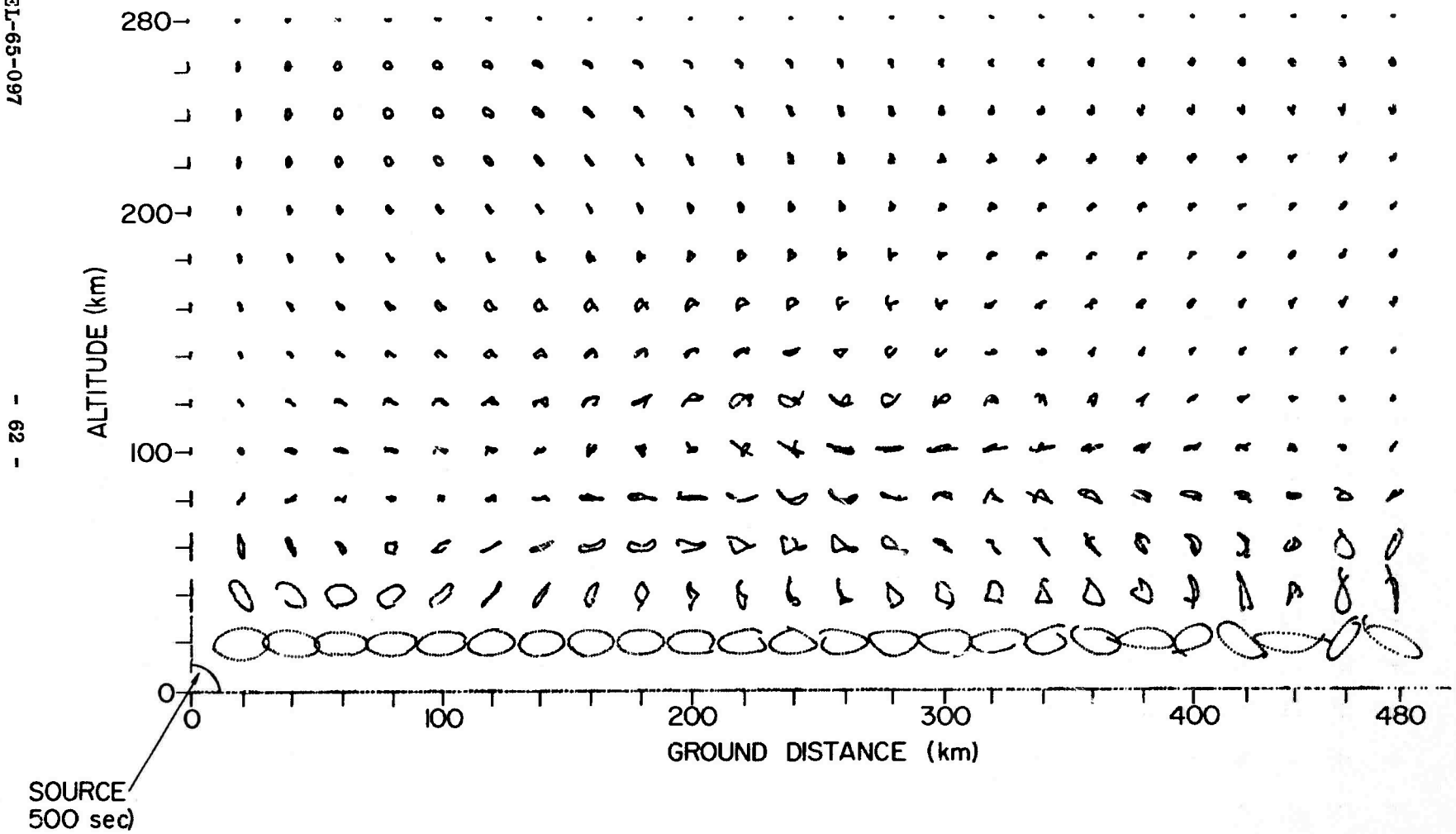

FIG. 27. EQUILIBRIUM AIR-CELL ORBITS RESULTING FROM A 500-SEC, SINUSOIDAL POINT SOURCE.

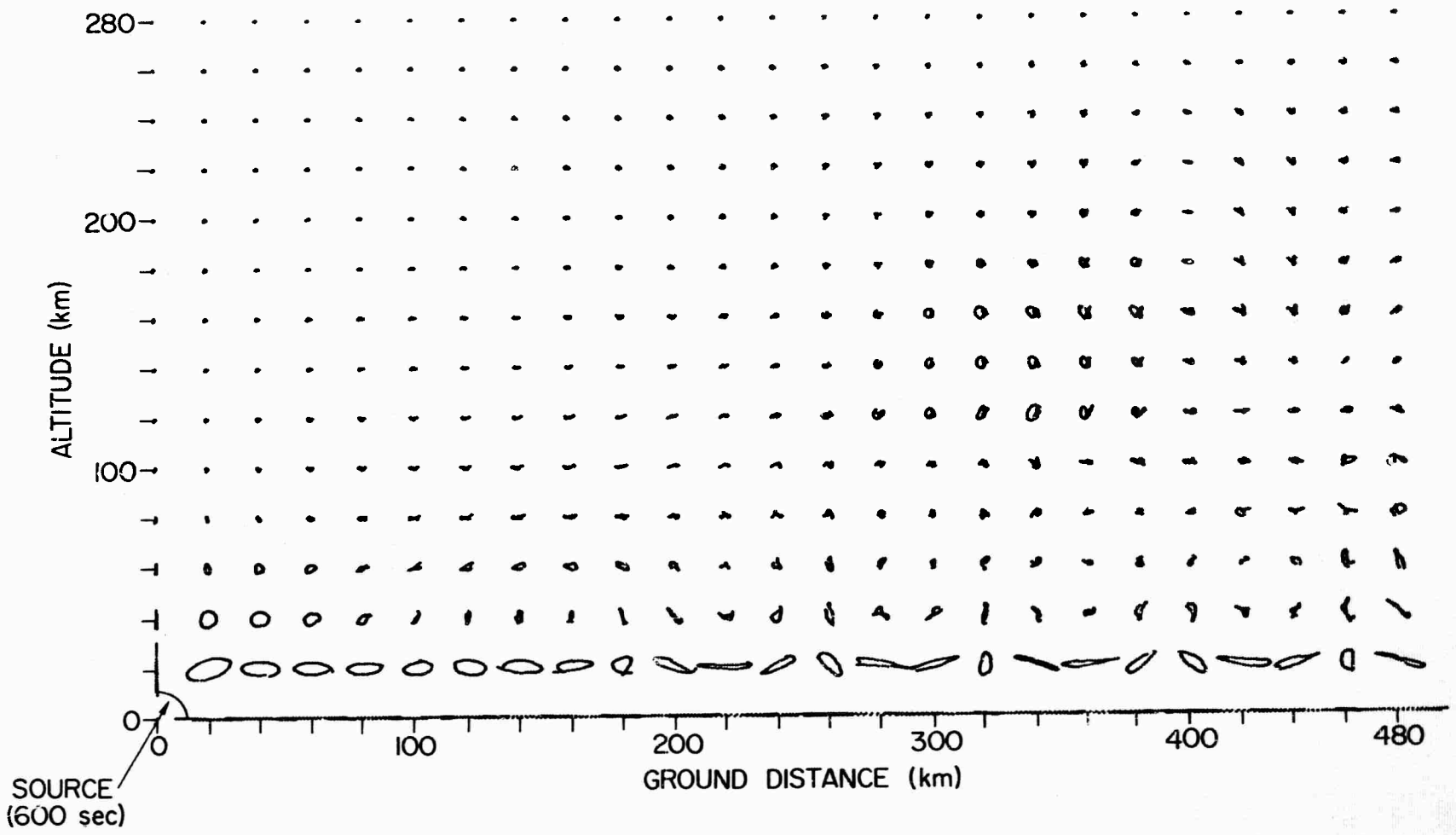

FIG. 28. EQUILIBRIUM AIR-CELL ORBITS RESULTING FROM A 600-SEC, SINUSOIDAL POINT SOURCE.

SEL-65-097

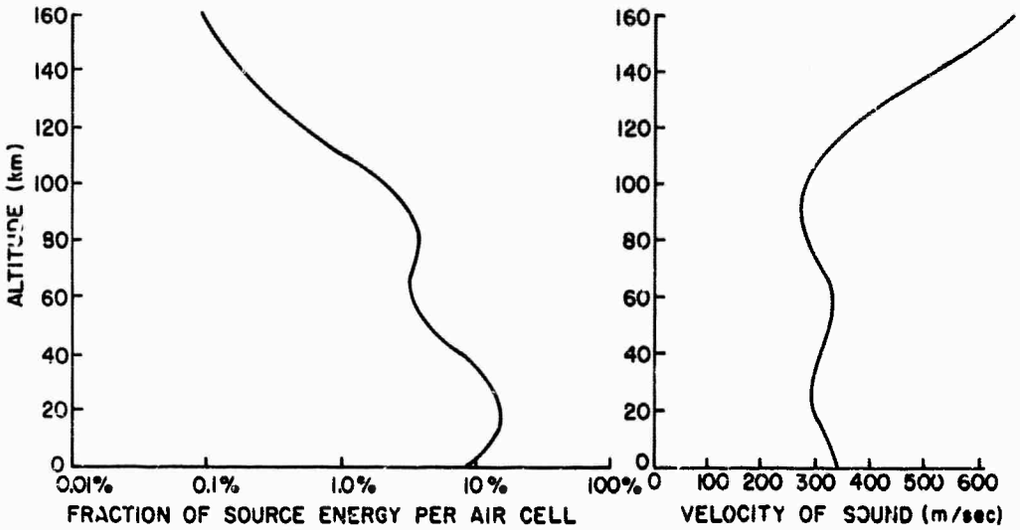

34147

FIG. 29. VERTICAL ENERGY DISTRIBUTION AT A 100-KM GROUND DISTANCE FROM A 200-SEC, GROUND-LEVEL POINT SOURCE.

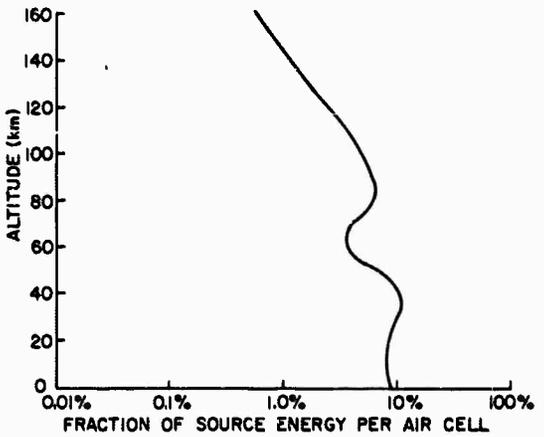

34148

FIG. 30. VERTICAL ENERGY DISTRIBUTION AT A 100-KM GROUND DISTANCE FROM A 300-SEC, GROUND-LEVEL POINT SOURCE.

This similarity agrees with the original "intuitions" gained from ray theory that low-frequency energy cannot propagate vertically in the atmosphere, but only "sideways."

For a 500-sec, ground-level source as shown in Fig. 32, nearly all of the released energy is confined to the ground. At distances close to the source, energy decreases exponentially with altitude, or directly proportional to the variation of mass density with altitude. This is to

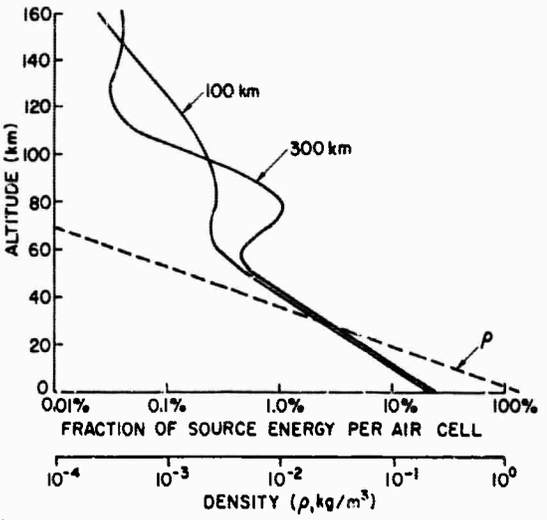

34149

FIG. 31. VERTICAL ENERGY DISTRIBUTIONS AT VARIOUS GROUND DISTANCES FROM A 400-SEC, GROUND-LEVEL POINT SOURCE.

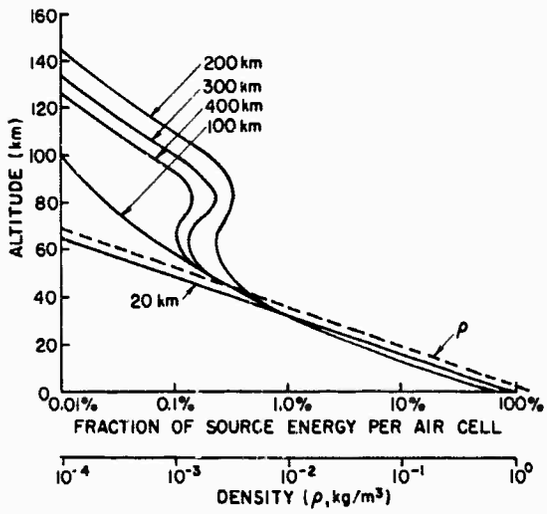

34150

FIG. 32. VERTICAL ENERGY DISTRIBUTIONS AT VARIOUS GROUND DISTANCES FROM A 500-SEC, GROUND-LEVEL POINT SOURCE.

be expected since, for frequencies below the atmospheric cutoff frequency, every air cell directly above the source moves with exactly the same velocity and the same maximum displacement. The vertical energy distribution is thus directly proportional to the vertical mass distribution.

At greater ground distances from the source, the vertical energy distribution decreases exponentially with altitude, but less severely than at close distances. A small amount of energy is trapped in the high-altitude sound duct at 90 km. For even lower frequencies, as shown in Fig. 33 for a 600-sec source, energy decreases exponentially with altitude even at great distances from the source. A very small amount of energy is still trapped in the high-altitude sound duct, but even this effect is beginning to vanish.

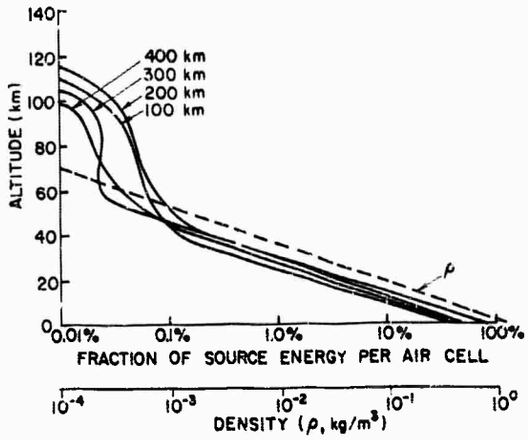

34151

FIG. 33. VERTICAL ENERGY DISTRIBUTIONS AT VARIOUS GROUND DISTANCES FROM A 600-SEC, GROUND-LEVEL POINT SOURCE.

Corresponding points on the vertical energy-distribution curves at various ground distances may be connected to provide constant-energy contours throughout the atmosphere, as shown in Fig. 34 for the 500-sec, ground-level point source. These contours should not be confused with the raytracings shown in Fig. 24, since the contours in Fig. 34 do not represent "energy-flux tubes" through which energy flows as do the raytracings. The curves in Fig. 34 represent only contours below which a constant fraction of the steady-state source energy is contained. The severe difference between the two concepts may be appreciated by considering areas in the atmosphere where the raytracings intersect as shown in Fig. 24.

Figure 34 defines a "forbidden-cone" area, above the source, in which only a very small amount of energy propagates. Nearly all of the total energy emitted by the source lies below the top contour. Only 0.1 percent of the total energy is channeled between the top two contours, while 96 percent of the energy is confined below the 40-km altitude in the atmosphere. From the curves of maximum takeoff angle and reflection height vs wave period derived from the refractive-index surface calculations in Chapter II, a 500-sec, ground-level pressure disturbance

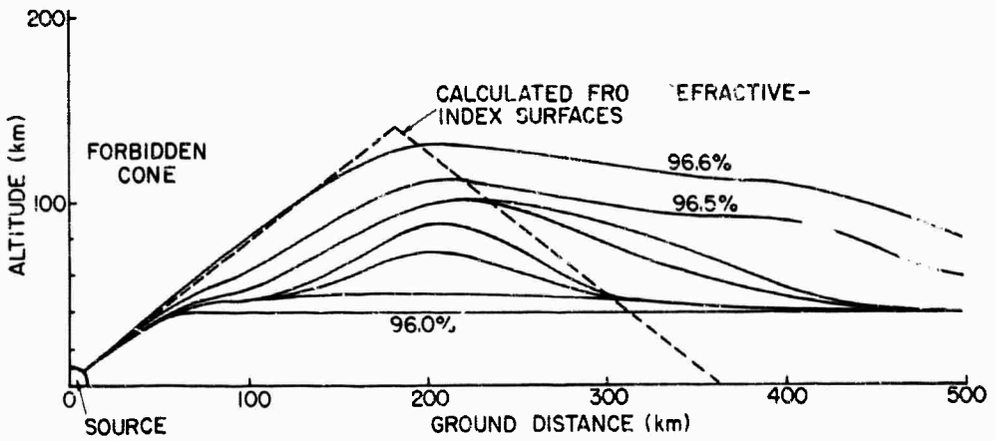

34152

FIG. 34. CONSTANT ENERGY-DENSITY CONTOURS FROM A 500-SEC, GROUND-LEVEL POINT SOURCE.

would be expected to be reflected at about a 140-km altitude, with all of the energy emitted below a 37-deg elevation angle. This situation is represented by the dashed line in Fig. 34 which compares well with the solid lines, which represent the results of the air-cell model close to the source; however, the computer model reveals focusing and ducting effects at greater distances from the source.

2. Conclusions

A number of fundamental conclusions concerning the propagation of acoustic-gravity waves in the atmosphere may be made from the analysis of air-cell orbits resulting from sinusoidal, ground-level point sources

above. Energy released by a ground-level source is confined to low altitudes for frequencies below the vertical atmospheric cutoff frequency. The degree of confinement is directly proportional to the frequency of the disturbance. Nearly all of the released energy is confined to the ground for frequencies corresponding to periods longer than 600 sec (10 min).

A smooth transition band of frequencies is observed between purely acoustic disturbances and the ground-confined, low-frequency, acoustic-gravity-wave disturbances. There is no well-defined cutoff frequency separating acoustic and acoustic-gravity disturbances. However, this transition band is approximately defined at the high-frequency end by the ground-level, vertical atmospheric cutoff frequency (corresponding to a period of about 300 sec for the computer model). This cutoff frequency depends critically on the mass-density gradient, and is therefore dependent on the temperature distribution at low altitudes in the atmosphere.

Since lower frequencies are more confined to ground level than are the higher acoustic frequencies, an observer on the ground would receive low frequencies before the higher frequencies released by a ground-level source emitting a band of frequencies. That is, group velocity inversely proportional to frequency would be deduced by the ground-level observer. Which of the low frequencies arrives earliest depends on the temperature in the lower portion of the atmosphere. This agrees with Press and Harkrider's [Ref. 14] conclusion that, "early arrivals corresponding to group velocity plateaus are controlled by the atmospheric structure below 50 km." This characteristic of acoustic-gravity waves becomes more evident in the consideration of explosive sources in a following section.

C. HIGH-ALTITUDE, SINUSOIDAL POINT SOURCES

Figure 35 displays the equilibrium air-cell orbits resulting from a sinusoidal source with a 500-sec period located at a 100-km altitude. The air-cell orbits in this figure are normalized to the same values as the ground-level sources in the preceding section.

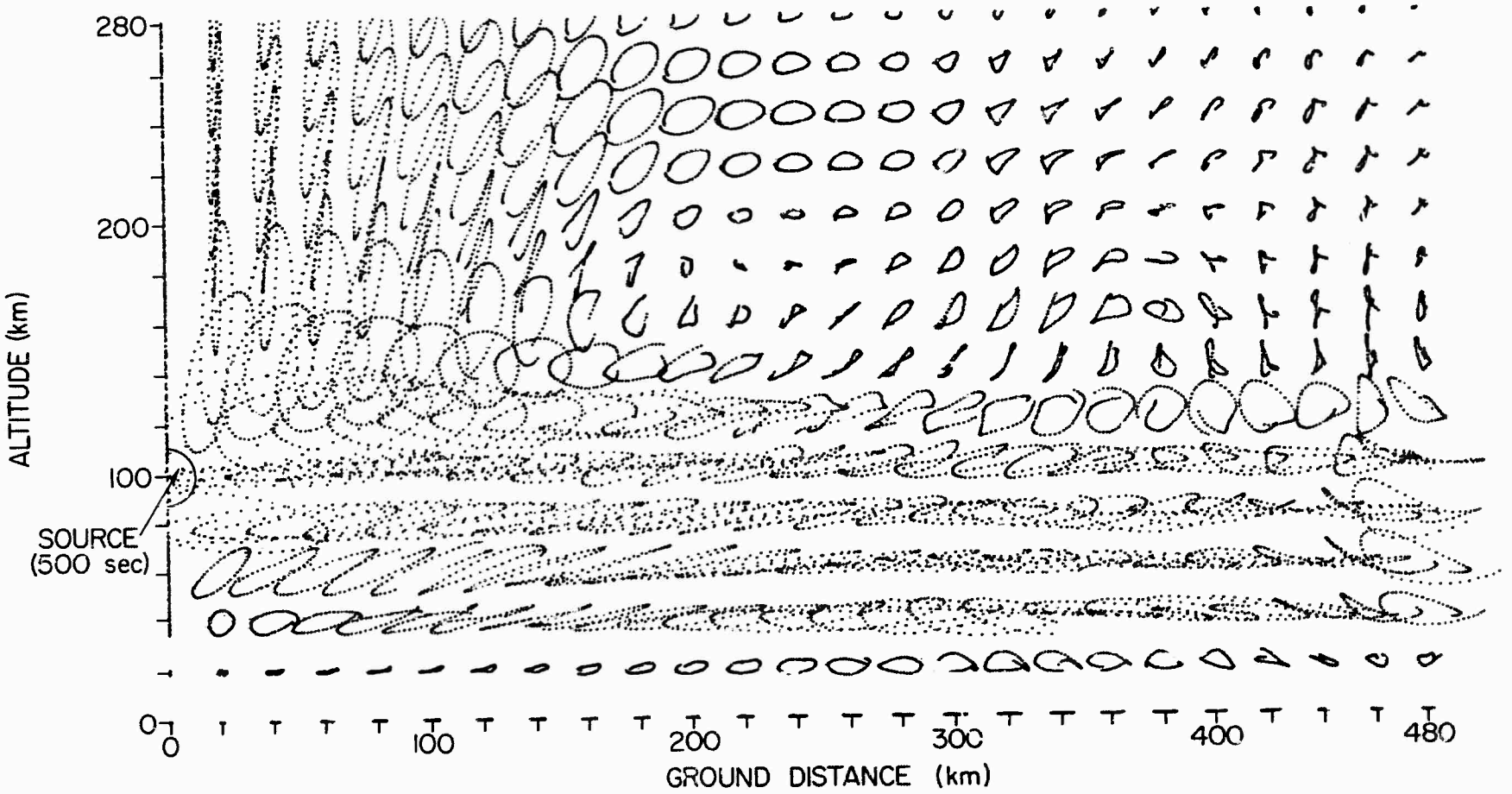

FIG. 35. EQUILIBRIUM AIR-CELL ORBITS RESULTING FROM A 500-SEC, SINUSOIDAL, 100-KM-HIGH POINT SOURCE.

The vertical atmospheric cutoff frequency depends on the vertical mass-density gradient, which varies with altitude so that the cutoff frequency will also be a function of altitude. At ground level, this cutoff corresponds to a period of 300 sec, while at a 140-km altitude the cutoff period is about 500 sec. In the area slightly above the source in Fig. 35 the 500-sec wave may propagate as an acoustic wave, but below the source this same disturbance may propagate as only an acoustic-gravity wave. A conclusion that may be drawn is that, for the low-frequency acoustic-gravity waves there is very little energy propagation in the vertical direction because the air-cell orbits are "flattened out" along the horizontal direction, as evidenced in the area below the source in Fig. 35. The area above the source appears as an acoustic medium to the high-altitude source, allowing the air-cell orbits to "stand vertically." Figure 36 displays raypaths from a 100-km-high acoustic source computed from Snell's law as described earlier, modified to eliminate the low-altitude rays. A comparison of these raypaths with the air-cell orbits in the upper portion of Fig. 35 reveals that the 500-sec source produces acoustic waves at high altitudes.

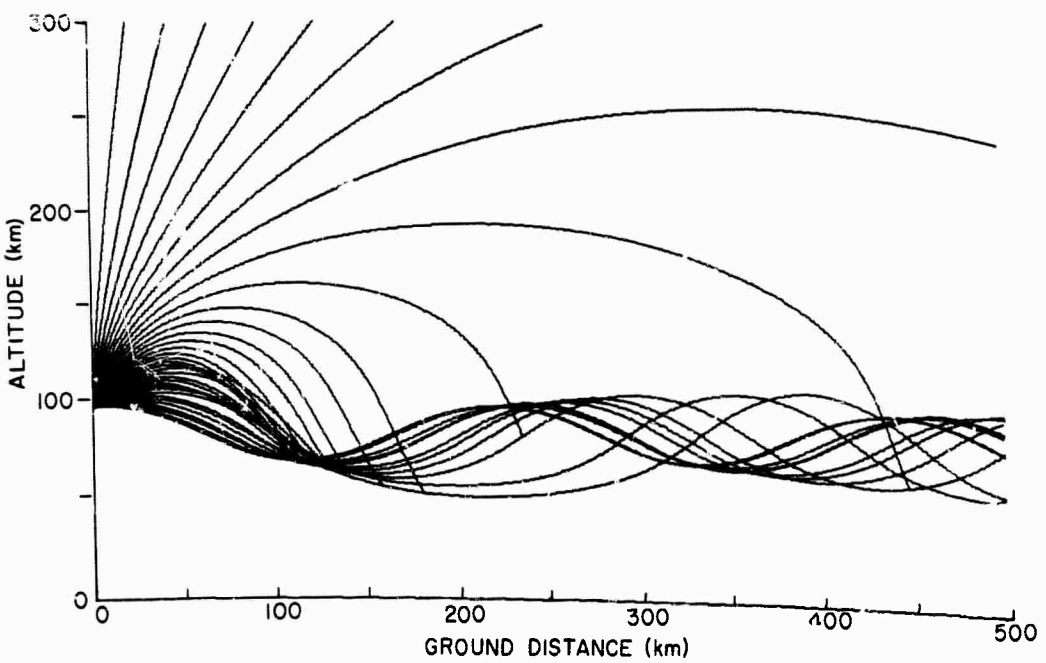

FIG. 36. RAYTRACINGS FROM A 100-KM-HIGH ACOUSTIC SOURCE (LOW-ALTITUDE RAYS REMOVED).

1. Energy Distributions

From the air-cell oribts, vertical energy-density contours at various horizontal distances from the source were calculated and appear in Fig. 37. Also in this figure is the energy distribution over a vertical path located 100 km away from the source for a uniform medium. Ground reflections will produce standing-wave patterns throughout the atmosphere for a continuous, sinusoidal source; but the wavelengths are so long (on the order of 150 km) that interference patterns do not appear.

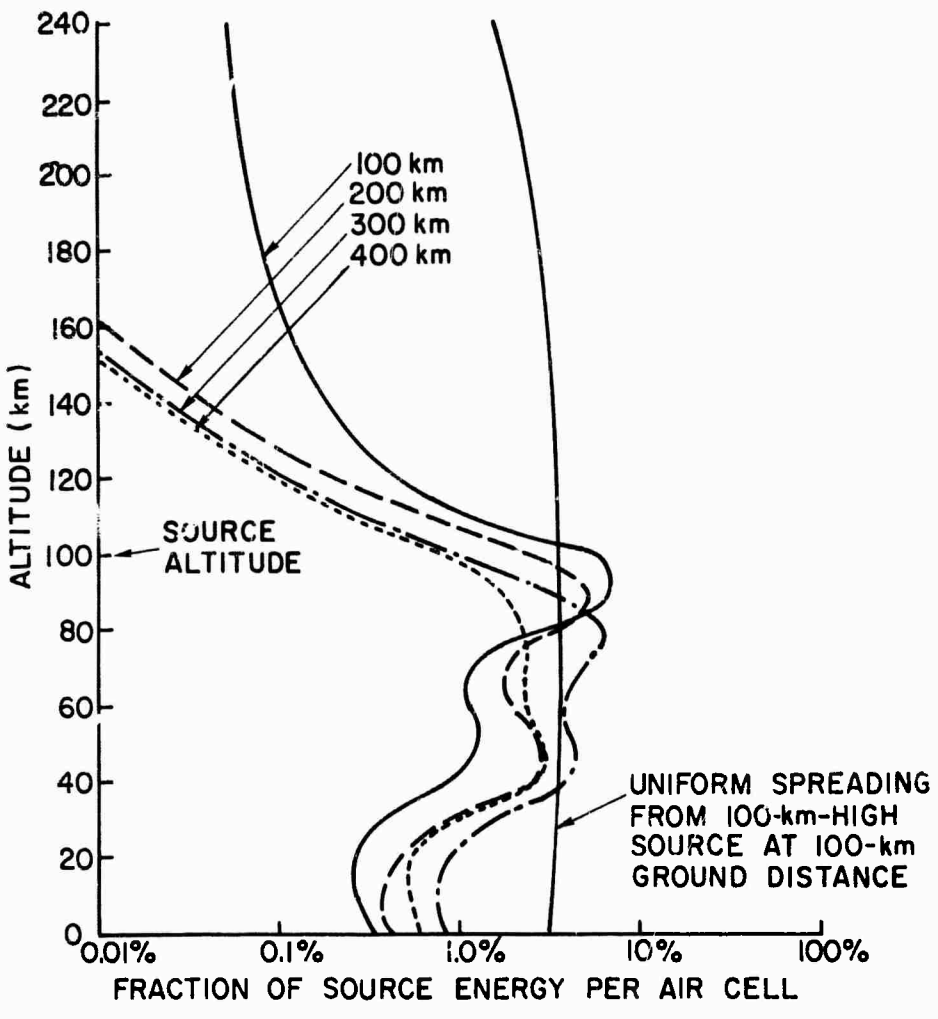

FIG. 37. VERTICAL ENERGY DISTRIBUTIONS AT VARIOUS GROUND DISTANCES FROM A 500-SEC POINT SOURCE 100-KM HIGH.

The distribution below the 100-km-altitude source is the inverse of the corresponding portion of the curve for the 200-sec, ground-level source (Fig. 29). To understand this situation, consider the following tapered electrical-transmission-line problem.

2. Electrical Analogy

Voltage e and current i measured at a distance y along a transmission line are given by

$$\frac{de}{dy} = Zi \qquad \frac{di}{dy} = Ye \ .$$

Assume a tapered transmission line for which the impedance Z and admittance Y vary as

$$Z = Z_o \exp\,[-\alpha y] \qquad Y = Y_o \exp\,[\alpha y] \ .$$

Solving for voltage e gives

$$\frac{d^2e}{dy^2} + \alpha \frac{de}{dy} - \beta^2 e = 0 \tag{4.1}$$

where $\beta^2 = ZY$.

With voltage e varying as

$$\exp\,[i(\omega t + ky)] \tag{4.2}$$

a dispersion relationship is derived,

$$-k^2 + i\alpha k + \beta^2 = 0 \tag{4.3a}$$

and

$$k = -i\,\frac{\alpha}{2} \pm \frac{1}{2}\,(4\beta^2 - \alpha^2)^{1/2} \ . \tag{4.3b}$$

The low-frequency cutoff is given by

$$\omega_c = \frac{\alpha v_p}{2}$$

below which k is completely imaginary. Here v_p is the phase velocity,

$$v_p = \frac{\omega}{\beta} = [LC]^{-1/2}$$

for a lossless line. For frequencies well below the cutoff, the choices for propagation constants are

$$k = \begin{cases} -i\alpha \\ 0 \end{cases} . \qquad (4.4)$$

For the atmospheric problem, mass density ρ is analogous to impedance Z in the electrical problem where

$$\rho(y) = \rho_o \exp [-y/H] \qquad (4.5)$$

and H is the scale height of the atmosphere defined in Chapter III. It should be understood that this analogy is strictly valid only for an isothermal atmosphere, so that the wave number k does not depend on altitude and a Fourier solution may be used. The atmospheric cutoff frequency is therefore

$$\omega_c = \frac{\alpha c}{2} \rightarrow \frac{c}{2H} = \frac{\gamma g}{2c} . \qquad (4.6)$$

Though γ, g, and c are all functions of altitude in the atmosphere, we use the transmission-line analogy and define a cutoff frequency $\omega_c = \gamma g/2c$ which then becomes a function of altitude as mentioned earlier. For frequencies well below this cutoff ω_c, pressure waves propagate with

a vertical wave number k given by the choice of Eq. (4.4) above. The selection of the proper k will depend on the imposed boundary conditions.

3. Energy-Density Profiles

The energy density throughout the atmosphere is given by

$$\frac{1}{2}\rho\bar{v}^2 = \frac{1}{2}\rho\left(v_x^2 + v_y^2\right) \text{ joules/m}^3 . \qquad (4.7)$$

At frequencies below the atmospheric cutoff ω_c, the air-cell orbits are "flattened" in the horizontal direction--i.e., $v_x \gg v_y$. Since the atmosphere is uniform in any horizontal direction, the acoustic formula for power density is also valid for acoustic-gravity waves:

$$E_d = \frac{1}{2}\rho\frac{c^3}{\gamma^2}\left(\frac{\Delta p}{p_o}\right)^2 = \frac{1}{2}\rho_o \exp\left[-y/H\right]\frac{c^3}{\gamma^2}\left(\frac{\Delta p}{p_o}\right)^2 \text{ w/m}^2 , \qquad (4.8)$$

where $(\Delta p/p_o)$ varies vertically as $\exp[y/2H]$ or $\exp[0]$ as derived in Chapter II. The first variation is interpreted as the "voltage-transformer" characteristic of the atmosphere. The two choices for the vertical energy distributions are found by inserting the two above variations into Eq. (4.8), yielding Eqs. (4.9) and (4.10) and are shown in Fig. 38.

$$E_{d1} = \frac{1}{2}\rho_o\frac{c^3}{\gamma^2}\exp[0] \qquad (4.9)$$

$$E_{d2} = \frac{1}{2}\rho_o\frac{c^3}{\gamma^2}\exp\left[-y/H\right] . \qquad (4.10)$$

It should be remembered that spreading and focusing effects must also be considered, but both are absent in the expressions above. For a ground-level source, E_{d1} would not be possible because the energy integral over an infinite path would not converge. The distribution

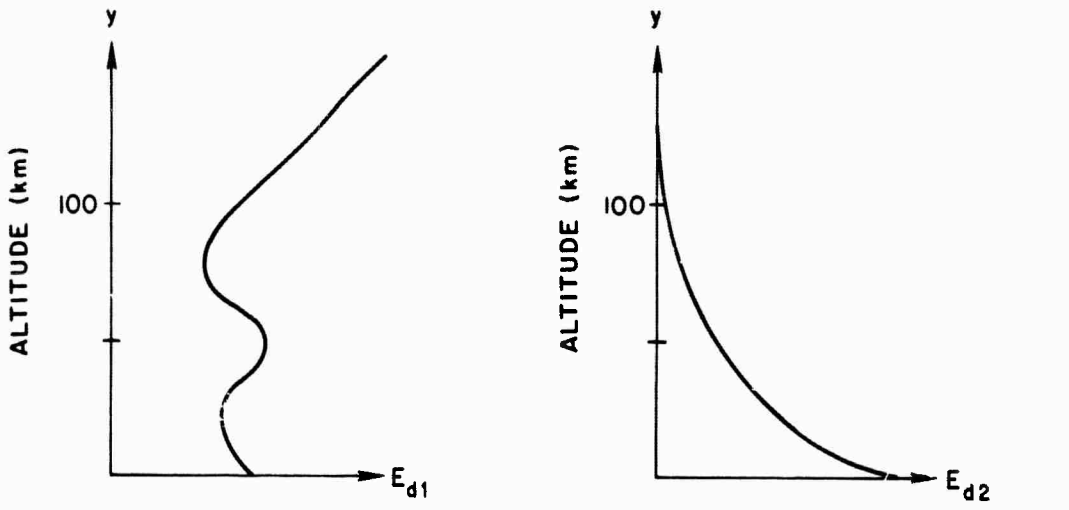

FIG. 38. CHOICES FOR VERTICAL ENERGY-DENSITY DISTRIBUTIONS.

E_{d2} would be appropriate in this case as shown in Fig. 38 for the 500-sec, ground-level point source (Fig. 32). For a high-altitude source (such as in Fig. 37), the distribution E_{d2} would not be valid below the source, since this would imply an exponential increase of energy downward. In this case the distribution E_{d1} must apply, supported by the results of the air-cell computer model as shown in Fig. 37. These energy contours include the effects of normal energy spreading ($1/r$ for the two-dimensional case where r is the distance from the source) and focusing, but more clearly have the shape of the cube of the sound-velocity profile, as would be expected from the discussion above. For the region above the source, the normal exponential distribution E_{d2} must be used.

4. Mechanical Analogy

Energy profiles in the atmosphere may be analyzed by considering a mechanical analog. Consider a one-dimensional array of particles and springs representing a vertical segment of the atmosphere in which the particle masses and spring constants generally decrease with altitude. The mechanical analog of a "sound duct," or region of sound-velocity minimum in the atmosphere, is an area of "weak springs" in the array, as shown in Fig. 39. Energy is released into the mechanical array at high altitudes by displacing the top particle very slowly at a typical acoustic-gravity-wave frequency. Since the mass of particles in the array increases

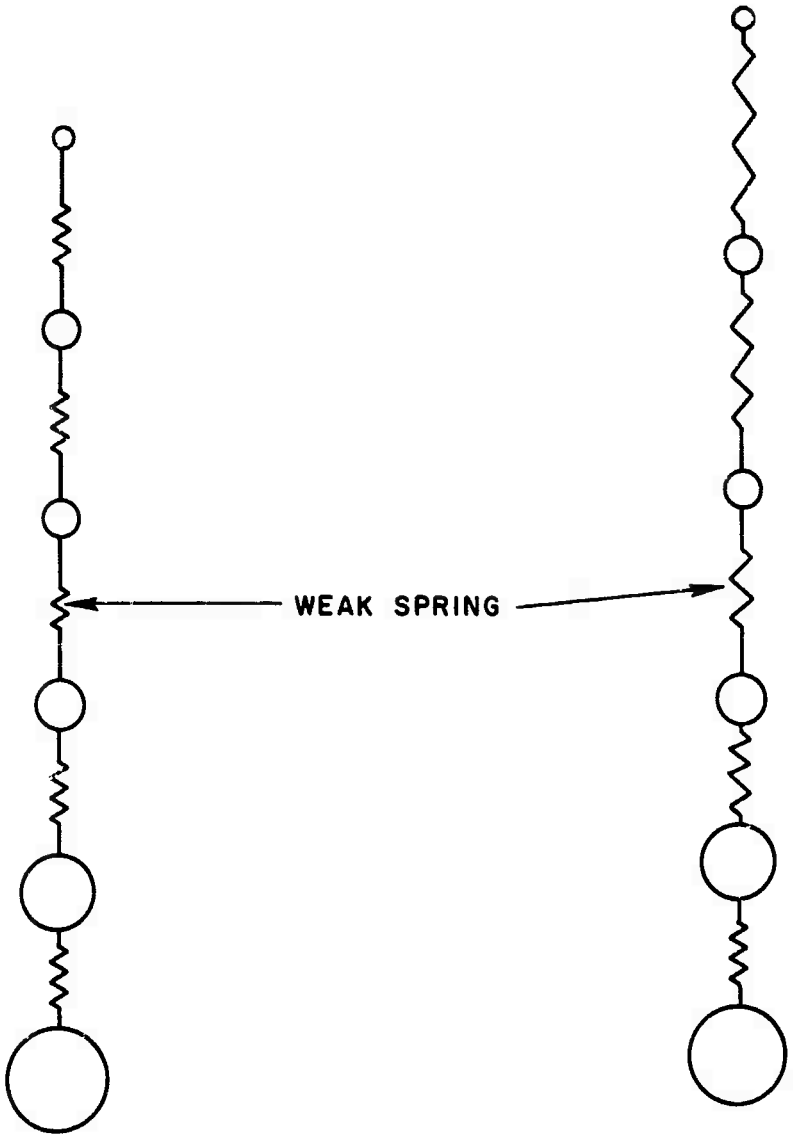

FIG. 39. MECHANICAL ANALOGY OF A SOUND DUCT.

with distance downward from the source, the displacements of these particles will decrease with downward distance, if, for the moment, we ignore the spring constants. The weak spring representing the area of the sound duct will stretch more than the neighboring springs above and below that segment and the particles in the sound duct will be displaced less. Energy minima will be found at altitudes corresponding to the sound ducts and the vertical energy profile will be proportional to the vertical sound-velocity or temperature profile in the atmosphere.

Figure 40 displays the energy contours throughout the atmosphere resulting from a 500-sec, sinusoidal source located 100 km high. As explained earlier, the number on each contour specifies the fractional portion of source energy contained below this contour. Again, these contours should not be confused with acoustic raytracings.

The high-altitude, 500-sec point source is a particularly interesting example because it vividly illustrates the differences between wave propagation in an acoustic medium and an acoustic-gravity-wave medium. In the area below the source in Fig. 35 the medium presents a higher acoustic impedance in the vertical direction than in the horizontal direction, as evidenced by the air-cell orbits. Energy is so constrained to move only in the horizontal direction below the source that hardly any energy at all propagates directly downward. A forbidden-cone area is discernable below the source in which energy is almost completely absent. For this example, at least, it could be concluded that the safest place to be during a high-altitude explosion containing no higher frequencies than 1/500 cps (2 mc) is directly below the blast!

On the other hand, the character of the atmosphere at high altitudes is such that the area above the source in Fig. 35 represents a nearly perfect acoustic medium, as evidenced by the arbitrary orientation of air-cell ellipses. Most of the energy released by the source is forced to escape upward as acoustic waves.

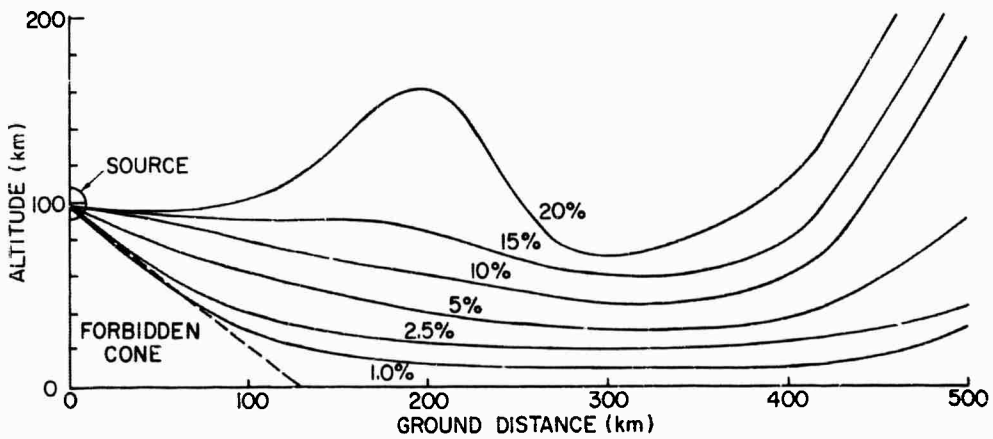

34154

FIG. 40. ENERGY-DENSITY CONTOURS RESULTING FROM A 500-SEC POINT SOURCE AT A 100-KM ALTITUDE.

D. EXPLOSIONS IN THE ATMOSPHERE

At distances close to an explosive source in the atmosphere, the situation is nonlinear and the resulting shock wave cannot be analyzed with the linear air-cell computer model. However, at greater distances from the blast the magnitude of the shock wave is sufficiently reduced to allow a linear treatment of the resulting pressure disturbance. Detailed calculations of pressures, densities, temperatures, and velocities vs time resulting from a spherical blast have been made by Brode [Ref. 27], whose findings have been verified in experiments involving actual explosions. The distance from the blast center to the linear region, and the wave shapes of pressure vs time are both dependent on the blast energy. The linear pressure disturbance may be filtered to eliminate frequencies above the useful range of the air-cell computer model and then programmed into the computer model.

The Defense Research Division of Sweden has conducted measurements of pressure disturbances resulting from Russian nuclear tests in 1962 [Ref. 28]. The locations of the microbarographs used in these experiments at Kiruna, Uppsala, and Stockholm are shown in Fig. 41 with respect to the Russian testing area. The frequency response of these barographs is shown in Fig. 42. The highest useful frequency for the air-cell computer model is 1/200 cps or 5 mc. A ground-level explosive impulse (properly

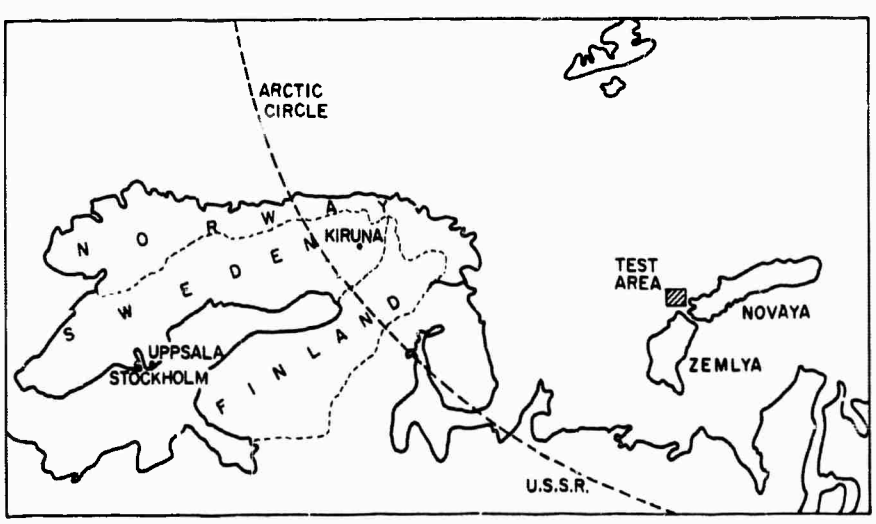

FIG. 41. MICROBAROGRAPH LOCATIONS WITH RESPECT TO RUSSIAN NUCLEAR EXPLOSIONS.

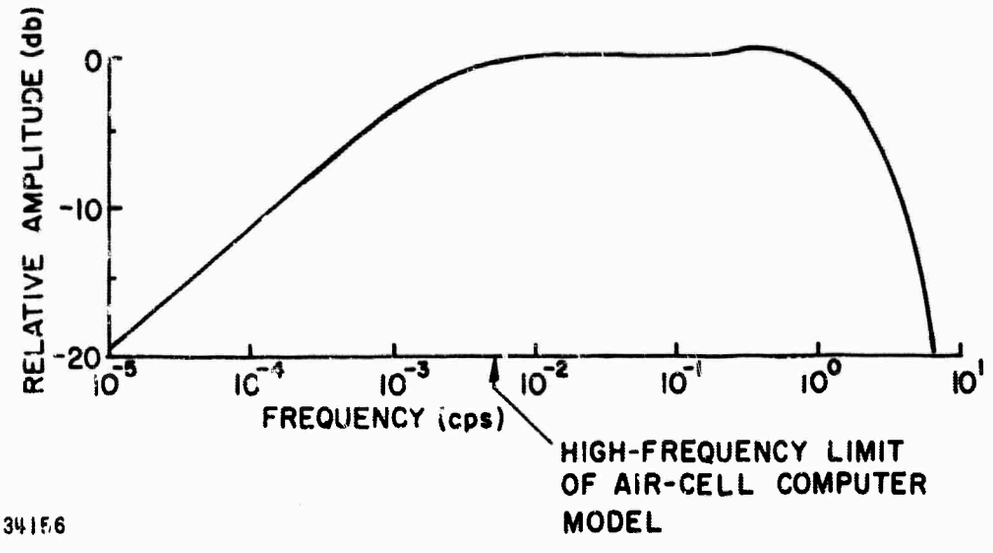

FIG. 42. FREQUENCY RESPONSE OF BAROGRAPHS USED AT KIRUNA, UPPSALA, AND STOCKHOLM.

filtered) was programmed into the computer model and the resulting ground-level barogram at a 450-km distance from the blast is shown in Figs. 43 and 44 for comparison with actual experimental barograms resulting from nuclear explosions. The vertical scale is measured in microbars (μb), where the ambient pressure p_o is 10^6 μb or 1 bar; the ordinate is time with a 10-min scale, as indicated. The closest available barogram was recorded at Kiruna, at a distance of approximately 1350 km in comparison with the 450 km distance of the synthetic barogram. The most significant factor affecting the structure of these barograms, however, is the temperature of the lower atmosphere. Distance to the source merely determines the scale of maximum overpressure, as can be seen by comparing records made at greater distances at Uppsala and Stockholm. The experimental barograms in Fig. 44 are catagorized by Wägner, Araskog, and Edin [Ref. 28] as an "A1 type gravity wave" and, in the opinion of these authors, "can appear in a textbook as a typical example of gravity waves. The A1 gravity wave is characterized by a slow first period followed by 4 - 5 periods with almost twice the frequency of the first. The amplitude is sustained for these cycles." This observation coincides with the data recorded in Great Britain after the Great Siberian Meteor on 30 June 1908 [Ref. 8] and also agrees with the barograms recorded during nuclear tests over a world-wide network of instruments reported by Donn and Ewing [Refs. 7, 9]. The experimental barograms in Fig. 43 are classified by

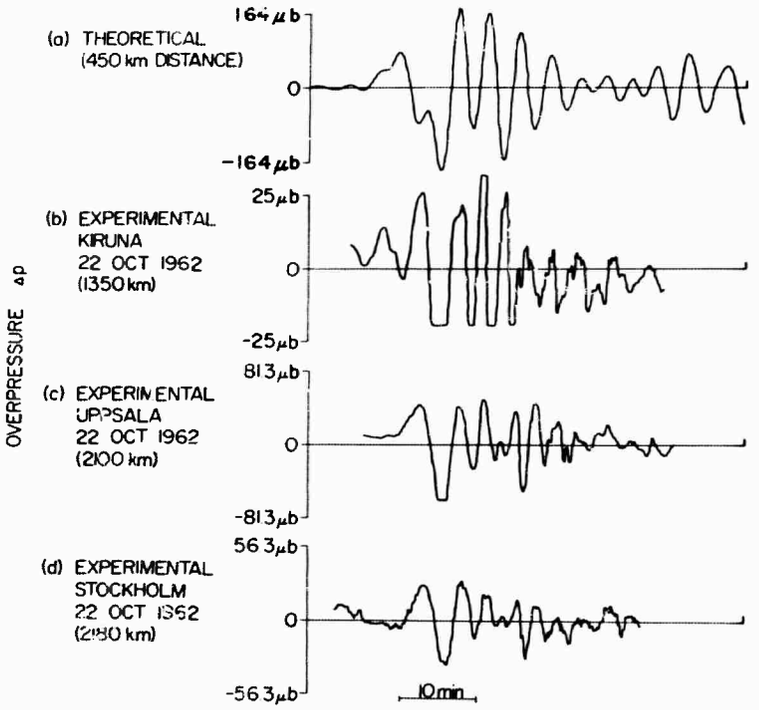

FIG. 43. COMPARISON OF THEORETICAL BAROGRAMS COMPUTED FROM THE AIR-CELL MODEL WITH BAROGRAMS RECORDED AFTER THE RUSSIAN NUCLEAR EXPLOSION AT NOVAYA ZEMLYA ON 22 OCTOBER 1962 (0906 GMT).

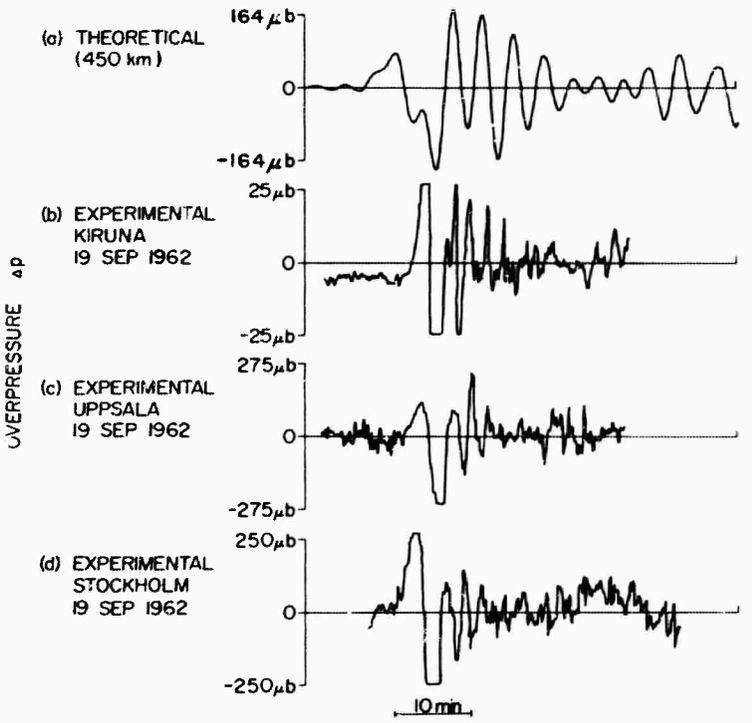

FIG. 44. COMPARISON OF THEORETICAL BAROGRAMS COMPUTED FROM THE AIR-CELL MODEL WITH BAROGRAMS RECORDED AFTER THE RUSSIAN NUCLEAR EXPLOSION AT NOVAYA ZEMLYA ON 19 SEPTEMBER 1962 (2042 GMT).

Wägner, Araskog, and Edin as an "A2 gravity wave," where "A2 is a modification of type A1. The frequency does not change so abruptly and the amplitude starts to decrease sooner."

1. Temperature Effects

A comparison of theoretical and experimental barograms in Figs. 43 and 44 reveals the importance of the vertical temperature profile at low altitudes in the atmosphere.

The atmospheric resonant frequency, or Väisälä frequency introduced in Chapter II and discussed with the help of an electrical analogy in Section C of this chapter, depends on the variation of density in the atmosphere. The density profile in the atmosphere is determined by the vertical temperature gradients.

The experimental records were made within the Arctic Circle, where temperatures in the lower atmosphere are much colder than that of the "Standard Atmosphere" used for the computer model. Figure 45a compares the two different temperature profiles. Colder temperatures at the base of the atmosphere will result in steeper mass-density changes with altitude as shown in Fig. 45a. The net effect is that the atmospheric resonant frequency is increased as shown in Fig. 45b.

Figure 45b shows the variation of the resonant frequency with altitude for the two different temperature profiles.

The period of the earliest arriving pressure disturbance is defined by aeronomists as the "fundamental period" of the acoustic-gravity wave [Ref. 20] and is dependent on the Väisälä frequency, as indicated by the results of the previous equilibrium analysis. The fundamental period is defined as the time between arrival times of the first two positive-pressure peaks. The barograms in Figs. 43 and 44 reveal a fundamental period of 450 sec for the computer-model data and fundamental periods between 250 and 300 sec for the experimental data. The Väisälä frequencies at ground level for the two different cases are 500 sec and 280 sec respectively, as shown in Fig. 45b.

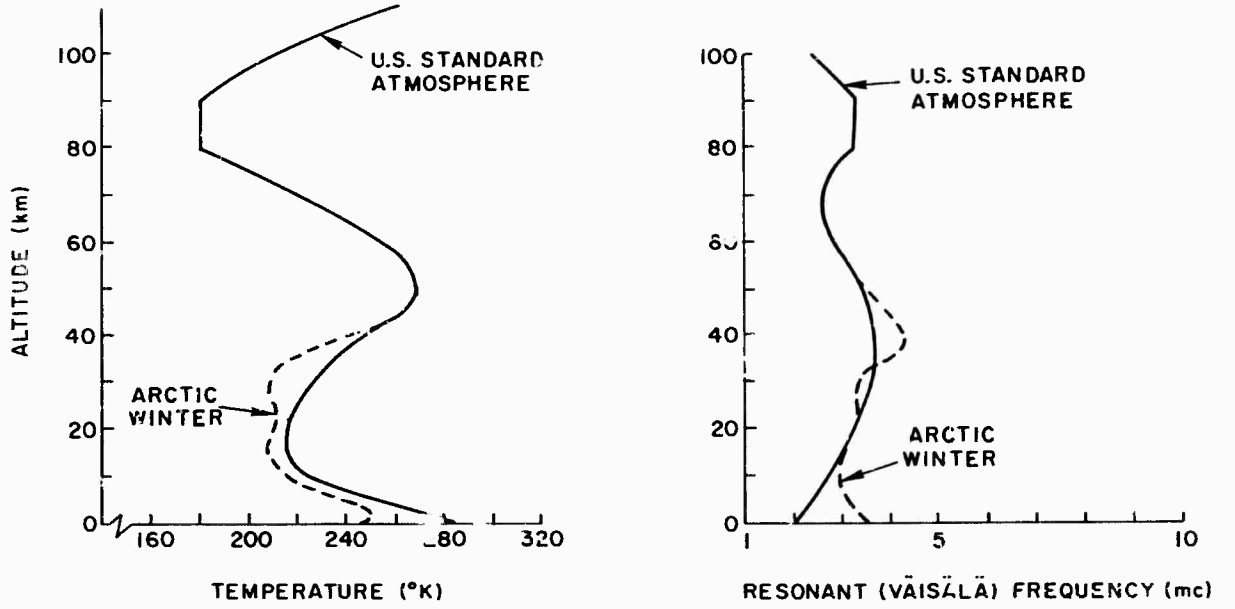

35380

a. Temperature profiles

b. Resonant (Väisälä) frequencies

FIG. 45. COMPARISON OF ARCTIC WINTER WITH U.S. STANDARD ATMOSPHERE.

2. Scale of Pressure Disturbance

The estimated yields of the Russian nuclear tests of 19 September 1962 and 22 October 1962 were on the order of 10 MT (megatons). The pressure waveform at a 31.2-km distance from a 10-MT explosion is shown in Fig. 46a as extrapolated from Brode's calculations [Ref. 27]. The

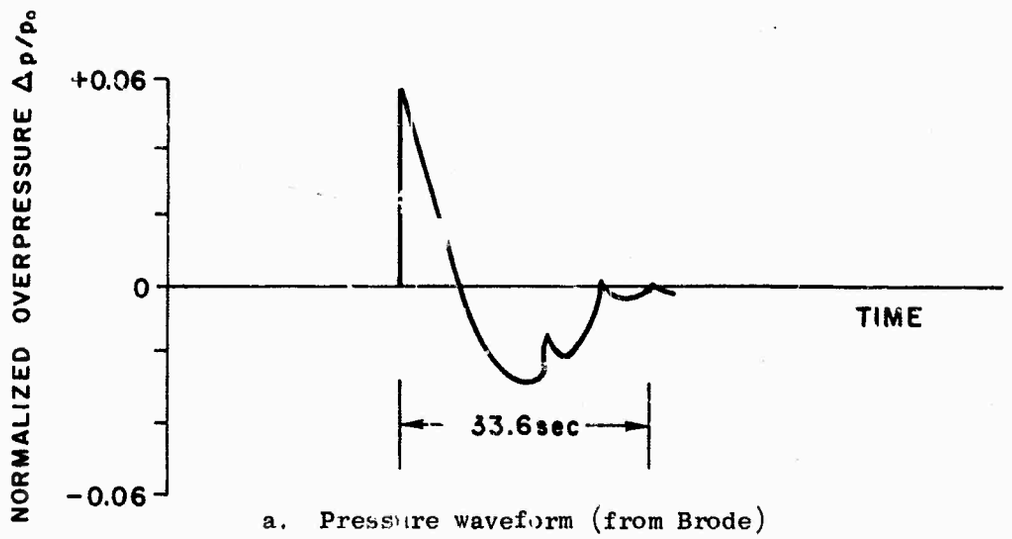

a. Pressure waveform (from Brode)

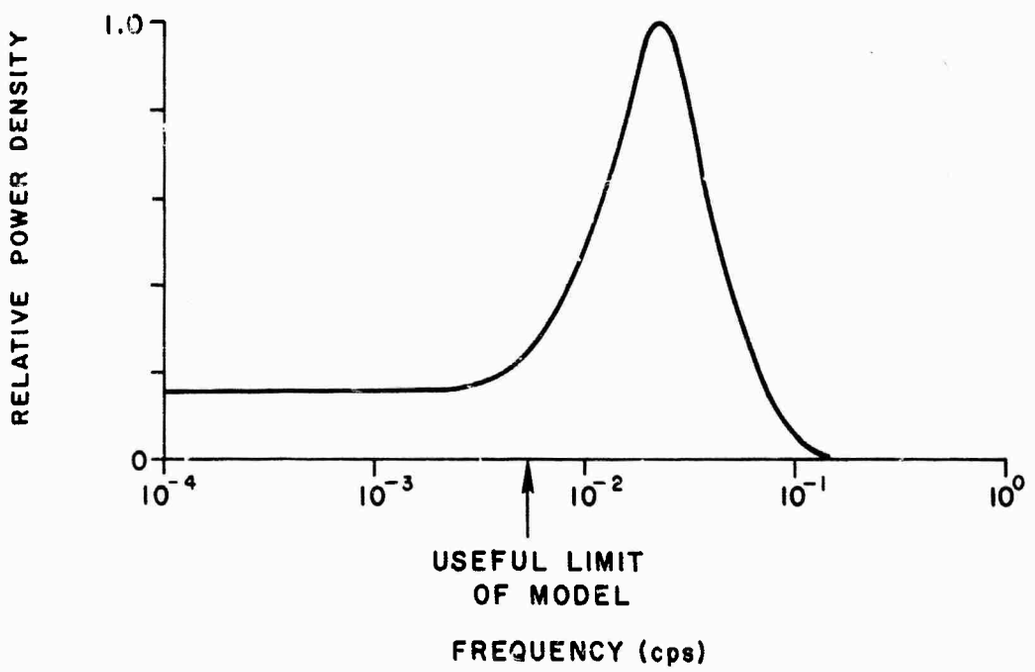

35379

b. Power spectrum of waveform

FIG. 46. PRESSURE DISTURBANCE OF 10-MT EXPLOSION AT 31.2-KM DISTANCE.

power spectrum of this pressure waveform is shown in Fig. 46b with the maximum useful frequency of the air-cell computer model also indicated. As stated above, all frequencies above the useful cutoff frequency of the model are filtered and the resulting waveform is programmed into the model. The scale of the resulting pressure waveform is calculated as follows.

As stated in Chapter III, it is assumed that at very close distances (of the order of a cell dimension d_o) to an energy source in the computer model, waves begin to propagate as if in a uniform medium, forming symmetrical cylindrical wavefronts, but at greater distances are deformed because of nonuniformity of the medium. A point source in the real atmosphere is corrected to a filament source in the computer model by a $1/r$ factor, where r is the radial distance from the source. A $1/r$ factor is also used to correct energy densities calculated at great distances from the source in the computer model back to the real atmosphere. The only purpose of this tenuous calculation is to provide a "ball-park" check of the theoretical barograms with the experimental data.

Applying these corrections, we calculate pressure from the computer model at a 450-km distance from the source (including all spreading effects);

$$\frac{\Delta p}{p_o} \text{ (450 km)} = 0.0068 \ .$$

From Fig. 46b only 0.058 percent of the total energy contained in this pressure waveform resides below the model cutoff frequency of 5 mc. Therefore, the maximum normalized overpressure of the synthetic barogram should be given as

$$\frac{\Delta p}{p_o} \text{ (450 km)} = 0.0068 \times (5.8 \cdot 10^{-4})^{1/2} = 1.64 \times 10^{-4} \ .$$

The ambient pressure p_o is 10^6 μb, so that the maximum overpressure is

$$\Delta p_{max} = 164 \text{ μb} .$$

The calculated scale for the synthetic barogram is comparable with the experimental records.

3. Summary

The most obvious characteristic of acoustic-gravity waves resulting from surface explosions and recorded on the ground is the dispersive relationship whereby group velocity decreases with increasing period (wavelength). The period of the earliest arriving disturbance in the dispersive wavetrain is critically dependent on the lower-altitude temperature profile in the atmosphere. Donn and Ewing [Ref. 7] in fact recommend that, as is done for seismic studies, the atmospheric model should be adjusted for the best fit between empirical and theoretical data on acoustic-gravity waves to provide a reliable description of the atmosphere.

In the very low frequency range of acoustic-gravity-wave propagation, the frequency spectra of the pressure waveforms resulting from even the largest explosions are essentially "flat," so that the waveshapes of the received barograms are nearly independent of blast size.

E. HIGH-ALTITUDE BAROGRAMS RESULTING FROM A GROUND-LEVEL SOURCE

Figure 47 displays barograms at various altitudes in the atmosphere, all at a 450-km ground distance from a ground-level explosive source. As would be expected, the waveforms contain little low-frequency energy. And since frequencies above the model cutoff have been filtered, these pressure waveforms contain frequencies in a very limited range between this cutoff and the lower limit provided by the ground confinement of acoustic-gravity waves. The most significant features of these barograms are the arrival times of the disturbances, which may be directly explained by existing geometric acoustic theory and the raytracings in Fig. 24.

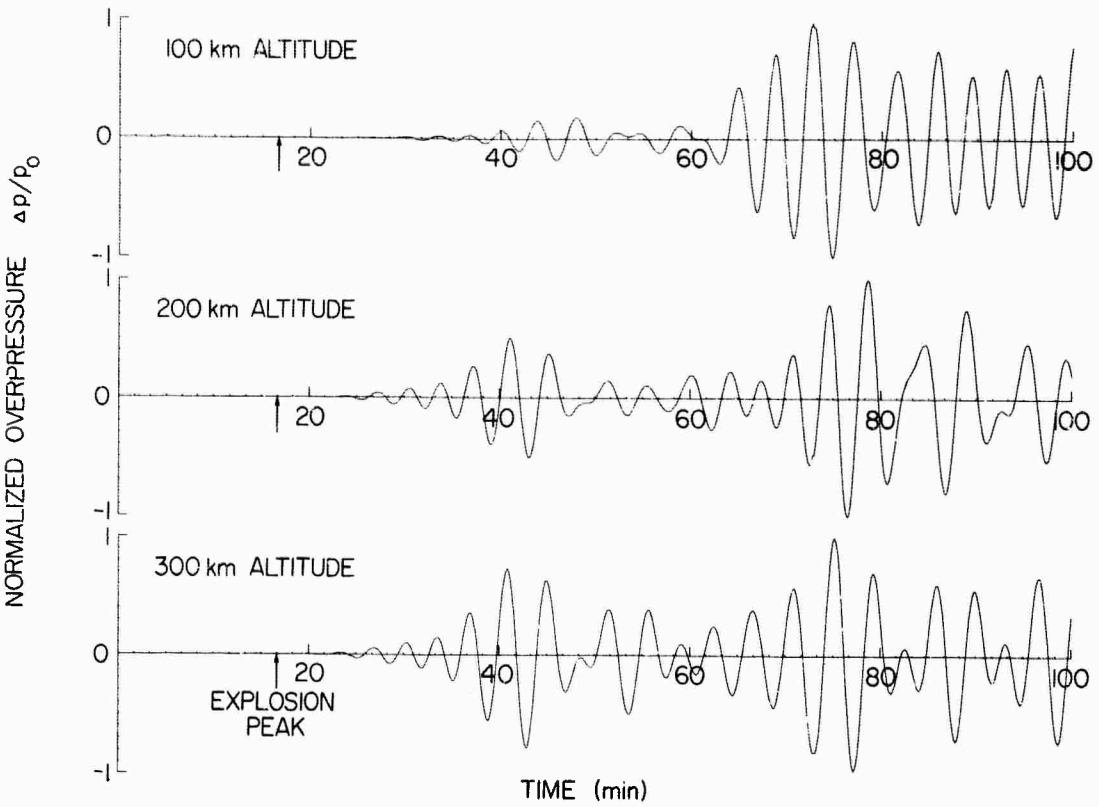

FIG. 47. THEORETICAL BAROGRAMS AT VARIOUS ALTITUDES IN THE ATMOSPHERE AT A GROUND DISTANCE OF 450 KM FROM A GROUND-LEVEL EXPLOSION.

F. HIGH-ALTITUDE EXPLOSION

An explosive source at a 100-km altitude was programmed into the air-cell computer model. As in the ground-level explosion, the most appropriate medium for analyzing the "transient" behavior of the atmosphere is a motion picture, which cannot be displayed in this report. Figure 48, however, does show a number of ground-level barograms resulting from a high-altitude explosion at various ground distances. All of these waveforms have been normalized to the same scale. As would be expected, magnitudes and arrival times decrease with increasing distance. Also as would be predicted from the equilibrium analysis above, an increase of lower-frequency energy is observed with increasing ground distance.

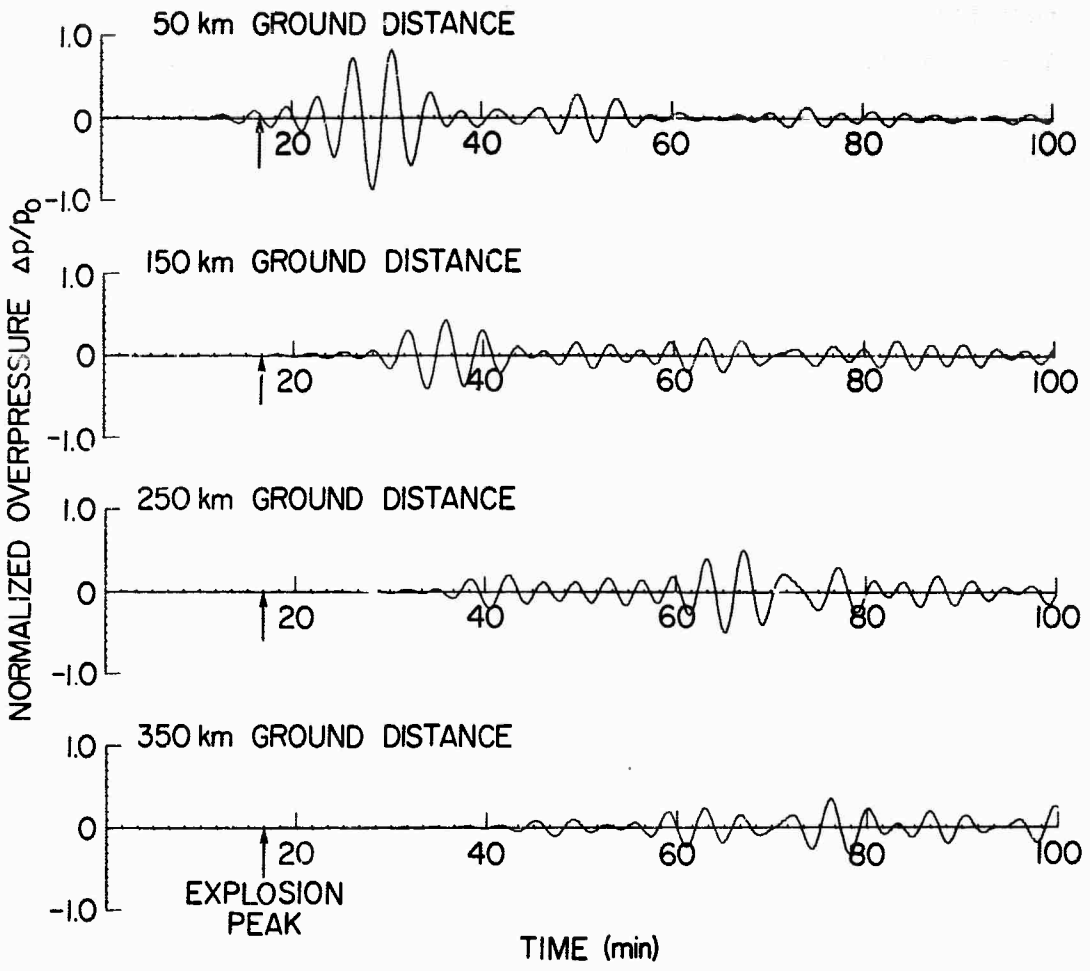

FIG. 48. THEORETICAL GROUND-LEVEL BAROGRAMS AT VARIOUS DISTANCES FROM AN EXPLOSION AT 100-KM ALTITUDE IN THE ATMOSPHERE.

G. MOTION-PICTURE OUTPUT OF THE COMPUTER MODEL

Motion pictures were produced by plotting the position of each particle on a frame of 35-mm photographic film and advancing the film at each time increment (equal to 10 sec). The 35-mm film strip was reduced to 16 mm and projected with a standard "home-movie" projector. Tapes of data prepared by an IBM 7090 digital computer were processed by a Stromberg-Carlson 4020 High-Speed Microfilm Recorder to produce the movie. A motion picture depicting motions resulting from the 200-sec, ground-level sinusoidal source, the ground-level explosion, and the 100-km-high explosion has been produced and may be obtained from the author. This movie,

entitled "The Air-Cell Computer Model of the Atmosphere" [Ref. 29] runs approximately 5 min and may be projected on a standard 16-mm silent projector. New details and perspective on mechanical wave motions in the atmosphere can be appreciated only by viewing this movie.

V. CONCLUSIONS

A computer model specifically developed to analyze the behavior of acoustic-gravity waves in the atmosphere has revealed a number of important characteristics of very low-frequency pressure-wave propagation in the atmosphere:

1. A definite "cutoff frequency" separating acoustic from acoustic-gravity-wave disturbances does not exist; rather, a smooth transition band of frequencies (corresponding to a band of periods of the order of a few hundred seconds) separates the two types of wave propagation.

2. Acoustic-gravity-wave energy released by ground-level sources is confined to low altitudes in the atmosphere. The degree of confinement depends on the period (wavelength) of the disturbance to such an extent that energy released from ground-level sources with periods longer than 10 min travels very close to the ground.

3. The low-altitude confinement of acoustic-gravity waves mentioned above accounts for an increasing group velocity with decreasing source-frequency relationship observed for many years on ground-based barograph records made during explosions in the atmosphere.

   Higher-frequency acoustic energy is released into the upper atmosphere more effectively than is the lower-frequency acoustic-gravity-wave energy, but arches downward to earth because of the change of sound speed with altitude in the atmosphere. The lower-frequency acoustic-gravity-wave energy travels at very low altitudes. Therefore acoustic-gravity-wave energy has a shorter distance to travel between source and receiver than the higher-frequency acoustic energy, as shown in Fig. 49, accounting for the early arrival of low-frequency energy.

4. The frequency of the earliest-arriving disturbance is critically dependent on the temperature of the lower atmosphere. This effect is possibly best understood with the help of the tapered-electrical-transmission-line analogy, where changes in temperature have the effect of altering the taper and hence the cutoff frequency of the electrical line. An adjustment of the atmospheric model to provide the best agreement between theoretical and empirical barograms might provide a good description of the lower atmosphere.

5. A forbidden-cone area above ground level, and above and below a high-altitude acoustic-gravity source may be discerned.

   Only a very small fraction of the released energy propagates into this area. This is, in fact, only a restatement of Item 2 above. The apex angle of this cone depends on the period (wavelength) of the source.

6. Because of the ground confinement of acoustic-gravity-wave energy, low frequencies are almost completely filtered out of high-altitude barograms resulting from ground-level explosions. This suggests that a completely geometric acoustic analysis is a good approximation for this situation.

7. The animated output of the computer model also provides new insight into the propagation of acoustic-gravity waves in the atmosphere which can be appreciated only by viewing a motion picture. Transient phenomena and large-scale motions in the atmosphere resulting from explosions are displayed by this motion-picture technique.

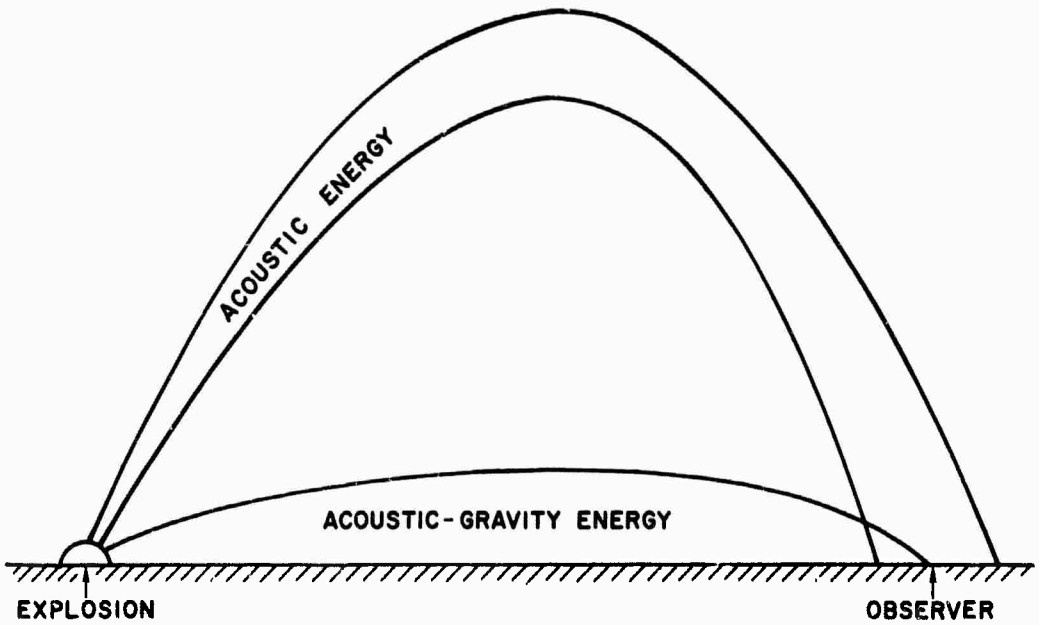

34391

FIG. 49. GROUND CONFINEMENT OF ACOUSTIC-GRAVITY WAVES.

VI. POSSIBLE FUTURE EXTENSIONS

The results of this report (cell orbits, pressure wave forms, energy spreading, etc.) are obtained by programing on a digital computer the equations of motion (Eqs. 3.63 and 3.64) of a mechanical array of masses and springs. The model can be shown to be a rigorous analog of the atmosphere only for irrotational motion. This limitation should not affect the validity of the results presented here since only irrotational sources of energy were considered. It has been suggested, however, that second-order errors (arising from the use of finite difference equations rather than differential equations) may introduce shear motions into the model. Energy stored in shear stresses might then propagate through the model in a manner not typical of the atmosphere. The difficulty could be overcome by programing instead the true hydrodynamic equations (Eqs. 3.56 and 3.57). This was attempted once without success, for reasons not understood. A successful programing of these equations and duplication of the present results using them would not only strengthen one's confidence in the results, but would also allow the model to be used for more general sources of energy, including those which involve a curl.

It was suggested in Chapter III that the present two-dimensional array with mass and spring constants independent of horizontal distance could be replaced by an array whose constants vary with distance. It would be possible in this way to simulate the behavior of rings concentric to a vertical line of symmetry, and the response of the three-dimensional atmosphere to a point source of energy could then be rigorously simulated.

The present model assumes linearity throughout. It is known that this assumption is violated in the case of high-energy disturbances (such as atomic bombs, volcanic eruptions, and probably earthquakes). The model could be extended to portray the nonlinear case by substitution of nonlinear springs in the computer model.

It might be possible to use the present model in reverse to locate or describe an energy source from an observed pressure disturbance. One would insert as initial conditions (necessarily curl-free with the present mass-and-spring model) the observed pressure disturbance and observe this distributed energy as it converges onto a source.

The flexibility of the air cell computer model is limited only by the available display facilities. With the motion picture output of the computer, incomprehensible quantities of numbers are eliminated as the standard form of computer output and new details and insight into mechanical wave propagation in the atmosphere are provided--details never before obtainable. Computer calculations need be performed only once for a given energy input configuration and the resulting atmospheric oscillations are recorded on magnetic tape. These data may be reinserted into the model any number of times to extend the solutions in either the vertical or horizontal directions. The major computational effort is thereby reduced to extracting the desired data from the magnetic tapes.

REFERENCES

1. C. O. Hines, "Internal Atmospheric Gravity Waves at Ionospheric Heights," Can. J. Phys., 38, 1960, pp. 1441-1481.

2. C. O. Hines, "Correction to 'Internal Atmospheric Gravity Waves at Ionospheric Heights'," Can. J. Phys., 42, 1964, pp. 1424-1427.

3. I. Newton, Principia, Book II, 1686.

4. G. Symond (editor), The Eruption of Krakatoa and Subsequent Phenomena, Trubner and Co., London, 1888.

5. R. Verbeek, "Krakatoa," Batavia, 1886.

6. Lt. Cen. Strachey, "The Eruption of the Krakatoa," Report of the Krakatoa Committee of the Royal Society, 1888.

7. W. L. Donn and M. Ewing, "Atmospheric Waves from Nuclear Explosions--Part II; The Soviet Test of 30 October 1961," J. Atmospheric Sci., 19, May 1962, pp. 264-273.

8. F. J. W. Whipple, "The Great Siberian Meteor and the Waves, Seismic and Aerial, Which It Produced," Quart. J. Roy. Met. Soc., 56, 1930, p. 287.

9. W. L. Donn and M. Ewing, "Atmospheric Waves from Nuclear Explosions," J. Geophys. Res., 65, 1962, pp. 1855-1866.

10. P. S. Laplace, Traite de Mechanique Celeste, 1799.

11. Sir Horace Lamb, Hydrodynamics, 6th edition, Cambridge University Press (also Dover), 1932.

12. C. L. Pekeris, "The Propagation of a Pulse in the Atmosphere," Proc. Roy. Soc., A 171, 1939, pp. 434-449.

13. C. L. Pekeris, "The Propagation of a Pulse in the Atmosphere, Part II," Phys. Rev., 73, 3, 15 Jan 1948, pp. 145-154.

14. F. Press and D. Harkrider, "Propagation of Acoustic-Gravity Waves in the Atmosphere," J. Geophys. Res., 67, 10, Sep 1962, pp. 3889-3908.

15. D. Harkrider, "Theoretical and Observed Acoustic-Gravity Waves from Explosive Sources in the Atmosphere," J. Geophys. Res., 69, 24, Dec 1964, pp. 5295-5321.

16. R. L. Pfeffer, "A Multi-Layer Model for the Study of Acoustic-Gravity Wave Propagation in the Earth's Atmosphere," J. Atmospheric Sci., 19, May 1962, pp. 251-255.

17. R. L. Pfeffer and J. Zarichny, "Acoustic-Gravity Wave Propagation in an Atmosphere with Two Sound Channels," Geofisica Pura e Applicata, 1963, pp. 54-56.

18. R. L. Pfeffer and J. Zarichny, "Acoustic-Gravity Wave Propagation from Nuclear Explosions in the Earth's Atmosphere," J. Atmospheric Sci., 19, May 1962 pp. 256-263.

19. Ivan Tolstoy, "Modes, Rays, and Travel Times," J. Geophys. Res., 64, 7, Jul 1959, pp. 815-821.

20. Carl Eckart, Hydrodynamics of Oceans and Atmospheres, Pergamon Press, London, 1960.

21. L. Brillouin, Wave Propagation in Periodic Structures, McGraw-Hill Book Company (also Dover), 1946.

22. F. Harlow and J. Fromm, "Computer Experiments in Fluid Dynamics," Sci. Am., 212, 3, Mar 1965 p. 104.

23. H. Kolsky, "A Method for the Numerical Solution of Transient Hydrodynamic Shock Problems in Two Space Dimensions," Los Alamos Sci. Lab. Rept. LA-1867, Sep 1954.

24. Martha Evans and Francis H. Harlow, "The Particle-in-Cell Method for Hydrodynamic Calculations," Los Alamos Sci. Lab. Rept. LA-2139, Sep 1954.

25. G. Barry, "Ray Tracings for Acoustic Waves in the Upper Atmosphere," J. Atmospheric Terrest. Phys., 25, Nov. 1963, pp. 621-629.

26. NASA, USAF, U.S. Weather Bureau, "U.S. Standard Atmosphere, 1962."

27. Harold L. Brode, "Blast Wave from a Spherical Charge," Phys. Fluids, 2, 2, Mar-Apr 1959, pp. 217-229.

28. H. Wägner, R. Araskog, and K. Edin, "Microbarographic Recordings of Nuclear Weapon Tests, May 6 - Dec 25, 1962," Forvarets Forskningsanstalt Avdelning, Stockholm, Jul 1963.

29. T. A. Potemra, "The Air-Cell Computer Model of the Atmosphere," Tech. Motion Picture TMP-110, Stanford Electronics Laboratories, Stanford, Calif., Oct 1965.

UNCLASSIFIED
Security Classification

DOCUMENT CONTROL DATA - R&D

(Security classification of title, body of abstract and indexing annotation must be entered when the overall report is classified)

1. ORIGINATING ACTIVITY *(Corporate author)*
Stanford Electronics Laboratories
Stanford University, Stanford, California

2a. REPORT SECURITY CLASSIFICATION
UNCLASSIFIED

2b. GROUP

3. REPORT TITLE
ACOUSTIC-GRAVITY WAVES IN THE ATMOSPHERE

4. DESCRIPTIVE NOTES *(Type of report and inclusive dates)*
Technical Report

5. AUTHOR(S) *(Last name, first name, initial)*
T. A. Potemra

6. REPORT DATE	7a. TOTAL NO. OF PAGES	7b. NO. OF REFS
November 1965	93	29

8a. CONTRACT OR GRANT NO.	9a. ORIGINATOR'S REPORT NUMBER(S)
ONR Contract Nonr-225(64)	SU-SEL-65-097
b. PROJECT NO.	Technical Report No. 110
c.	9b. OTHER REPORT NO(S) *(Any other numbers that may be assigned this report)*
d.	

10. AVAILABILITY/LIMITATION NOTICES
Qualified requesters may obtain copies from DDC. Foreign announcement and dissemination by DDC is not authorized.

11. SUPPLEMENTARY NOTES	12. SPONSORING MILITARY ACTIVITY
	ONR

13. ABSTRACT

The purpose of this research was to obtain a panoramic view of acoustic-gravity-wave motions throughout the atmosphere. A one-dimensional array of particles and springs, conceived by Newton to study sound waves in the atmosphere, was extended to two dimensions by means of 1500 particles interconnected by springs. Variations of density and pressure with altitude are represented by variations in mass and spring constants. This new model has provided means by which acoustic-gravity-wave motions in the atmosphere are solved on a high-speed digital computer, and a new animated-computer-output technique is used. A motion picture--automatically plotted by the computer, a frame at a time--provides greater detail and perspective of mechanical wave motions in the atmosphere than has ever been obtainable before. Ground-level and 100-km-high explosions were investigated with this computer model, and the resulting transient motions of the atmosphere were displayed by means of a motion picture produced by digital techniques. Computed ground-level barograms resulting from a ground-level explosion compare well with experimental barograms recorded during ground-level nuclear explosions.

DD FORM 1 JAN 64 1473

UNCLASSIFIED
Security Classification

14. KEY WORDS	LINK A		LINK B		LINK C	
	ROLE	WT	ROLE	WT	ROLE	WT
ACOUSTIC-GRAVITY WAVES PRESSURE DISTURBANCES IN THE ATMOSPHERE MOTION PICTURE COMPUTER OUTPUT						

INSTRUCTIONS

1. ORIGINATING ACTIVITY: Enter the name and address of the contractor, subcontractor, grantee, Department of Defense activity or other organization *(corporate author)* issuing the report.

2*a*. REPORT SECURITY CLASSIFICATION: Enter the overall security classification of the report. Indicate whether "Restricted Data" is included. Marking is to be in accordance with appropriate security regulations.

2*b*. GROUP: Automatic downgrading is specified in DoD Directive 5200.10 and Armed Forces Industrial Manual. Enter the group number. Also, when applicable, show that optional markings have been used for Group 3 and Group 4 as authorized.

3. REPORT TITLE: Enter the complete report title in all capital letters. Titles in all cases should be unclassified. If a meaningful title cannot be selected without classification, show title classification in all capitals in parenthesis immediately following the title.

4. DESCRIPTIVE NOTES: If appropriate, enter the type of report, e.g., interim, progress, summary, annual, or final. Give the inclusive dates when a specific reporting period is covered.

5. AUTHOR(S): Enter the name(s) of author(s) as shown on or in the report. Enter last name, first name, middle initial. If military, show rank and branch of service. The name of the principal author is an absolute minimum requirement.

6. REPORT DATE: Enter the date of the report as day, month, year; or month, year. If more than one date appears on the report, use date of publication.

7*a*. TOTAL NUMBER OF PAGES: The total page count should follow normal pagination procedures, i.e., enter the number of pages containing information.

7*b*. NUMBER OF REFERENCES: Enter the total number of references cited in the report.

8*a*. CONTRACT OR GRANT NUMBER: If appropriate, enter the applicable number of the contract or grant under which the report was written.

8*b*, 8*c*, & 8*d*. PROJECT NUMBER: Enter the appropriate military department identification, such as project number, subproject number, system numbers, task number, etc.

9*a*. ORIGINATOR'S REPORT NUMBER(S): Enter the official report number by which the document will be identified and controlled by the originating activity. This number must be unique to this report.

9*b*. OTHER REPORT NUMBER(S): If the report has been assigned any other report numbers *(either by the originator or by the sponsor)*, also enter this number(s).

10. AVAILABILITY/LIMITATION NOTICES: Enter any limitations on further dissemination of the report, other than those imposed by security classification, using standard statements such as:

(1) "Qualified requesters may obtain copies of this report from DDC."

(2) "Foreign announcement and dissemination of this report by DDC is not authorized."

(3) "U. S. Government agencies may obtain copies of this report directly from DDC. Other qualified DDC users shall request through _____."

(4) "U. S. military agencies may obtain copies of this report directly from DDC. Other qualified users shall request through _____."

(5) "All distribution of this report is controlled. Qualified DDC users shall request through _____."

If the report has been furnished to the Office of Technical Services, Department of Commerce, for sale to the public, indicate this fact and enter the price, if known.

11. SUPPLEMENTARY NOTES: Use for additional explanatory notes.

12. SPONSORING MILITARY ACTIVITY: Enter the name of the departmental project office or laboratory sponsoring *(paying for)* the research and development. Include address.

13. ABSTRACT: Enter an abstract giving a brief and factual summary of the document indicative of the report, even though it may also appear elsewhere in the body of the technical report. If additional space is required, a continuation sheet shall be attached.

It is highly desirable that the abstract of classified reports be unclassified. Each paragraph of the abstract shall end with an indication of the military security classification of the information in the paragraph, represented as *(TS)*, *(S)*, *(C)*, or *(U)*.

There is no limitation on the length of the abstract. However, the suggested length is from 150 to 225 words.

14. KEY WORDS: Key words are technically meaningful terms or short phrases that characterize a report and may be used as index entries for cataloging the report. Key words must be selected so that no security classification is required. Identifiers, such as equipment model designation, trade name, military project code name, geographic location, may be used as key words but will be followed by an indication of technical context. The assignment of links, rules, and weights is optional.